ABSTRACT

Electrostatic Control of Cu, Zn Superoxide Dismutase Aggregation in Amyotrophic Lateral Sclerosis: from Lysine Modification to Interaction with Lipid Membranes

Sanaz Rasouli, Ph.D.

Advisor: Bryan F. Shaw, Ph.D.

Cu, Zn superoxide dismutase (SOD1) is a ubiquitous metalloprotein, which is responsible for protecting living cells from oxidative stress via disproportionation of superoxide ions. Misfolding and subsequent aggregation of SOD1 is casually linked to familial and sporadic cases of amyotrophic lateral sclerosis (ALS). Symptoms of ALS include weakness in arms and legs and respiratory failure, which lead to death within a few years. The deposition of SOD1 amyloid fibrils (i.e., gain of toxic function) in axons causes the selective death of motor neurons, a hallmark of neurodegeneration. In this dissertation, I use various bioanalytical and biophysical techniques to study aggregation of wild-type (WT) and ALS-variant apo-SOD1 in both *in vitro* and *in vivo* conditions, in the context of ALS.

In Chapter Two of this dissertation, I first show how acylation of lysine residues in WT apo-SOD1 affects the kinetics and morphology of amyloid formation during microplate-based (*in vitro*) assays. Moreover, the ability of WT SOD1 fibrils to seed the aggregation of ALS-variant SOD1 in organotypic spinal cord derived from transgenic YFP-G85R-SOD1 mice is studied. I show, for the first time, that minimal acylation of apo-SOD1 with small moieties carrying a high negative charge increases the probability of formation of non- toxic SOD1 oligomers. The results from this study are crucial for designing small molecules that can selectively bind to and inhibit the propagation of toxic SOD1 fibrils.

In Chapter Three, I determine the rate, mechanism of formation, and morphology of aggregated forms of WT apo-SOD1 in the presence of small unilamellar vesicles (SUVs) composed of identical hydrophobic chains, but headgroups of variable charge i.e., anionic, zwitterionic, and cationic. The aggregation of eight different ALS variants of apo-SOD1 was also examined in the presence of SUVs. I found that SOD1 aggregation can be triggered by negatively-charged liposomes, which is very significant considering that cell-to-cell propagation of SOD1 is mediated by its interaction with lipid membranes.

Electrostatic Control of Cu, Zn Superoxide Dismutase Aggregation in Amyotrophic Lateral Sclerosis: from Lysine Modification to Interaction with Lipid Membranes

by

Sanaz Rasouli, B.Sc., M.Sc.

A Dissertation

Approved by the Institute of Biomedical Studies

_____

Robert R. Kane, Ph.D., Director

Submitted to the Graduate Faculty of
Baylor University in Partial Fulfillment of the
Requirements for the Degree
of

Doctor of Philosophy

Approved by the Dissertation Committee

_____

Bryan F. Shaw, Ph.D., Chairperson

_____

Robert R. Kane, Ph.D.

_____

Michael A. Trakselis, Ph.D.

_____

Bessie W. Kebaara, Ph.D.

_____

Carlos E. Manzanares, Ph.D.

Accepted by the Graduate School

August 2018

_____

J. Larry Lyon, Ph.D., Dean

Page bearing signatures is kept on file in the Graduate School.

TABLE OF CONTENTS

LIST OF FIGURES vii

LIST OF TABLES xi

LIST OF SCHEMES xii

ACKNOWLEDGMENTS xiii

CHAPTER ONE 1

Protein Aggregation and Neurodegenerative Diseases 1

Introduction 1

SOD1 and ALS 3

Prion-like behavior of SOD1: where lipid membranes become important in SOD1-linked ALS pathogenesis 7

Effect of net charge on aggregation of SOD1 8

Statement of Contribution 9

CHAPTER TWO 10

Lysine acylation in superoxide dismutase-1 electrostatically inhibits formation of fibrils with prion-like seeding 10

Abstract 10

Introduction 11

Materials and Methods.....14

Results and Discussion 20

Conclusion 44

CHAPTER THREE 48

Glycerolipid headgroups control rate and mechanism of SOD1 aggregation and accelerate fibrillization of slowly aggregating ALS mutants…… 48

Abstract.....48

Introduction.....49

Results and Discussion 53

Conclusion 74

Materials and Methods.....77

CHAPTER FOUR.....82

Supporting Information.....82

Lysine acylation in superoxide dismutase-1 electrostatically inhibits formation of fibrils with prion-like seeding……..82

Glycerolipid headgroups control rate and mechanism of SOD1 aggregation and accelerate fibrillization of slowly aggregating ALS mutants……..94

REFERENCES 97

LIST OF FIGURES

Figure 1.1 Schematic representing mechanism of formation of fibrillar aggregates from an amyloidogenic protein. 3

Figure 1.2 Disproportionation (dismutation) activity of SOD1 via scavenging superoxide ions to produce oxygen molecule and hydrogen peroxide 5

Figure 1.3 Fibrillization of SOD1 in the absence of any post-translational modifications 5

Figure 1.4 Three-dimensional ribbon structure of WT human SOD1 dimer (PDB entry: 2V0A 7

Figure 2.1 Increasing the net negative charge (Z) of apo-SOD1 via acylation of lysine-ε-NH_3^+ 14

Figure 2.2 Natural (N) and unnatural (U) acyl modifications examined in this chapter 22

Figure 2.3 Quantifying charge regulation associated with lysine acylation using "protein charge ladders" and CE 25

Figure 2.4 Effect of lysine acylation on the thermostability of WT apo-SOD1 26

Figure 2.5 Effect of fractional acylation of WT apo-SOD1 with highly charged groups ($\Delta Z_{formal} = -4$) on SOD1's fibrillization into ThT-positive species 28

Figure 2.6 Effect of fractional acylation of WT apo-SOD1 with weakly charged groups ($\Delta Z_{formal} \leq -2$) on SOD1's fibrillization int ThT-positive species 30

Figure 2.7 Effect of acylation on the probability of SOD1 aggregation studied with Kaplan-Meier estimators 34

Figure 2.8 Effect of apo-SOD1 acylation on the rate of formation of ANS-positive complexes 38

Figure 2.9 Seeding properties of unmodified (a-c) and singly pyromellitylated fibrils (d-f) of WT apo-SOD1 after four-week incubation with organotypic spinal cord cultures from transgenic ALS mice 41

Figure 2.10 Pyromellitylation of 4.16 lysine residues (37 % of all lysines in SOD1) abolishes the ability of SOD1 to form ThT-positive fibrils in microplate assays and inhibits seeding in organotypic spinal cord cultures.....42

Figure 3.1 Iterate thioflavin-T fluorescence assays of WT apo-SOD1 fibrillization in the presence of anionic, cationic, and zwitterionic liposomes.....55

Figure 3.2 Average ThT fluorescence of WT apo-SOD1 as a function of [Lipid]:[SOD1] for **(a)** anionic, **(b)** cationic, and **(c)** zwitterionic liposomes. Each plot is an average of data points from plots in Figure 3.1. Plots of **(d)** average ThT fluorescence intensity, **(e)** average lag time, and **(f)** average propagation rate versus increasing [Lipid]:[SOD1] ratios for the aggregation of WT apo-SOD1 in the presence of anionic DOPCA liposomes.....59

Figure 3.3 Filter-trap assays of binding of soluble WT apo-SOD1 to liposomes before fibrillization.....64

Figure 3.4 Fully metallated SOD1 does not fibrillize into ThT(+) species in the absence or presence of DOPCA liposomes 66

Figure 3.5 Iterate thioflavin-T fluorescence assays of fibrillization of WT and ALS-variant apo-SOD1 in the presence of anionic DOPCA liposomes ([Lipid]:[SOD1] = 30:1) (pH 7.4, 37ºC) 69

Figure 3.6 Comparison of rank order of **(a-b)** fibril nucleation, and **(c-d)** fibril elongation rate of ALS variant apo-SOD1 proteins when assays are carried out semi-quiescently in the presence of anionic DOPCA liposomes (without a Teflon bead) versus agitation with a Teflon bead (without liposomes). **(e)** Kaplan-Meier analysis of aggregation of WT and 8 ALS-variant apo-SOD1 proteins in the presence of anionic DOPCA liposomes ([Lipid]:[SOD1] = 30:1). **(e)** Kaplan-Meier analysis of aggregation of WT and 8 ALS-variant apo-SOD1 proteins in the presence of anionic DOPCA liposomes ([Lipid]:[SOD1] = 30:1)……..72

Figure 3.7 Primary nucleation mechanism of lipid-catalyzed SOD1 fibrillization 72

Figure 4.1 Mass spectra of WT apo-SOD1 proteins modified with **(a)** BP (0.70), **(b)** BT (0.98), and **(c)** CB (1.45).....82

Figure 4.2 Mass spectra of WT apo-SOD1 proteins modified with **(a)** SA(0.90), CA(1.10), GA(0.89), PhA(1.07), AA(1.05), and **(b)** SA(1.94), CA(2.22), GA(1.91), and PhA(1.82)……82

Figure 4.3 Acylation of WT apo-SOD1 with BP and BT modifications.....83

Figure 4.4 Acylation of WT apo-SOD1 with PM and CB modifications.....84

Figure 4.5 Acylation of WT apo-SOD1 with CA modification.....85

Figure 4.6 Acylation of WT apo-SOD1 with GA and SA modifications.....86

Figure 4.7 Acylation of WT apo-SOD1 with PhA and AA modifications.....87

Figure 4.8 Charge calculation for the minor charge ladder observed in the electropherograms of SOD1 proteins modified with acyl groups with $\Delta Z_{formal} = -2$.....88

Figure 4.9 TEM micrographs of acylated and unacylated apo-SOD1 proteins collected after the termination of ThT assay ($\Delta Z_{formal} = -4$).....88

Figure 4.10 **(a-e)** Histograms of fibril length (average ± SD) for variably acylated and unmodified apo-SOD1 proteins ($\Delta Z_{formal} = -4$), measured from TEM micrographs ($n_{unmod} = 265$; $n_{PM} = 234$; $n_{BT} = 112$; $n_{BP} = 239$; $n_{CB} = 214$) 89

Figure 4.11 TEM micrographs of acylated and unacylated apo-SOD1 proteins collected after the termination of ThT assay ($\Delta Z_{formal} \leq -2$).....89

Figure 4.12 Representative TEM micrographs taken from wells that show sigmoidal (left) and exponential (right) kinetics, during ANS fluorescence aggregation assays of acylated and unmodified apo-SOD1 proteins 90

Figure 4.13 **(a)** Replicate ThT fluorescence assays of aggregation of WT apo-SOD1 seeded with acylated SOD1 fibrils that were ThT-negative and ThT-positive. The fibrils that were used to seed SOD1 are composed of preformed, singly pyromellitylated SOD1. The black trace in each

ç

(b) average lag time, and **(c)** average propagation rate for SOD1 aggregation in the absence and presence of different seeds (SD: standard deviation). P-values for ThT-negative and ThT-positive conditions are calculated with respect to control (unseeded) data, using an Unpaired Student's t-test. **(d)** Kaplan-Meier analysis of aggregation of WT apo-SOD1 seeded with ThT-negative and ThT-positive SOD1 fibrils.....91

Figure 4.14 Characterization of zwitterionic, anionic, and cationic SUVs 94

Figure 4.15 Small lipid vesicles do not disassemble during the course of aggregation assays 95

Figure 4.16 TEM micrographs of **(A)** ThT(+), and **(B)** ThT(-) wells after completion of aggregation assays of ALS-variant apo-SOD1 proteins in the presence of anionic DOPCA liposomes, [Lipid]:[SOD1] = 30:1. SDS-PAGE gels of the supernatants from **(C)** ThT(+), and **(D)** ThT(-) wells containing ALS-variant apo-SOD1 proteins in the presence of anionic DOPCA liposomes ([Lipid]:[SOD1] = 30:1) after the termination of aggregation assay. SDS-PAGE gel of soluble control WT apo-SOD1 from a 30 μM stock solution is shown in panel D as control (right gel).....95

LIST OF TABLES

Table 2.1 Kinetic parameters of *in vitro* fibrillization of WT apo-SOD1 (100 mM TCEP 37 °C, pH 7.4) before and after acylation 23

Table 3.1 Kinetic parameters of non-liposomal (T) and liposomal (L) assays of apo-SOD1 fibrillization (10 mM TCEP, 37 °C, pH 7.4)……..67

Table 4.1 MS/MS analysis of WT apo-SOD1 tryptic digests modified with different acylating groups (Ac(~1))……..87

Table 4.2 MS/MS analysis of WT apo-SOD1 tryptic digests modified with different acylating groups with $\Delta Z_{formal} = -2$ for the purpose of measuring ΔZ of acylation (Ac(~2))……..88

Table 4.3 Metal content of WT and ALS-variant apo-SOD1 proteins measured with ICP-MS……..88

LIST OF SCHEMES

Scheme 3.1 Lipids used to prepare SUVs.....48

ACKNOWLEDGMENTS

To my lovely best friend and husband, Alireza, who has been a constant source of support and encouragement during the challenges of graduate school and life. I am truly thankful for having you in my life.

I would like to express my sincere gratitude to my advisor Prof. Bryan Shaw for the continuous support of my PhD study and research, for his patience, motivation, enthusiasm, and immense knowledge.

I am grateful to my family, my father, Dr. Mojtaba Rasouli, and my older sisters, Dr. Ousha Rasouli and Dr. Soora Rasouli, who have always loved me unconditionally and whose good examples have taught me to work hard for the things that I aspire to achieve.

With a special mention to all my friends and colleagues; Devon, Corbin, Aleks, Collin, Lindsay, Katelyn, Keats, Aaron, Richard, and Mark. I hope I have not missed anyone. It was fantastic to have the opportunity to work with you!

I am also grateful to all the faculty members and staff of Institute of Biomedical Sciences, Department of Chemistry and Biochemistry, and Department of Biology, specially Prof. Bob Kane, Prof. Bessie Kebaara, Prof. Michael Trakselis, Prof. Carlos Manzanares, Prof. Christopher Kearney, and Prof. Mary Lynn Trawick.

Thanks for all your encouragement!

CHAPTER ONE

Introduction

Protein Aggregation and Neurodegenerative Diseases

Millions of people are affected by neurodegenerative disorders such as Alzheimer's disease (AD), Parkinson's disease (PD), Huntington's disease (HD), amyotrophic lateral sclerosis (ALS or Lou Gehrig's disease), and other prion diseases worldwide.[1] Among these, the two most common neurodegenerative diseases are AD and PD.[1] In 2015, ~ 30 million people suffered from AD and ~ 6 million people were diagnosed with PD.[2] The diagnosis and treatment of neurodegenerative diseases costs millions of dollars per year. Unfortunately, the exact molecular mechanism(s) of these diseases is not well-understood, and currently there are no effective therapies for them.[1] Neurodegenerative diseases have several typical symptoms such as memory loss, muscle weakness, fatigue, ataxia, seizures, anxiety, and insomnia.[3]

Almost all neurodegenerative disorders involve a common pathogenic pathway that is associated with accumulation of insoluble protein aggregates in both central nervous system (CNS) and peripheral nervous system (PNS).[3] The most important implication of this pathway, sometimes known as the amyloid hypothesis, is neuron death which leads to neurodegeneration. The primary driving force for pathogenesis in all neurodegenerative diseases is amyloid hypothesis.[4] Examples include, but are not limited to: the aggregation of amyloid beta protein ($A\beta_{1\text{-}40}$ and $A\beta_{1\text{-}42}$) and tau protein in AD,[5] aggregation of copper, zinc superoxide dismutase (SOD1) in ALS,[6] and aggregation of α-synuclein in PD.[7]

Almost all of the neurodegenerative diseases have a similar mechanism for aggregation of amyloidogenic proteins.[4] This mechanism involves a three-step pathway (Figure 1.1): 1) the nucleation step (i.e., lag phase)[8] in which a "critical nucleus" is formed. This critical nucleus is composed of a certain number of misfolded, monomeric polypeptide units, that assemble together through interaction of exposed hydrophobic residues in each polypeptide; 2) the elongation step (i.e., log phase), in which oligomeric protofibrils are formed via addition of monomeric polypeptides to the critical nucleus; 3) the termination step (i.e., plateau phase), in which mature fibrils are formed via assembly of intermediate oligomers and protofibrils, and chemical equilibrium has reached. This means that rate of addition of monomeric species to these mature fibrils is equal to the rate of dissociation of monomers, and thus fibrils will not further elongate.[8]

The length of amyloid fibrils that are formed from amyloidogenic proteins are usually in nanometer scale.[9] They typically consist of multiple protofilaments that twist around each other to form mature fibrils. X-ray crystallography have shown that the core of each protofilament adopts a cross-β structure, in which β-strands form effective and continuous hydrogen-bonded β-sheets that run along the length of the fibril.[10] X-ray crystallography has also revealed the atomic structure of fibril. First shown by David Eisenberg laboratory on 2007,[11] the backbone structure of an amyloid fibril consists of intertwined hydrophobic residues from constituent β-strands. These structures are called "steric zippers", and are unique for each amyloidogenic protein.[11]

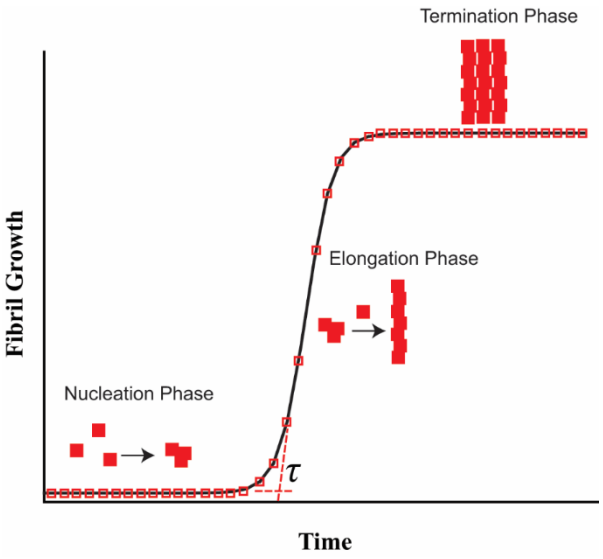

Figure 1.1 Schematic representing mechanism of formation of fibrillar aggregates from an amyloidogenic protein. The time required for the formation of "critical nucleus" is known as fibrillization lag time (τ). Each red square illustrates a single polypeptide. Black line is the sigmoidal curve that is mathematically fit to protein aggregation data and is used to extract kinetic parameters of protein aggregation.

SOD1 and ALS

Amyotrophic lateral sclerosis (ALS) is a fatal neurodegenerative disease that affects motor neurons in the spinal cord, brainstem, and motor cortex.[12] ALS is a protein misfolding disease in which, similar to other motor neuron disorders (MNDs),[13, 14] abnormal self-assembly of a handful of amyloidogenic proteins play an important role in the pathogenesis of disease. Most ALS cases (~ 90 %) are sporadic (i.e., sALS), while 10 % of ALS cases are familial (i.e., fALS). Both sALS and fALS show similar clinical symptoms, however, in some cases of fALS, earlier disease onset occurs compared to sALS.[15] Approximately 20 % of fALS cases (2 % of all ALS cases) are arising from mutations in the gene encoding ubiquitous metalloprotein copper/zinc superoxide dismutase 1 (SOD1).[16]

Eukaryote SOD1 is a 32-kD homodimeric protein containing 153 amino acids, and found predominantly in the cytosol but also in the nucleus, mitochondrial membrane space, peroxisomes, and lysosomes.[17] Each subunit contains an eight-stranded, Greek-key β-barrel, a binuclear copper/zinc site, and one intramolecular disulfide bond between Cys 57 and Cys 146. The insertion of copper into SOD1[18] and formation of disulfide bond which is induced by molecular oxygen[19] are facilitated by the copper chaperon for SOD1 (CCS), which belongs to metallochaperones family.[20] Although the majority of human SOD1 (hSOD1) maturation is CCS dependent,[21] some studies have revealed that activation of hSOD1 can also be CCS independent. In this scenario, copper is delivered into SOD1 through reduced gluthathione (GSH) and oxidation of disulfide bond without molecular oxygen.[22, 23]

Antioxidant activity of SOD1 was first reported by McCord and Fridovich.[24] SOD1 converts two superoxide radicals into oxygen molecule and hydrogen peroxide (Figure 1.2). The copper ion in SOD1 active site cycles between Cu^{2+} to Cu^{1+} redox states. The first superoxide molecule transfers an electron to Cu^{2+}, thereby reducing it to Cu^{1+}. The His63 residue (i.e., imidazolate anion) detaches from Cu^{1+} and binds to a proton.[25] This proton is then transferred to the second superoxide radical in the active site, neutralizing the negative charge on the second superoxide molecule, and forming hydrogen peroxide (Figure 1.2).[24] The zinc ion is not involved in the catalytic disproportionation of superoxide, but provides structural support in the active site.[26]

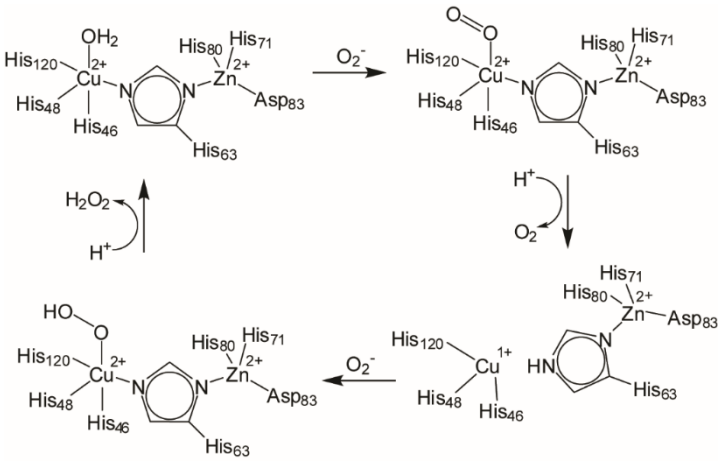

Figure 1.2. Disproportionation (dismutation) activity of SOD1 via scavenging superoxide ions to produce oxygen molecule and hydrogen peroxide. H_2O_2 is then converted into oxygen and water via enzyme catalase.

SOD1 activation and maturation involves several post-translational modifications including copper/zinc binding, formation of intramolecular disulfide bond, and SOD1 dimerization.[27] Absence of any of these processes could result in a buildup of unfolded SOD1 and could trigger the formation of SOD1 insoluble fibrils (Figure 1.3).[28] Accumulation of insoluble SOD1 fibrils has been proposed to disrupt several cellular activities such as axonal transport and mitochondrial function, leading to neuronal cell death.[29]

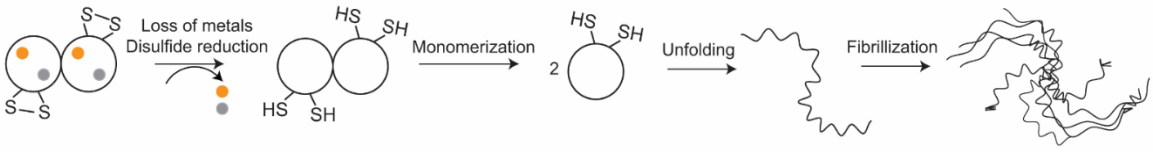

Figure 1.3. Fibrillization of SOD1 in the absence of post-translational modification.

In the 25 years from the time that SOD1 was identified for ALS,[30] more than 160 mutations have been reported (http://alsod.iop.kcl.ac.uk/).[31] The positions of SOD1 mutations are scattered throughout SOD1 polypeptide (Figurer 1.4), including residues in the dimer interference.[32] SOD1 mutations are divided into two major groups based on their biophysical properties: wild type-like SOD1 mutants and metal binding region mutant proteins.[33, 34] Wild-type like SOD1 mutants exist as fully functional SOD1 proteins and have full SOD1 enzyme activity. Moreover, wild-type-like SOD1 mutations can have a very severe phenotype. For example, A4V is the most aggressive form of ALS in North America with ~ 1 year survival time after diagnosis.[35] Conversely, mutations falling into the second category (i.e., metal-binding deficient mutants) such as H46Q show different physical properties (i.e., reduced ability to bind copper and zinc) compared to wild-type like SOD1 variants.[33] However, a fraction of SOD1 mutants linked to ALS do not alter any physical properties significantly. These mutants which are called "cryptic" mutations (e.g., D90A, E100K, D101N, and N139K) promote fibrillization by reducing the formal net charge of SOD1 by one or two units.[36, 37]

Loss of function of SOD1 enzyme activity was initially suggested for phenotypes arise from ALS caused by SOD1 mutations.[38] However, this mechanism became less favored compared to gain of toxic property mechanism because: (i) in humans, there is no correlation between reduced enzyme activity of SOD1 and disease severity.[39] (ii) loss of lower motor neurons and ALS symptoms has been developed in transgenic mice overexpressing human SOD1.[32]

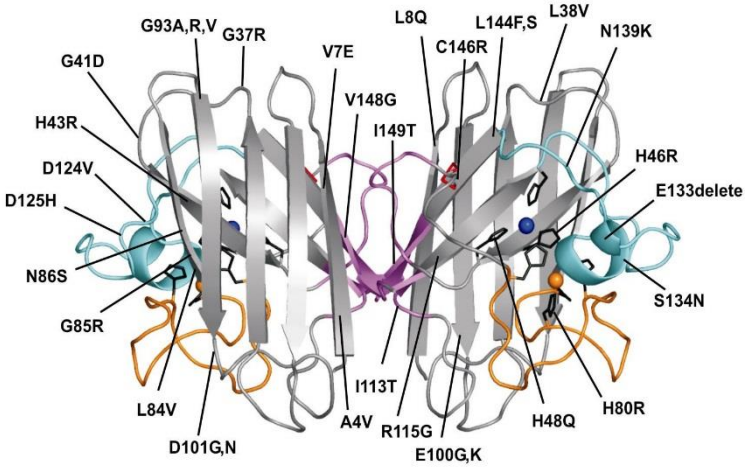

Figure 1.4. Three-dimensional ribbon structure of WT human SOD1 dimer (PDB entry: 2V0A). Various mutations of SOD1 are shown that are scattered throughout SOD1 structure.

Prion-like Behavior of SOD1: Where Lipid Membranes Become Important in SOD1-linked ALS Pathogenesis

Prions are infectious protein species that are capable of spreading between living cells.[40] Prion-like propagation involves entering of misfolded proteins into the cells upon interaction with cellular membrane, and transmitting pathogenic proteins in a prion-like manner via seeding the aggregation of normally folded proteins.[41] The mechanism by which pathogenic proteins gain access to the cytoplasmic compartment to propagate toxic oligomers is not fully understood in the context of neurodegenerative diseases.[7, 42]

It has been shown that SOD1 oligomers are able to seed fibrillization of folded proteins in a prion-like manner.[43, 44] Indeed, SOD1 aggregates can be taken up efficiently and rapidly into living cells,[45] including motor neurons. Several studies have suggested that aggregated forms of SOD1 derived from recombinant protein or from homogenates of spinal cords of transgenic mice expressing human mutant SOD1 can trigger the formation of protein aggregates in normal cells.[46]

During their prion-like propagation, monomeric or oligomeric SOD1 species interact with cellular or vesicular membranes.[47] Misfolded SOD1 can be transmitted between the cells via endocytosis and exocytosis processes.[42] Interaction of SOD1 with lipid membranes might also trigger self-assembly of SOD1 monomers.[48, 49] Moreover, it has been shown that interactions between SOD1 and mitochondrial membranes are involved in oligomerization of SOD1 under *in vivo* condition.[50] Mitochondrial dysfunction has been observed in ALS transgenic mice due to accumulations of SOD1 in mitochondrial outer membrane, intermembrane space, and matrix.[50, 51] Moreover, increasing the negative charge of SOD1 oligomers would presumably impede their interaction with cellular membrane and would inhibit their diffusion across the cell membrane. These evidences concomitantly point out the important role of lipid membranes in the context of SOD1-linked ALS.

Effect of Net Charge on Aggregation of SOD1

The net charge of protein is one of the factors that can affect aggregation propensity of SOD1 polypeptides. SOD1 is a negatively charged protein with Z = -6.05 per monomeric protein.[37] Some ALS-mutations decrease the net negative charge of SOD1 (pushing the protein towards neutrality) and increase the aggregation propensity of SOD1 polypeptide by reducing repulsive Coulombic forces between individual SOD1 polypeptides.[52] The reduced repulsive force lowers the kinetic barrier for aggregation and promotes SOD1 aggregation.[53]

Moreover, it has been shown that increasing the negative charge of SOD1 via covalent modification with aspirin, which acetylates the lysine residues in SOD1, inhibits aggregation by increasing electrostatic repulsions between SOD1 polypeptides.[54]

Statement of Contribution

I am more than grateful that I have been able to contribute to the publication of six peer-reviewed publications under the supervision of Prof. Bryan F. Shaw, in two of which I contributed as the first author. These comprise the chapters two and three of this dissertation, and are as follows: (1) Lysine acylation in superoxide dismutase-1 electrostatically inhibits formation of fibrils with prion-like seeding; (2) Glycerolipid headgroups control rate and mechanism of SOD1 aggregation and accelerate fibrillization of slowly aggregating ALS mutants.

Dr. Alireza Abdolvahabi, Mr. Corbin Croom, Mr. Devon Plewman, Dr. Yunhua Shi, and Dr. Jacob Ayers contributed in performing experiments, data analysis, and writing of manuscript for the publication "Lysine acylation in superoxide dismutase-1 electrostatically inhibits formation of fibrils with prion-like seeding". Dr. Alireza Abdolvahabi, Mr. Corbin Croom, Mr. Devon Plewman, and Dr. Yunhua Shi contributed in conducting experiments and analysis of data in the publication "Glycerolipid headgroups control rate and mechanism of SOD1 aggregation and accelerate fibrillization of slowly aggregating ALS mutants".

CHAPTER TWO

Lysine Acylation in Superoxide Dismutase-1 Electrostatically Inhibits Formation of Fibrils with Prion-like Seeding

This chapter is published as:
Rasouli S, Abdolvahabi A, Croom CM, Plewman DL, Shi Y, Ayers JI, Shaw BF. Lysine acylation in superoxide dismutase-1 electrostatically inhibits formation of fibrils with prion-like seeding (2017) Lysine acylation in superoxide dismutase-1 electrostatically inhibits formation of fibrils with prion-like seeding. *Journal of Biological Chemistry*. **292**, 19366-19380.[55]

Abstract

The acylation of lysine residues in superoxide dismutase-1 (SOD1) has been previously shown to decrease its rate of nucleation and elongation into amyloid-like fibrils linked to amyotrophic lateral sclerosis (ALS). The chemical mechanism underlying this effect is unclear, *i.e.* hydrophobic/steric effects *versus* electrostatic effects. Moreover, the degree to which the acylation might alter the prion-like seeding of SOD1 *in vivo* has not been addressed. Here, I acylated a fraction of lysine residues in SOD1 with groups of variable hydrophobicity, charge, and conformational entropy. The effect of each acyl group on the rate of SOD1 fibril nucleation and elongation was quantified *in vitro* with thioflavin-T (ThT) fluorescence, and I performed 594 iterate aggregation assays to obtain statistically significant rates. The effect of the lysine acylation on the prion-like seeding of SOD1 was assayed in spinal cord extracts of transgenic mice expressing a G85R SOD1—yellow fluorescent protein construct. Acyl groups with > 2 carboxylic acids diminished self-assembly into ThT-positive fibrils and instead promoted the self-assembly of ThT-negative fibrils and amorphous complexes. The addition of ThT-negative, acylated SOD1 fibrils to organotypic spinal cord failed to produce the SOD1 inclusion pathology that typically

results from the addition of ThT-positive SOD1 fibrils. These results suggest that chemically increasing the net negative surface charge of SOD1 via acylation can block the prion-like propagation of oligomeric SOD1 in spinal cord.

Introduction

The role that long-range Coulombic interactions play in the nucleation, propagation, and toxicity of amyloid-like oligomers is generally overlooked. These electrostatic forces scale with the net charge (Z) of the self-assembling proteins, unlike short-range Coulombic interactions that scale with local patterns of surface charge.[54, 56-59] In the hydrophobic core of a protein or protein aggregate, these long-range Coulombic forces can extend dozens of angstroms further than through aqueous solution, where the Debye radius is only ~ 10 Å at pH 7.4, I = 0.1 M.[60, 61]

Can long-range electrostatic forces be medicinally targeted, for example, to increase electrostatic repulsion between protein subunits that self-assemble into neurotoxic complexes? Can "Z" be viewed as a druggable parameter, and chemically permuted like other classic parameters in biochemistry such as an enzyme's V_{max} or K_m? To date, there have been only a handful of studies to determine whether such electrostatic forces can be chemically (medicinally) amplified to inhibit self-assembly.[54, 62, 63] This potentially new sub-field of medicinal chemistry is obscured by the general difficulty in quantifying the net charge of a folded protein in solution, and the lack of tools available for measuring the net charge of a folded protein in solution.[60] For example, the magnitude by which "Z" is affected by a missense mutation, post-translational modification, fluctuation in subcellular pH, or co-factor binding has only been measured for a few proteins, using "protein charge

ladders".[60, 64, 65] In these cases, measured values of net charge can differ in magnitude (and sign/polarity) from predicted values.[60, 64, 65]

In this chapter, I hypothesize that lysine acylation (lysine-ε-NH_3^+ → lysine-ε-NHCOR) represents a plausible mechanism by which protein self-assembly might be controlled electrostatically. Although this electrostatic hypothesis is unconventional, it is not unreasonable. Pharmacological agents such as aspirin, the simplest aryl ester, can transfer acetyl groups directly to lysine residues of ~ 100 different proteins.[66-69] In general, the neutralization of a single lysine-ε-NH_3^+ in a protein is expected to have a large effect on its overall net charge because proteins are predicted to have low values of net charge to begin with ("low" defined as Z between -10 and +10).[70] Could acyl groups function as potent electrostatic inhibitors of undesired interactions between proteins? I conducted this chapter to begin to answer this question, within the context of the amyloidogenesis of SOD1.[71, 72] The self-assembly of SOD1—a net negatively charged protein at pH 7.4—into amyloid-like complexes is regarded as one of many causes of a subset of ALS.[73-75]

The toolbox of lysine acyl modifications utilized by biological systems is broader than once assumed and includes methylation, formylation, propionylation, butyrylation, crotonylation, malonylation, succinylation, glutarylation, and myristoylation.[76] Previous studies have shown that acetylation of lysine residues (and other types of chemical modifications) in neurotoxic proteins can affect processes linked to neurodegeneration,[77-79] but the biochemical mechanisms are unclear. For example, acetylation of lysine residues in TDP-43 is enhanced by oxidative stress, and disrupts RNA and DNA binding sites and triggers TDP-43 aggregation.[78] In mice, SOD1 has been reported to undergo succinylation and acetylation at multiple lysine residues, however, any role in ALS is unclear.[80] The

acetylation of tau can either promote or decrease aggregation depending on the site of acetylation.[79] In the case of SOD1, palmitoylation of cysteine has been shown to cause partitioning of SOD1 to cell membranes, which might increase its aggregation propensity by increasing the probability of surface-catalyzed aggregation.[81]

We have recently shown that acetylation of multiple lysine residues in apo-SOD1 (up to ~ 6 out of 11 lysines in the SOD1 chain) with aspirin impedes the (*in vitro*) nucleation and elongation of amyloid fibrils as measured by microplate-based ThT assays.[54] This protective effect was rationalized to be electrostatic in nature and originate from the increased electrostatic repulsion of acetylated SOD1 via neutralization of lysine-ε-NH_3^+ to lysine-ε-$NHCOCH_3$. For example, apo-SOD1 has a net negative charge of -6.92 ± 0.14 per subunit,[65] which is increased by ~ -0.9 units per acetyl group. While our previous study proved that post-translational modifications can inhibit SOD1 fibrillization via transferring of acetyl groups, it did not examine: (i) whether acetylation promoted alternate (amorphous) pathways of SOD1 aggregation;[82] (ii) if natural and unnatural acyl modifications of greater negative charge (i.e., $\Delta Z > 1$) could inhibit SOD1 fibrillization into amyloid by a greater magnitude than acetyl modifications; and (iii) whether acylation of lysine residues in SOD1 could inhibit the prion-like seeding of SOD1 complexes in living systems. In this chapter, I answer these three questions.

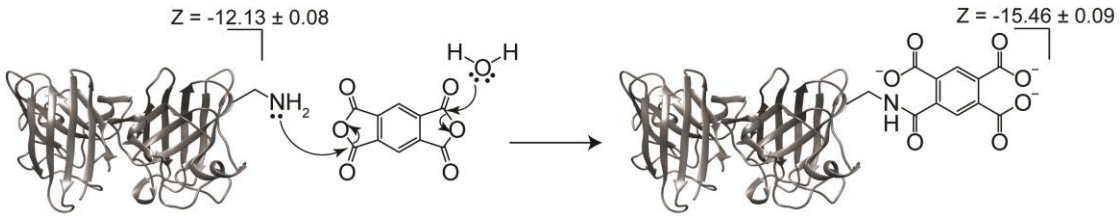

Figure 2.1 Increasing the net negative charge (Z) of apo-SOD1 via acylation of lysine-ε-NH_3^+. Acylation of SOD1 by pyromellitic dianhydride (PM) is shown as an example. The net charge of WT apo-SOD1 is -12.13 ± 0.08 (per dimer) at pH 7.4, 10 mM potassium phosphate buffer.[65] The formal change in charge upon attachment of PM group to lysine is ΔZ_{formal} = -4.0. The actual change in charge upon acylation of lysine in SOD1 (ΔZ_{CE}; determined in this chapter) is -3.33 ± 0.04, because of "charge regulation".[83, 84] Values of ΔZ_{formal} and ΔZ_{CE} are listed for each acyl group studied in this chapter in Figure 2.2

Materials and Methods

Expression, Purification, and Demetallation of Human WT SOD1

Human WT SOD1 was recombinantly expressed in *S. cerevisiae*, purified, demetallated, and characterized as previously described.[54] Briefly, *S. cerevisiae* cells were shaken at 30 °C for ~ 7 days post-inoculation (to obtain an average optical density of 1.8 a.u.), and were centrifuged at 4500 rpm. Cell pellets were lysed using 0.5 mm glass beads, followed by ammonium sulfate precipitation and three successive chromatographic separations: hydrophobic interaction chromatography, ion-exchange chromatography, and size-exclusion chromatography. Upon the completion of size-exclusion chromatography, purified SOD1 proteins were demetallated via dialysis in three demetallation buffers (~ 6 days), which are as follows: (i) 100 mM sodium acetate, 10 mM EDTA, pH 3.8; (ii) 100 mM sodium acetate, 10 mM NaCl, pH 3.8; and (iii) 100 mM sodium acetate, pH 5.5. All demetallated proteins were flash frozen with liquid nitrogen and kept at -80 °C.

*Inductively Coupled Plasma Mass Spectrometry (ICP-MS)***:**

The absence of metal ions in purified WT SOD1 proteins was confirmed using a 7900 ICP-MS instrument (Agilent Technologies, Santa Clara, CA). All WT apo-SOD1 proteins contained < 0.02 molar equivalents of zinc or copper.

*Acylation of WT apo-SOD1 with Different Acylating Groups***:**

Acylating agents that were used to modify WT apo-SOD1 were purchased from Sigma-Aldrich and include: cyclobutane-1,2,3,4-tetracarboxylic dianhydride (CB), pyromellitic dianhydride (PM), benzophenone-3,3′,4,4′-tetracarboxylic dianhydride (BT), 3,3′,4,4′-biphenyltetracarboxylic dianhydride (BP), succinic anhydride (SA), citraconic anhydride (CA), glutaric anhydride (GA), phthalic anhydride (PhA), and acetic anhydride (AA). To perform acylation reactions, WT apo-SOD1 proteins were first transferred to a reaction buffer containing 100 mM HEPBS (N-(2-hydroxyethyl)piperazine-N′-(4-butanesulfonic acid); pH 9.0). Stock solutions of different acylating agents were prepared by dissolution in either dimethyl sulfoxide (DMSO), 1,4-dioxane, or dimethylformamide (DMF) to a final concentration of 1 M (except for CB and BP, which were dissolved to a final stock concentration of 0.5 M). Different degrees of WT apo-SOD1 acylation were obtained by adding different molar equivalents of acylating agents to the reaction solution (to a final concentration of up to 1 mM; [SOD1] = 10 μM), followed by constant and gentle stirring for 2 hr at 4 °C. Identical volumes of DMSO, DMF, or dioxane were added to a solution of unmodified WT apo-SOD1 (i.e., the control solution) in order to account for any possible effects of organic solvents on the structure or stability of native SOD1. The final concentration of organic solvents in the aggregation assay (per modification) are as follows: 0.01 % DMSO (PM); 0.1 % DMF (CB); 0.04 % DMSO (BP); 0.01 % DMSO

(BT); 0.02 % DMSO (SA); 0.01 % DMSO (CA); 0.01 % DMSO (GA); 0.01 % DMSO (PhA); 0.04 % dioxane (AA). Acylation reactions were stopped after 2 hr, and 10 μL aliquots were taken for further characterization, as described below.

Mass Spectrometry (MS):

Acylated WT apo-SOD1 proteins were diluted in 0.1 % formic acid solution to a final concentration of 1 μM, and analyzed using a Synapt G2 ion-mobility spectrometry mass spectrometry (IMS-MS) instrument under positive ion mode. Proteins were desalted for 10 min on a C-18 trapping column (98 % water, 2 % acetonitrile) prior to MS. Mass spectra of proteins were then deconvoluted using MaxEnt1 module in MassLynx software (Waters Corporation, MA, USA). The number of modifications per SOD1 subunit was calculated from deconvoluted spectra. In particular, we expressed the number of modifications as the weighted average of each modification per SOD1 subunit.

*Trypsin Digestion, Tandem Mass Spectrometry (MS/MS), and Proteomics Analysis***:**

Partially acylated apo-SOD1 protein solutions were transferred to 50 mM Tris-HCl buffer, pH 8.8 (to achieve optimal trypsin activity), using centrifugal filtration. Transferred protein solutions were digested with trypsin Gold (Promega®, WI, USA) at a ratio of 1:20 (trypsin:SOD1; [SOD1] = 150 μM*).* Dithiothreitol (DTT) was added to SOD1:trypsin mixture at a final concentration of *2 mM* to ensure complete disulfide reduction. The SOD1 tryptic digest was incubated at 37 °C for 24 hr, prior to mass spectrometry analysis. A LTQ LX/Orbitrap Discovery LC/MS instrument (Thermo Fisher Scientific, MA, USA) was used to acquire mass spectra for apo-SOD1 tryptic peptides. SOD1 tryptic digests were separated on a reversed-phase C-18 column using a gradient mixture of water and

acetonitrile as mobile phase. The proteomics analysis was performed using the SEQUEST protein identification software (Thermo Fisher Scientific, MA, USA).

Human SOD1 amino acid sequence was used as the template for protein identification. The sequence coverage amongst all acylated SOD1 proteins varied from 98 % to 100 %. Only peptides with Xcorr $\geq$ 4.0 and ppm $\leq$ 0.05 were considered as positive hits.

Capillary Electrophoresis (CE):

The degree to which each modification altered the net charge of WT apo-SOD1 was quantified using CE, as previously described.[65] Briefly, acylated and unmodified apo-SOD1 proteins were transferred to CE running buffer (10 mM KPO_4, pH 7.4) and analyzed using a Beckman P/ACE instrument, equipped with a bare fused-silica capillary. All CE experiments were performed at 22 °C.

Differential Scanning Calorimetry (DSC):

The impact of all acyl modifications on the thermostability of WT apo-SOD1 was measured using DSC. Unmodified and acylated proteins were transferred to 10 mM KPO_4 buffer (pH 7.4), and heated from 20 °C to 80 °C at a scan rate of 1 °C/min, using a MicroCal VP-DSC calorimeter (Malvern Instruments, UK). Normalization of protein concentration and baseline correction were performed on DSC thermograms prior to fitting with a 2-state non-binding model, from which the values of melting temperature (T_m) were extracted.

Thioflavin-T (ThT) and 1-Anilino-8-Naphthalenesulfonate (ANS) Aggregation Assays:

High-throughput ThT and ANS aggregation assays were performed, as previously described.[54, 82] Briefly, acylated and unmodified WT apo-SOD1 proteins were transferred to aggregation buffer (10 mM KPO_4, 5 mM EDTA, pH 7.4) via centrifugal filtration (4-5 cycles of 1:10 dilution, followed by 10-fold concentration). Solutions were then filtered using a 200-μm GHP Acrodisc® syringe filter. Concentration of all apo-SOD1 solutions (modified and unmodified) were measured using Bradford assay and bicinchoninic acid (BCA) assay (instead of UV-vis spectrophotometry), because of the high UV absorption of aromatic moieties in PM, BT, BP, and PhA modifications. Both Bradford and BCA assays were performed according to well-established, standard procedures.[85, 86] Bovine serum albumin (BSA) was used as standard protein for both Bradford and BCA assays.

After quantifying the concentration of all modified and unmodified SOD1 proteins, tris(2-carboxyethyl)phosphine (TCEP) was added to each protein solution ([TCEP] = 100 mM, [SOD1] = 30 μM per dimer), and solutions were gently shaken at room temperature for 6 hr to achieve ~ 90 % disulfide reduction.[82] Solutions were then filtered with a 0.2-μm GHP Acrodisc® syringe filter to remove any preformed oligomers that might possibly seed apo-SOD1 aggregation. ThT and/or ANS were added to WT apo-SOD1 solutions at a final concentration of 20 μM, thoroughly mixed, and solutions were aliquoted (200 μL each) into the wells of a 96-well, nonbinding black polystyrene plate. Each well contained a clean and dust-free 1/8" Teflon bead (McMaster-Carr®). The plate was firmly sealed with a polypropylene seal to prevent solvent evaporation and TCEP oxidation. Assays were performed using an Ascent® Fluoroskan FL microplate reader (Thermo Fisher Scientific, MA, USA) with a built-in temperature controller (37 °C). Fluorescence was recorded every

15 min for up to ~ 168 hr, with intermittent orbital gyration at 360 rpm (gyration occurred every 15 sec, for 15 sec; gyration diameter = 3 mm).

Analysis of SOD1 aggregation data, including fitting kinetic traces, extraction of mean kinetic parameters (i.e., lag time, propagation rate, ThT/ANS fluorescence intensity), construction of Kaplan-Meier plots, and calculation of Hazard ratios were performed as previously described.[54, 87]

Transmission Electron Microscopy (TEM):

To determine the morphology of SOD1 aggregates after the termination of each aggregation assay, I performed TEM microscopy using a JEOL JEM-1010 transmission electron microscope (JEOL Ltd., MA, USA). TEM samples for SOD1 aggregates were prepared, as previously described.[87]

Mice:

Studies that involved transgenic mice were approved by the Institutional Animal Care and Use Committee (IACUC) at the University of Florida in accordance with the NIH guidelines. All animals were housed (between one to five to a cage) and nourished on ad libitum food and water. A 14-hr light and 10-hr dark cycle was used. The construction and pathology of transgenic G85R-SOD1:YFP mice have been previously described,[88] and are maintained on the FVB/NJ background.

Organotypic Spinal Cord Cultures:

The organotypic spinal cord slice cultures were prepared as previously described.[89] Briefly, G85R-SOD1:YFP mouse pups were euthanized at 7 days old by CO_2 asphyxiation and were immediately decapitated. Spinal cords were dissected and cut to a length of 350

μm using a McIlwain Tissue Chopper. Spinal cord slices were cultured on 0.4 μm Millipore Millicell-CM membrane inserts and incubated in medium containing 50 % (v/v) minimal essential medium, 25 mM HEPES, 25 % (v/v) heat-inactivated horse serum, 25 % (v/v) Hank's Balanced Salt Solution (HBSS), and supplemented with 6.4 mg/mL glucose and 2 mM glutamine. Cultures were incubated at 37 °C in a 5 % CO_2/95 % air humidified environment.

To perform the seeding experiments, fibril homogenates from *in vitro* microplate preparations were vigorously shaken and 1 μL of homogenate was micropipetted directly to the top of each spinal cord section (after the cross section was incubated for ~ 1 week). Sections were incubated for 1 month after the addition of aggregated SOD1 from *in vitro* microplate assays. To image sections, samples were fixed with 4 % paraformaldehyde for 4 hr, rinsed in PBS, and put directly onto slides. The slides were then cover-slipped in Vectastain mounting media containing 4′,6-diamidino-2-phenylindole (DAPI). Images were visualized using an Olympus DSU-IX81 spinning disc confocal microscope.

Results and Discussion

The natural and unnatural acyl modifications examined in this study increase the magnitude of net negative charge of SOD1 by -1 to -4 formal units; hydrophobicity of the lysine-ε-NH_3^+ is increased from log P ≈ +1.0 to log P ≈ -2.0 (Figure 2.2). Purified, recombinant WT apo-SOD1 were acylated with different anhydrides at various stoichiometric ratios that resulted—through trial and error—in the desired average stoichiometry of ~ 1 acyl group per SOD1 monomer for each type of acyl group (Table 2.1). The average number of acylated lysine (Table 2.1) was determined by integration of mass spectra and weighted averaging of each "rung" (Figure 2.3a-b and Figures 4.1 and

4.2). Stoichiometries ranged from 0.70 acyl groups per monomer for tricarboxybiphenylated SOD1 to 1.45 for tricarboxycyclobutylated SOD1, however, stoichiometries for all other groups ranged fom 0.89 to 1.22 acyl groups per monomer (Table 2.1). The percent of SOD1 that remained unacylated after addition of anhydrides ranged from 10.7 % in tricarboxycyclobutylated samples to 40.9 % in tricarboxybiphenylated samples, however, unacetylated SOD1 ranged from 20.8 % to 34.3 % for all other types of acyl groups (Table 2.1). These stoichiometries were also confirmed with capillary electrophoresis (CE), which detects proteins by absorbance at 214 nm (Figure 2.3c-d). Thus, this study examined how partially acylated SOD1 proteins—mixtures of regioisomers that contain subpopulations of unmodified SOD1—affect aggregation.

Trypsin digestion and tandem mass spectrometry resulted in between 98 % to 100 % sequence coverage and suggested that lysine residues were semi-randomly acylated by each anhydride (Figures 4.3-4.7, and Table 4.1). Generally, the acylation of surface lysine-ε-NH_3^+ in proteins is not purely random *per se* and is not necessarily controlled by the solvent accessibility of a particular lysine (but rather the pK_a of lysine-ε-NH_3^+).[60] The CA and BT modifications did not result in as many measureable regioisomers as other modifications, according to MS/MS (Table 4.1). For example, only K36 and K128 were found to be acylated in SOD1-BT solutions, and only K9 in SOD1-CA. I do not know if these results are artifacts of altered trypsinization or reflect selective acylation. I also detected sporadic acylation at His, Thr, Ser, Cys, and Arg residues with

certain modifications (Table 4.1). The N-terminal α-NH_3^+ group was uniformly acetylated in all protein solutions prior to acylation with anhydrides as the N-terminal α-NH_3^+ group of human SOD1 is properly acetylated when expressed in yeast.

Chemical Structure	Abbreviation	ΔZ_{formal}	ΔZ_{CE}	Log P	Natural/Unnatural
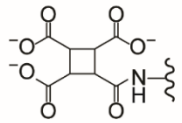	CB	-4	-3.06 ± 0.05	-2.09 ± 0.26	U
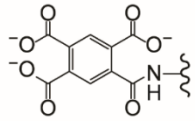	PM	-4	-3.33 ± 0.04	-0.40 ± 0.20	U
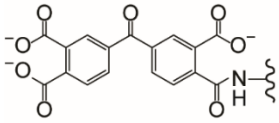	BT	-4	-3.22 ± 0.04	0.74 ± 0.34	U
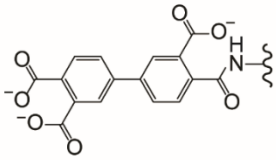	BP	-4	-3.17 ± 0.03	1.01 ± 0.26	U
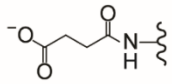	SA	-2	-1.82 ± 0.03	-0.97 ± 0.11	N
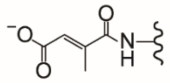	CA	-2	-1.64 ± 0.04	-0.51 ± 0.08	U
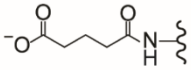	GA	-2	-1.74 ± 0.03	-0.36 ± 0.06	N
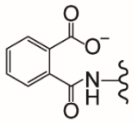	PhA	-2	-1.70 ± 0.04	0.51 ± 0.10	U
	AA	-1	-0.90 ± 0.01	-0.77 ± 0.02	N

Figure 2.2 Natural (N) and unnatural (U) acyl modifications examined in this chapter. ΔZ_{formal} refers to the formal difference in net charge upon acylation of a single lysine-ε-NH_3^+. ΔZ_{CE} refers to the measured difference in net charge upon acylation of a single lysine-ε-NH_3^+ that reflects charge regulation [83, 84] (measured in this chapter using CE). Errors represent the standard deviation (n = 3). Log P represents the calculated hydrophobicity for each acyl group. CB: tricarboxycyclobutyl; PM: pyromellityl; BT: tricarboxybenzophenonyl; BP: tricarboxybiphenyl; SA: succinyl; CA: citraconyl; GA: glutaryl; PhA: phthalyl; AA: acetyl. Errors represent the standard deviation of hydrophobicity calculations from Chemdraw and ChemAxon programs.

Table 2.1 Kinetic parameters of *in vitro* fibrillization of WT apo-SOD1 (100 mM TCEP, 37 °C, pH 7.4) before and after acylation. Data are shown as mean ± standard deviation (SD).

Modification Ac(N)[a]	Lag time ratio[b]	Propagation rate ratio[b]	Maximal ThT fluorescence ratio[b]	Hazard ratio[c]	% unmodified SOD1[d]	ΔT_m (°C)[e]
CB Ac(1.45)	1.37 ± 0.17 (p = 0.09)	0.94 ± 0.30 (p = 0.8)	0.45 ± 0.35 (p = 0.08)	0.48 (p = 0.15)	10.7 %	-3.2
PM Ac(1.22)	1.88 ± 0.08 (p < 0.0001)	0.94 ± 0.07 (p = 0.4)	0.36 ± 0.20 (p < 0.0001)	0.25 (p < 0.0001)	23.2 %	-3.6
BT Ac(0.98)	0.87 ± 0.08 (p = 0.09)	0.84 ± 0.24 (p = 0.5)	0.66 ± 0.18 (p = 0.02)	0.21 (p < 0.0001)	20.8 %	-4.5
BP Ac(0.70)	1.46 ± 0.09 (p = 0.0004)	1.48 ± 0.28 (p = 0.2)	0.35 ± 0.15 (p < 0.0001)	0.47 (p = 0.005)	40.9 %	-4.0
SA Ac(0.90)	0.98 ± 0.06 (p = 0.8)	1.03 ± 0.14 (p = 0.8)	1.25 ± 0.16 (p = 0.2)	2.95 (p = 0.001)	36.2 %	-2.1
CA Ac(1.10)	0.92 ± 0.09 (p = 0.3)	2.06 ± 0.06 (p < 0.0001)	1.37 ± 0.15 (p = 0.04)	3.83 (p < 0.0001)	27.9 %	-5.3
GA Ac(0.98)	0.99 ± 0.09 (p = 0.9)	4.42 ± 0.24 (p = 0.2)	0.61 ± 0.36 (p = 0.2)	1.18 (p = 0.61)	34.3 %	-3.8
PhA Ac(1.07)	1.01 ± 0.13 (p = 0.9)	0.87 ± 0.16 (p = 0.4)	1.18 ± 0.17 (p = 0.3)	1.11 (p = 0.69)	23.9 %	-4.0
AA Ac(1.05)	1.00 ± 0.06 (p = 0.9)	1.04 ± 0.07 (p = 0.6)	1.29 ± 0.15 (p = 0.07)	1.09 (p = 0.72)	29.7 %	-2.2

[a]Average stoichiometry of the acylated protein was calculated as a weighted average of integrated mass spectra. [b]Ratios for all kinetic parameters were calculated as τ_{mod}/τ_{unmod}, k_{mod}/k_{unmod}, and ThT_{mod}/ThT_{unmod}, with p-values calculated with respect to unmodified SOD1 using an unpaired Student's t-test at 95 % confidence interval ($p < 0.05$). [c]Hazard ratios and their corresponding p-values were calculated from the statistical comparison between Kaplan-Meier plots of each modified SOD1 and its corresponding unmodified protein, using Log-Rank (Mantel-Cox) algorithm at 95 % confidence interval ($p < 0.05$). [d]Calculated via integration of deconvoluted mass spectra. [e]Values of ΔT_m are calculated as $T_m(unmod) - T_m(acylated)$.

The formal (predicted) change in net charge of SOD1 imparted by each modification (ΔZ_{formal}) does not accurately reflect the actual change in the net surface charge of SOD1 because of "charge regulation" (the adjustment of pK_a's of functional groups in response to the neutralization of lysine or addition of charged groups).[83, 84] To determine the actual ΔZ for each type of acylation, I performed CE on both unmodified and modified proteins and calculated the ΔZ associated with each acylation using the "protein charge ladder" method[64, 65] (Figure 2.3c-f). To do so, I plotted the electrophoretic mobility of each acyl peak (each "rung") versus the number of acylations (N) associated with that rung (Figure 2.3,e-f). The actual ΔZ (denoted ΔZ_{CE}) was calculated by obtaining the x-intercept, which is equal to the quotient of the net charge of unmodified apo-SOD1 (previously determined to be Z_{CE} = -12.13 ± 0.08, per dimeric protein)[90] and the ΔZ imparted by each modification (Figure 2.3e-f). In the case of tricarboxylic acylating groups (ΔZ_{formal} = -4), I determined that ΔZ_{CE} values ranged from -3.06 ± 0.05 to -3.33 ± 0.04, with the average ΔZ_{CE} = -3.19 ± 0.10 (Table 2.1 and Figure 2.3e).

The ΔZ_{CE} of acylating groups with ΔZ_{formal} = -2 ranged from ΔZ_{CE} = -1.64 ± 0.04 to -1.82 ± 0.03, with the average ΔZ_{CE} = -1.72 ± 0.07 (Figure 2.3f). In these charge ladders, I also observed a secondary "charge ladder", that is, a distinct population of "rungs" in this same ladder. The "rungs" of this minor ladder are designated with asterisks in Figure 2.3d. This distribution of minor "rungs" exhibited a ΔZ_{CE} = -0.87 ± 0.02 per modification (Figure 4.8), which might be due to acylation of partially charged residues (e.g., serine or histidine; Table 4.2).

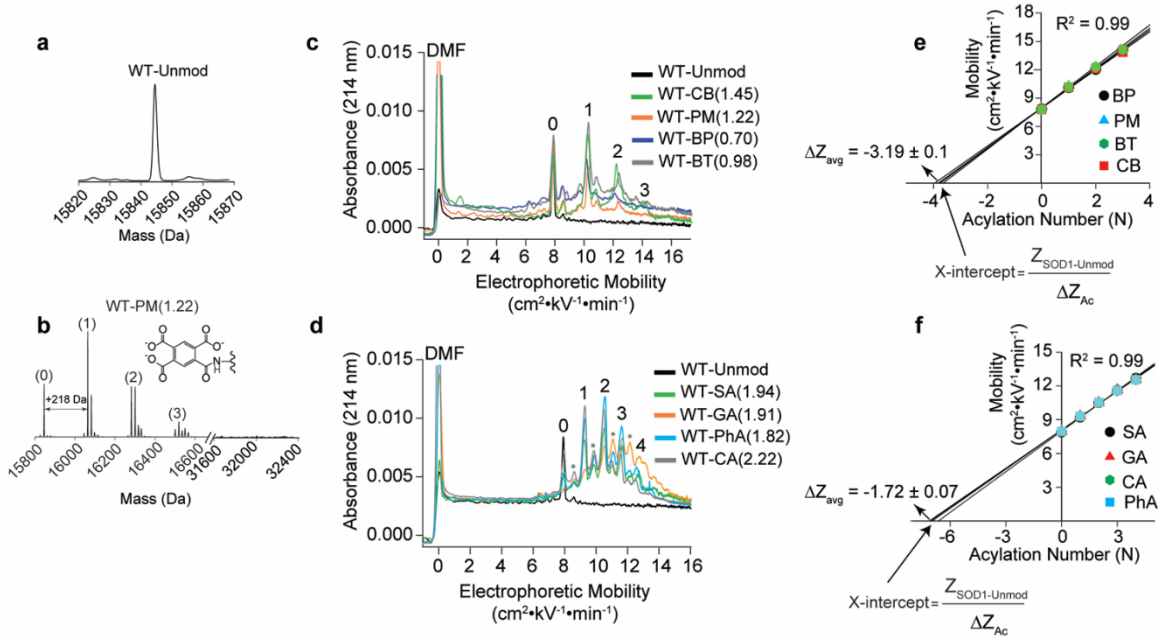

Figure 2.3 Quantifying charge regulation associated with lysine acylation using "protein charge ladders" and CE. Electrospray ionization mass spectra of **(a)** unmodified, and **(b)** pyromellitylated WT apo-SOD1 proteins (denoted as WT-PM(1.22)) used in amyloid assays. Mass spectra for all other acyl modifications are shown in Figures 4.1 and 4.2. CE electropherograms of protein charge ladders of WT apo-SOD1 with **(c)** acyl groups with ΔZ_{formal} = -4, and **(d)** acyl groups with ΔZ_{formal} = -2 for the purpose of measuring ΔZ of acylation. Average values of measured ΔZ (ΔZ_{CE}) for **(e)** all modifications with ΔZ_{formal} = -4, and **(f)** all modifications with ΔZ_{formal} = -2. The number of acyl modifications in CE electropherograms refers to the number of modifications per SOD1 dimer, whereas the number of acyl modifications in mass spectra refers to modifications per monomer (electrospray ionization leads to dissociation of SOD1 dimer). ΔZ_{CE} values in **(e)** and **(f)** are average values for each type of modification. Values of ΔZ_{CE} for each acyl group are listed in Figure 2.2.

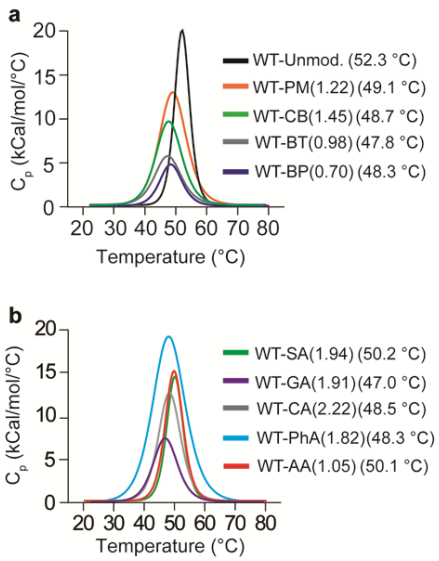

Figure 2.4 Effect of lysine acylation on the thermostability of WT apo-SOD1. DSC thermograms of unmodified and acylated WT apo-SOD1, modified with acyl groups with **(a)** ΔZ_{formal} = -4, and **(b)** $\Delta Z_{formal} \leq$ -2. The number of acyl modifications are listed per monomeric SOD1. Value in the paranthesis next to each SOD1 protein represents the corresponding melting temperature.

To determine the effect of acylating agents on the thermostability of WT apo-SOD1, I performed differential scanning calorimetry (DSC) on unmodified and variably acylated SOD1 proteins (Figure 2.4). All acyl modifications caused a modest decrease in melting temperature (T_m) of WT apo-SOD1, up to $\Delta T_m \sim$ -5 °C (Figure 2.4 and Table 2.1), which is similar to previous analyses of acylated SOD1[54, 90] and bovine carbonic anhydrase II[91] (acylation does not uniformly destabilize proteins, e.g., acetylation increases the thermostability of α-amylase).[92]

Effect of Surface Charge and Hydrophobicity on Fibril Nucleation and Elongation of WT Apo-SOD1 in Microplate Assays:

Similar to our previous studies,[54, 82, 90] I utilized a 96-well microplate-based ThT fluorescence assay (n_{total} = 594) to investigate the effect of acylation on the kinetics of apo-

SOD1 fibrillization. Because the aggregation of SOD1 is stochastic,[87] I performed ≥ 10 replicate assays for each type of acylated protein (i.e., analyzed ≥ 10 iterate wells) and calculated mean rates of fibril nucleation and elongation (Figure 2.5 and Figure 2.6). For each type of acylated protein, I also performed a control ThT-assay on unacylated SOD1 that was exposed to the same concentration of organic solvent as the acylated protein. Trace organic solvent (0.01-0.1 % vol/vol) is initially required to dissolve each anhydride into SOD1 solutions, but is washed out during centrifugal filtration and buffer transfer; nevertheless, I performed separate controls for each acyl group.

Iterate longitudinal plots of ThT fluorescence are shown in Figure 2.5 and Figure 2.6 for unmodified and singly acylated SOD1 proteins. Generally, all modifications with $\Delta Z_{formal} = -4$ diminished the rate of apo-SOD1 fibrillization into ThT-positive fibrils, and/or diminished the maximal fluorescence of fibrils (Figure 2.5a-c). Pyromellitylated SOD1 proteins showed a ~ 64 % decrease in the intensity of ThT fluorescence compared to unmodified proteins (Figure 2.5c). Moreover, pyromellitylated and tricarboxybiphenylated apo-SOD1 underwent amyloid nucleation (into ThT-positive fibrils) at slower rates than unmodified SOD1, whereas tricarboxybenzophenonylated and tricarboxycyclobutylated apo-SOD1 proteins showed no significant difference in lag time compared to unmodified apo-SOD1 ($p = 0.09$; Figure 2.5c and Table 2.1). Pyromellitylation also increased the number of wells that exhibited no apparent increase in ThT fluorescence. The absence of (or decrease in) ThT fluorescence is not definitive proof that a modification inhibited the fibrillization of SOD1. Amyloid fibrils of apo-SOD1 with minimal ThT fluorescence have been reported.[87]

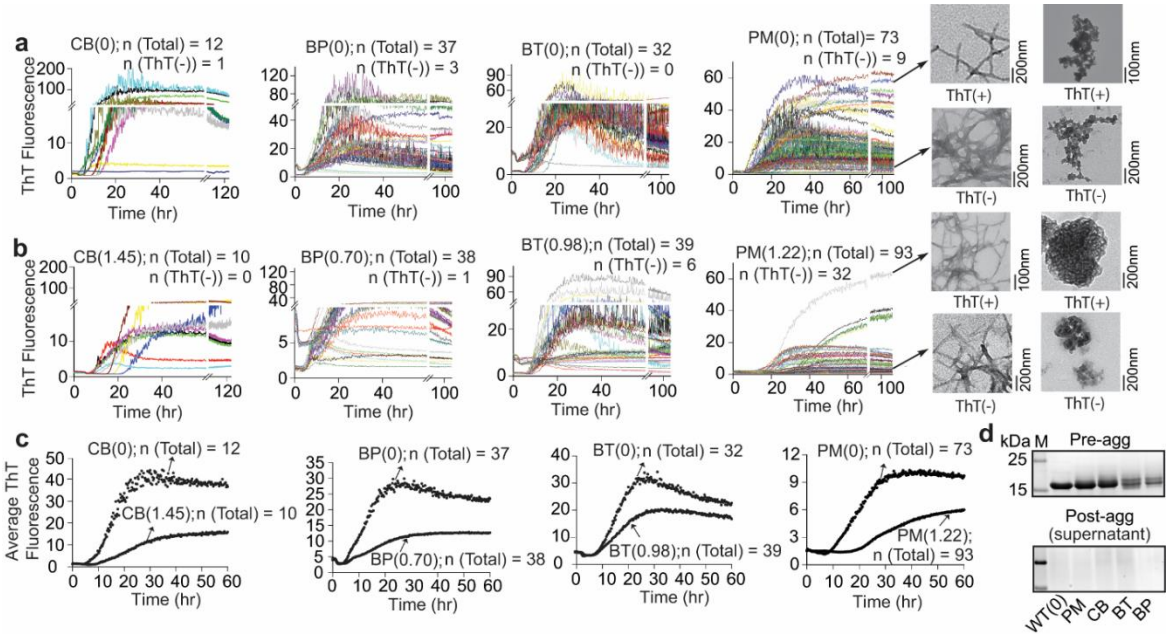

Figure 2.5 Effect of fractional acylation of WT apo-SOD1 with highly charged groups (ΔZ_{formal} = -4) on SOD1's fibrillization into ThT-positive species. (a-b) Replicate ThT fluorescence assays of **(a)** unmodified and **(b)** singly acylated WT apo-SOD1. Replicates that resulted in zero fluorescence (denoted ThT(-)) are also shown. Regions of lag phase are magnified to illustrate stochasticity. Insets show TEM micrographs of fibrillar and amorphous complexes of unmodified and pyromellitylated WT apo-SOD1 after the completion of ThT fibrillization assay (images are representative and include analysis of ThT-negative and ThT-positive wells). The TEM micrographs for all other modified and unmodified SOD1 fibrils are shown in Figure 4-9. **(c)** Average plots of ThT fluorescence for all acylated WT apo-SOD1 and their corresponding unmodified proteins (averaged from **a** and **b**). Replicates that resulted in zero fluorescence (i.e., ThT(-)) were included in average plots. **(d)** SDS-PAGE of SOD1 solutions before starting (upper gel) and after termination of ThT assay (lower gel).

To determine the morphology of acylated SOD1 aggregates, I performed transmission electron microscopy (TEM) on wells that contain both acylated and unmodified SOD1 aggregates (insets in Figure 2.5a-b, and Figure 4.9). All wells that exhibited increases in ThT fluorescence were found with TEM to contain a mixture of fibrillar and amorphous aggregates. The fraction of wells that exhibited no significant increase in ThT fluorescence also contained fibrillar and amorphous complexes, however, a few ThT-negative wells contained only amorphous aggregates (insets in Figure 2.5a-b).

The low level—or complete absence—of ThT fluorescence exhibited by many wells is not caused by incomplete aggregation or variation in concentration of SOD1 proteins. Analysis of the concentration of soluble SOD1 with SDS-PAGE, Bradford assay, and bicinchoninic acid (BCA) assay confirmed that proteins existed at similar concentrations prior to initiating the assay (Figure 2.5d). For example, SDS-PAGE bands for unmodified and singly tricarboxybiphenylated apo-SOD1 proteins had statistically similar intensities (2.8×10^3 a.u. and 3.1×10^3 a.u., respectively; Figure 2.5d, upper panel). Moreover, analysis of sample supernatants at the end of each aggregation assay (with SDS-PAGE) showed that SOD1 completely aggregated into sedimentable species (Figure 2.5d, lower panel). I reiterate that the analysis of ThT-negative wells with TEM also showed the presence of fibrillar SOD1 species (Figure 2.5a-b). Thus, the SOD1 protein self-assembles into ThT-negative fibrils and amorphous complexes, and acylation can increase the probability that SOD1 forms these ThT-negative assemblies.

The observation that polycarboxylic acyl groups promote the formation of fibrils with low (or zero) ThT fluorescence suggests that these acylated fibrils have different structures or gross morphologies than unmodified fibrils. I found that, in general, acylation of apo-SOD1 with modifications possessing $\Delta Z_{formal} = -4$ produced slightly shorter fibrils than unmodified protein (Figure 4.10). For example, singly pyromellitylated SOD1 fibrils were (on average) 17.8 ± 7.5 nm shorter than unmodified fibrils. Tricarboxycyclobutylation had the most pronounced effect on the length of SOD1 fibrils; these fibrils were shorter than unmodified fibrils by 38.7 ± 5.4 nm (Figure 4.10).

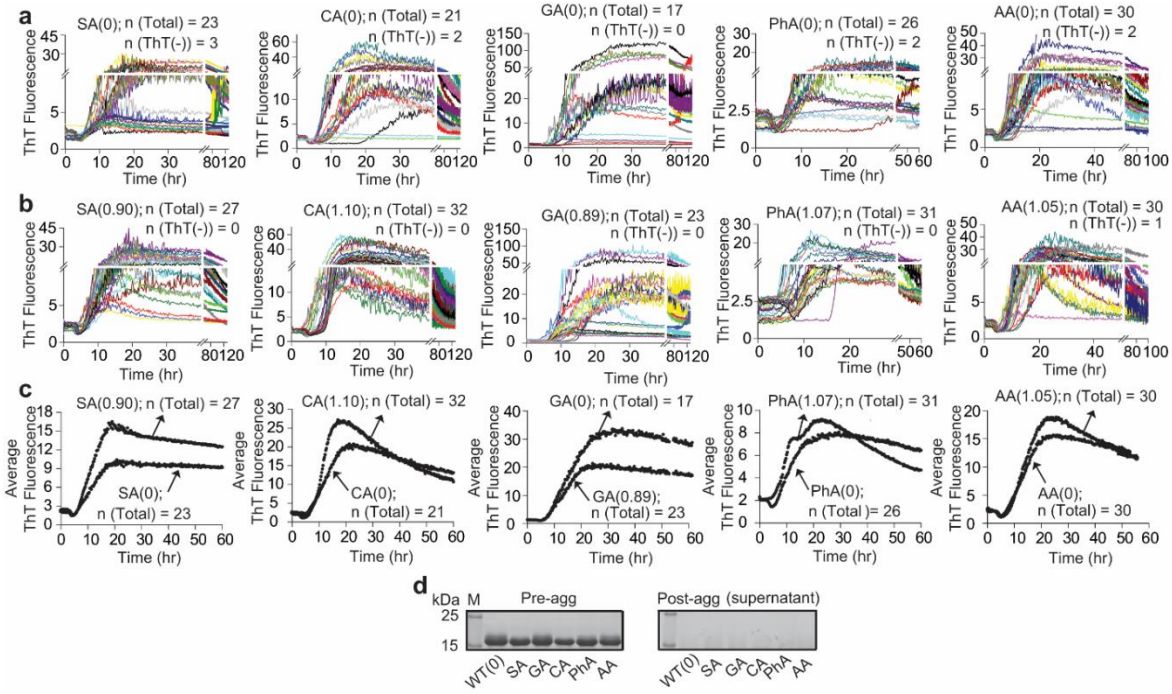

Figure 2.6 Effect of fractional acylation of WT apo-SOD1 with weakly charged groups ($\Delta Z_{formal} \leq -2$) on SOD1's fibrillization into ThT-positive species. (a-b) Replicate ThT fluorescence assays of **(a)** unmodified and **(b)** singly acylated WT apo-SOD1. Replicates that resulted in zero fluorescence (denoted ThT(-)) are also shown. **(c)** Plots of average ThT fluorescence for all unmodified and acylated WT apo-SOD1 (averaged from **a** and **b**). Replicates that resulted in zero fluorescence (i.e., ThT(-)) were included in average plots. **(d)** SDS-PAGE of all apo-SOD1 solutions before starting (left gel) and after termination of ThT assay (right gel). The TEM micrographs for all modified and unmodified SOD1 proteins are shown in Figure 4.11.

In summary, acyl groups that change the net charge of SOD1 by $\Delta Z_{formal} = -4$ generally inhibit the aggregation of SOD1 into ThT-positive fibrils, but promote the formation of shorter fibrils with lower or zero ThT fluorescence. The ability of polycarboxylic modifications such as PM to inhibit fibrillization into ThT-positive species could arise from: (i) increased electrostatic repulsions between SOD1 polypeptides,[54] and/or (ii) aromatic rings that might alter the packing of SOD1 polypeptides into ThT-positive fibrils.

To discern between electrostatic and hydrophobic effects, I modified WT apo-SOD1 with a series of aromatic and non-aromatic moieties that are rotational, aromatic, and electrostatic analogs of one another (GA, SA, PhA, CA, AA; Figure 2.2). ThT fluorescence aggregation assays were then performed on all modified proteins (Figure 2.6). These groups add either one or two formal units of net negative charge ($\Delta Z_{formal} \leq -2$) to apo-SOD1 upon lysine acylation (Figure 2.2 and Figure 4.2). Four of these acylating groups add a linear chain of 2-5 carbons (both saturated and unsaturated) to the protein sequence (Figure 2.2). One acyl group (from phthalic anhydride, PhA) possesses a benzene ring with a single carboxylic acid, thus acting as the steric analog of the pyromellityl group, but with a $\Delta Z_{formal} = -2$ (Figure 2.2). Another group, CA, represents a hydrophobic, rotationally locked (unsaturated) analog of SA.

In general, acyl groups that imparted ≤ -2 units of charge resulted in weaker inhibitory effects on SOD1 fibrillization (into ThT-positive species) compared to acyl groups with $\Delta Z_{formal} = -4$ (Figure 2.6a-c). Despite their structural similarity, phthalylation had a smaller kinetic effect on SOD1 aggregation than pyromellitylation. For example, the difference in fibrillization lag time ($\Delta\tau$) = 11.94 ± 1.54 hr for PM-SOD1 ($\Delta\tau$ is calculated as $\tau_{PM\text{-}SOD1} - \tau_{unmod\text{-}SOD1}$), whereas PhA-SOD1 showed only a minor difference in lag time compared to unmodified SOD1 ($\Delta\tau = 0.07 \pm 0.96$ hr; Figure 2.6a-c). The greater inhibitory effect of pyromellitylation compared to phthalylation ($\Delta\Delta\tau = 10.33 \pm 2.49$ hr) suggests that the 2 additional units of negative charge imparted to SOD1 by the PM modification is the source of PM's inhibitory effect, not the steric bulk added by the benzene ring.

The succinylation of ~ 0.90 lysines in SOD1 did not significantly alter the nucleation or propagation of ThT-positive fibrils (Figure 2.6a-c and Table 2.1). The

citraconylation of ~ 1.10 lysines in SOD1, on the other hand, accelerated the propagation of SOD1 by ~ 2-fold (Figure 2.6a-c and Table 2.1). The citraconyl group—the unsaturated, methylated analog of succinyl moiety—is both rigid and hydrophobic (it is the only modification in this study with a non-rotameric secondary methyl group, Figure 2.2). The isoelectric nature of citraconyl and succinyl groups (Figure 2.2) suggests that the acceleration of aggregation by CA groups is caused by their more rigid, hydrophobic groups, which I presume will drive burial and promote London dispersion interactions.

In addition to extracting standard metrics of aggregation (e.g., lag time, propagation rate) from ThT fluorescence assays, I also analyzed ThT fluorescence data with Kaplan-Meier estimators[93] to determine the probability that acylated SOD1 fibrillized into ThT-positive complexes versus ThT-negative complexes (Figure 2.7). We have recently shown that Kaplan-Meier estimators can be used to determine the probability that ALS-mutant SOD1 will fibrillize (*in vitro*) into ThT-positive species, relative to the probability that WT SOD1 will fibrillize into ThT-positive species. These probabilistic metrics scale better with patient phenotypes (i.e., survival time) than classical aggregation metrics and might be more clinically relevant.[93] Each downward step in the Kaplan-Meier plot (Figure 2.7) indicates the time at which an individual microplate well reached half of its maximum ThT fluorescence. This inflection point (X_0) therefore expresses both the nucleation rate and elongation (secondary nucleation) rate for fibrillizing proteins in each well,[8, 94] according to the formula $X_0 = \tau + 2/k$. In the present study, Kaplan-Meier estimators express the probability of fibrillization of acylated SOD1 into ThT-positive species relative to unacylated SOD1. The principal readout in this analysis is a Hazard ratio (HR) of fibrillization.[87] Hazard ratios > 1 indicate that acylation promoted fibrillization into ThT-

positive species; ratios < 1 demonstrate that modifications inhibited fibrillization into ThT-positive species; ratios = 1 demonstrate no effect.

The Kaplan-Meier plots of SOD1 fibrillization (Figure 2.7) provide a convenient "bird's eye" view of the fibrillization of SOD1 in all individual wells of the microplate, especially wells that did not fibrillize into ThT-positive species. At high TCEP concentrations (i.e., 100 mM), SOD1 does not always form ThT-positive species, that is, iterate wells do not exhibit fluorescence above baseline.[90] These negative effects have not been observed at 10 mM TCEP,[54, 87] and appear due to increasing ionic strength.[95] Kaplan-Meier analyses can account for (and quantify) the iterate assays that showed baseline (zero) ThT fluorescence (i.e., ThT-negative wells).[90]

Fibrillization of individual wells containing apo-SOD1 proteins with acyl modifications that imparted $\Delta Z_{CE} > -3.0$ occurred at a lower probability compared to wells with unmodified protein (Figure 2.7). Hazard ratios were calculated to be < 0.5 for SOD1 proteins modified with all tricarboxylic acyl groups (Figure 2.7). According to Kaplan-Meier analysis, modifications that imparted ≤ 2 formal units of charge led to minimal or no reduction in probability of fibrillization into ThT-positive species and in some cases increased probability of fibrillization (Figure 2.7). Citraconylation of SOD1 resulted in a significantly higher probability of aggregation into ThT-positive fibrils than unmodified SOD1 protein, with a Hazard ratio of 3.83 (Figure 2.7 and Table 2.1); succinylation also increased the probability of fibrillization into ThT-positive species, but to a lesser extent (HR = 2.95; Figure 2.7 and Table 2.1). Acetylation had a negligible effect on fibrillization (HR = 1.09; Figure 2.7 and Table 2.1).

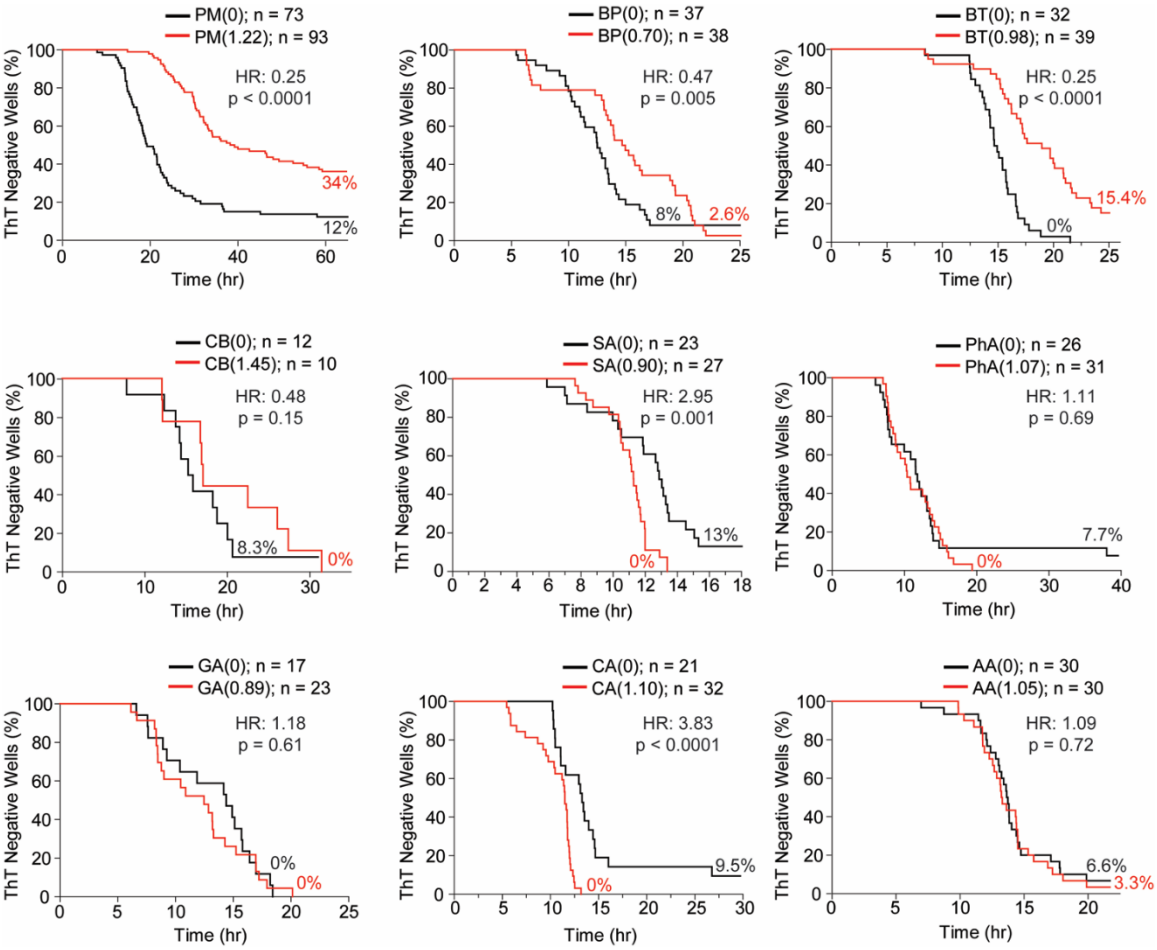

Figure 2.7 Effect of acylation on the probability of SOD1 aggregation studied with Kaplan-Meier estimators. Kaplan-Meier plots of SOD1 aggregation in microplate wells, extracted from ThT fluorescence data in Figure 2.5 and Figure 2.6. Each down-step represents aggregation of a single well into a ThT-positive species. The red trace in each plot represents acylated protein, and black trace represents the unacylated control. Values next to each plot indicate the percent of wells that showed no significant increase in ThT fluorescence over 120 h (i.e., ThT-negative wells). In all plots, p-values were calculated with respect to unmodified SOD1 using Log-Rank (Mantel-Cox) algorithm at 95 % confidence interval ($p < 0.05$). HR: Hazard ratio.

I point out that our previous report on the inhibitory effects of acetylation on SOD1 fibrillization do not necessarily conflict with the results here, as the proteins in the current study contain ~ 1 modification (on average; Table 2.1) per subunit—and a substantial

population of unmodified SOD1—whereas our previous study analyzed SOD1 proteins with up to ~ 6 acetyl modifications per subunit (and an absence of unacylated SOD1).[54]

The number of wells that do not aggregate into ThT-positive species in these microplate assays is, itself, an important metric. For unmodified SOD1 proteins, the percent of wells that failed to form ThT-positive fibrils varied from 0 % to 13 % of all wells (Figure 2.7).

Several different acyl groups increased the percent of wells that failed to form ThT-positive complexes. Pyromellitylation exhibited the largest effect and increased the probability that SOD1 formed ThT-negative complexes from 12 % of wells to 34 % of wells (Figure 2.7).

Effect of Lysine Acylation on the Pathway of SOD1 Aggregation:

The aggregation of SOD1 has been observed to occur stochastically and proceed along amorphous and fibrillar pathways that are in competition (have similar ΔE_a) at pH 7.4, 37 °C.[82] I sought to determine whether acylation alters these pathways of aggregation, e.g., favors non-fibrillar pathways over fibrillar or vice versa. Non-fibrillar aggregates cannot be detected with ThT fluorescence, but are detectable using 1-anilino-8-naphthalenesulfonate (ANS) fluorescence;[82, 95, 96] ANS produces a fluorescent readout when bound to either fibrillar or amorphous aggregates.[96] Microplate-based iterate ANS assays of WT and mutant apo-SOD1 aggregation yield a mixture of sigmoidal and exponential aggregation processes, that is, a minor fraction of iterate microplate wells rapidly form amorphous aggregates (exponential regime), while the majority of wells produce fibrillar aggregates (sigmoidal regime).[82]

Iterate assays of ANS fluorescence were performed on a subset of acylated SOD1 proteins (glutarylated, pyromellitylated, and tricarboxybenzophenonylated apo-SOD1 proteins; Figure 2.8a). Acylated and unacylated apo-SOD1 proteins each exhibited sigmoidal and exponential increases in ANS fluorescence (Figure 2.8a). Wells that exhibit sigmoidal kinetics were found with TEM to contain both fibrillar and amorphous species (Figure 4.12), whereas wells exhibiting exponential kinetics contained only amorphous aggregates (Figure 4.12), consistent with the results from our previous study on unmodified SOD1.[82]

The absolute nucleation rates (lag times) and propagation rates in ANS assays (i.e., the sigmoidal regime) were slower than in ThT assays (Figure 2.8), as I previously observed for unacylated SOD1.[82] This difference might be caused by the inhibitory effects that ANS can have on protein aggregation.[97] Despite these absolute differences in rates as measured by the two assays, the shift in the rate of SOD1 nucleation and propagation upon acylation were statistically similar in both ThT and ANS assays (Figure 2.5, Figure 2.6, and Figure 2.8). For example, single pyromellitylation delayed the nucleation of apo-SOD1 according to ANS and ThT fluorescence assays ($\Delta\tau_{ANS}$ = 9.34 ± 2.05 hr and $\Delta\tau_{ThT}$ = 11.94 ± 1.54 hr), but did not alter SOD1 propagation rate (Δk_{ANS} = 0.01 ± 0.003 hr^{-1} and Δk_{ThT} = 0.02 ± 0.02 hr^{-1}). Glutarylation and tricarboxybenzophenonylation did not significantly change the rate of nucleation or oligomer propagation of SOD1 in either assay (Figure 2.8a-b).

ANS fluorescence suggests that acylation can decrease the probability of fibrillar aggregation and increase the probability of amorphous aggregation. For example, ~ 41 % of wells containing unmodified apo-SOD1 aggregated in the exponential regime, whereas

~ 60 % of wells with glutarylated SOD1 aggregated exponentially (insets in Figure 2.8a). Similar trends were observed in the case of PM- and BT-modified SOD1 (insets in Figure 2.8a). Together, these results suggest that acylation (both natural and unnatural) can weakly favor (in our opinion) one specific SOD1 aggregation pathway over others (in this case amorphous pathways over fibrillar ones). Pyromellitylation imparts at least a fraction of its inhibitory effects on fibrillization via altering the mechanism (pathway) of SOD1 aggregation.

I also analyzed the sigmoidal and exponential aggregation of individual wells with Kaplan-Meier estimators (Figure 2.8c). Pyromellitylation diminished the probability of sigmoidal aggregation (Hazard ratio = 0.11, $p < 0.001$; Figure 8c), but had a statistically insignificant effect on exponential aggregation (Hazard ratio = 0.52, $p = 0.51$; Figure 2.8c). The fibrillization rate of BT-modified apo-SOD1 (i.e., the sigmoidal regime) was statistically similar to unmodified SOD1 (Hazard ratio = 0.74, $p = 0.49$; Figure 2.8c), as was the amorphous aggregation (i.e., exponential regime) of unmodified and BT-modified SOD1 (Hazard ratio = 0.26, $p = 0.13$; Figure 2.8c).

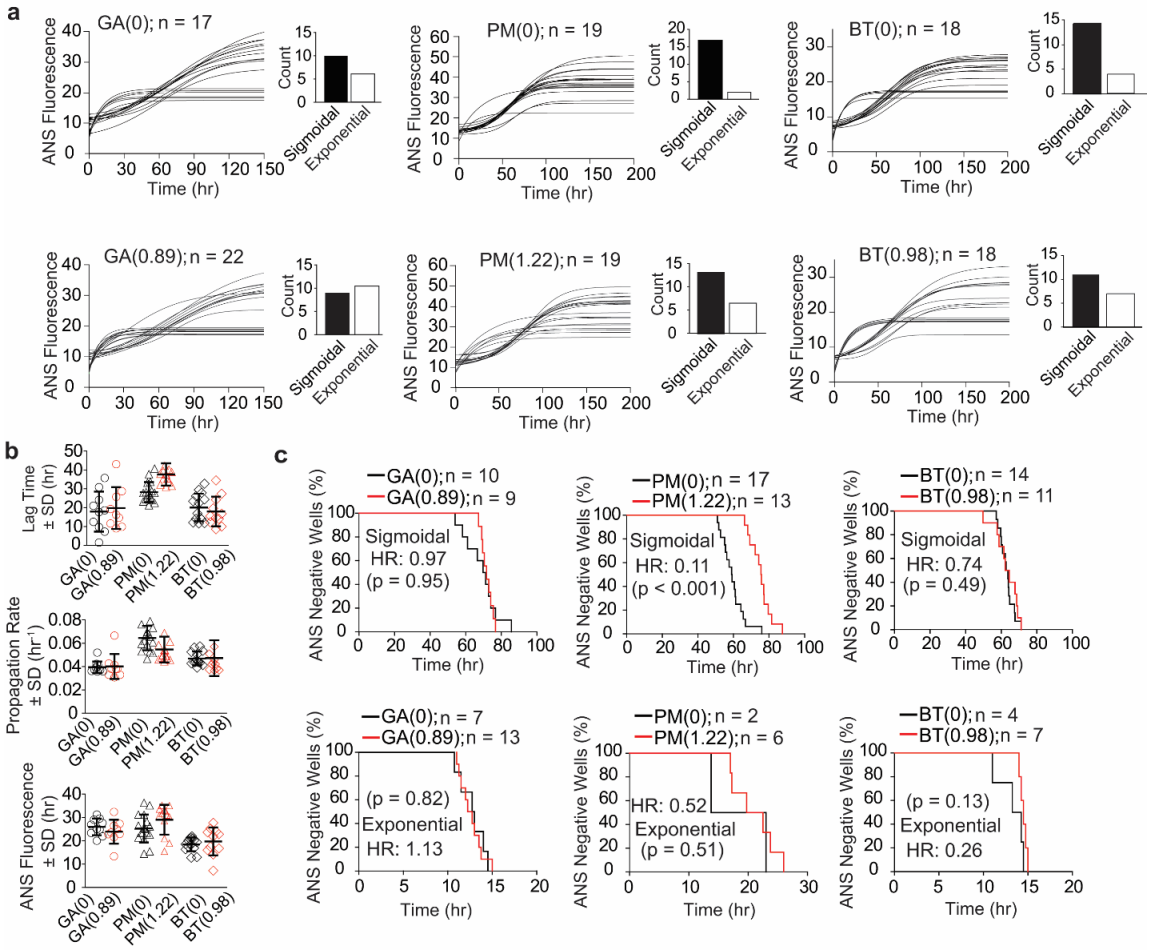

Figure 2.8 Effect of apo-SOD1 acylation on the rate of formation of ANS-positive complexes. (a) Longitudinal plots of ANS fluorescence for WT apo-SOD1 modified with GA(1.91), PM(1.22), and BT(0.98). **(b)** Comparison plots of average lag time, propagation rate, and ThT fluorescence intensity for the aggregation of all modified SOD1 proteins and their corresponding unmodified proteins. Data are extracted from sigmoidal regimes only. **(c)** Kaplan-Meier plots for the aggregation of acylated and unmodified SOD1 proteins extracted from data in **(a)**. Upper and lower plots in **(c)** show the Kaplan-Meier analysis for sigmoidal (top) and exponential (bottom) regimes. In all plots, p-values were calculated with respect to unmodified SOD1 using Log-Rank (Mantel-Cox) algorithm at 95 % confidence interval ($p < 0.05$). HR: Hazard ratio.

Effect of WT SOD1 Acylation on Seeding the Aggregation of G85R SOD1 in Organotypic Mouse Spinal Cord:

In transgenic mice, the co-expression of WT SOD1 protein increases the toxicity of the ALS-mutant SOD1.[98-100] The cause of this synergy is unknown, that is, it is not known if WT SOD1 directly interacts with mutant SOD1 in ways that promote the aggregation of mutant SOD1, or whether WT SOD1 competes with mutant SOD1 for protective factors.[101] Additionally, recent studies have demonstrated the ability for ThT-positive fibrils of recombinant WT SOD1 to induce SOD1 pathology and motor neuron disease (MND) in an *in vivo* model for SOD1 prion-like seeding.[89]

To determine how acylation of SOD1 affected the ability of its aggregates to seed the aggregation of ALS-variant SOD1 in living systems, I added acylated and unacylated aggregates (that formed in microplate wells during ThT assays) to organotypic spinal cord cultures prepared from the G85R-SOD1:YFP (yellow fluorescent protein) transgenic mouse model (Figure 2.9). This model expresses the ALS-linked G85R SOD1 transgene below the threshold level required to develop MND or inclusion pathology and has been used extensively to study the prion-like seeding of oligomeric SOD1 (to seed aggregation in pools of soluble SOD1).[89] These cultures can be kept alive for months[102] and provide a convenient platform for monitoring (using fluorescence microscopy) the ability of exogenously added solutions of aggregated SOD1 to induce formation of fluorescent inclusions from SOD1:YFP, that is endogenously expressed by the mice.[89] The readout in these qualitative assays are large, spatially localized inclusions of G85R-SOD1:YFP.[89] There is a positive correlation between the formation of these SOD1:YFP inclusions and the onset of ALS symptoms in mice.[103]

Spinal cord cultures were prepared from mice at ~ 7 days of age and treated with SOD1 fibrils from wells that produced fibrils with high, low, and zero ThT fluorescence (Figure 2.9). I found that the addition of WT SOD1 fibrils with high ThT fluorescence induced the formation of large, visible inclusions of G85R-SOD1:YFP, regardless of whether the aggregates were composed of acylated (pyromellitylated for these experiments) or unmodified apo-SOD1 (Figure 2.9a-b and e-f). In contrast, the addition of ThT-negative SOD1 fibrils did not induce the formation of G85R-SOD1:YFP inclusions, regardless of whether the aggregates were composed of acylated or unmodified apo-SOD1 (Figure 2.9c-d). When considering that acylation of SOD1 increases the probability that the protein forms a ThT-negative fibril or an amorphous oligomer (Figure 2.5, Figure 2.7, and Figure 2.8), the tissue culture assays suggest that the acylation of WT apo-SOD1 will inhibit its ability to seed further aggregation by driving the acylated protein into a ThT-negative assembly.

The ability of ThT-positive WT SOD1 fibrils to induce inclusions that I observed in this study is in agreement with our recent study[89] (Figure 2.9a-b and e-f). In this chapter, however, I also show that ThT-negative fibrils—produced simultaneously from the same batch of SOD1, in the same microplate—do not induce inclusions of ALS variant SOD1 (Figure 2.9c-d). In the context of ALS, the question of whether acylation of SOD1 would

increase or decrease the toxicity of SOD1 (i.e., accelerate or decelerate the onset or progression of neurodegeneration) depends on whether these large assemblies are protective or toxic.

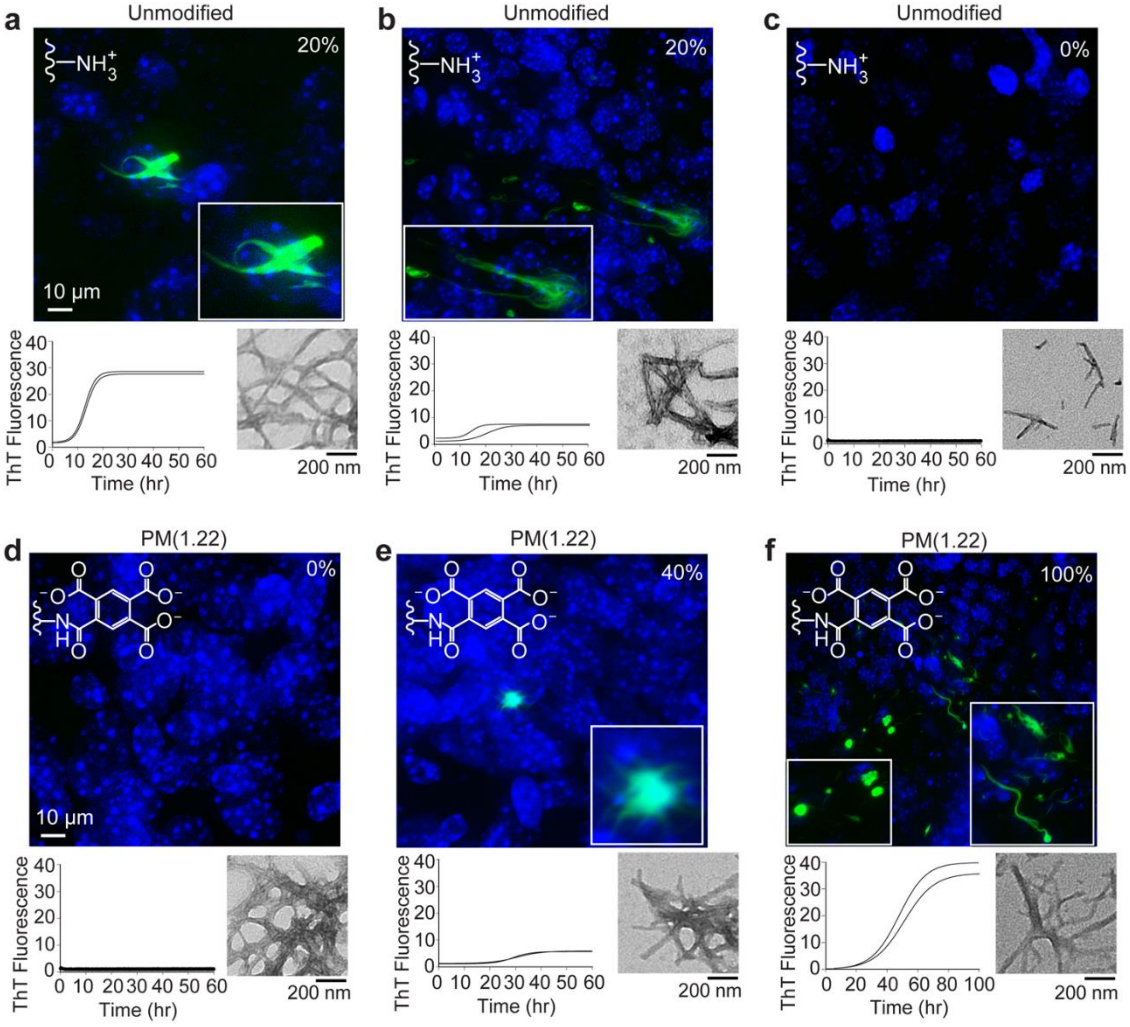

Figure 2.9 Seeding properties of unmodified (a-c) and singly pyromellitylated fibrils (d-f) of WT apo-SOD1 after four-week incubation with organotypic spinal cord cultures from transgenic ALS mice. Representative confocal micrographs of inclusion pathology induced in spinal cord slices from transgenic G85R-SOD1:YFP mice (harvested at ~ 7 days old). Fibrils were grown in microplate wells and added in well-specific manner to organotypic spinal cord as a function of ThT fluorescence: **(a,f)** high fluorescence; **(b,e)** low fluorescence; **(c,d)** zero fluorescence. The value on the top right of each confocal micrograph represents the percentage of replicate spinal cord slices that showed SOD1 inclusions (n = 5). Plots below confocal micrographs show ThT fluorescence traces (left) and TEM micrographs (right) corresponding to the particular microplate well/fibril solution that was added to spinal cord.

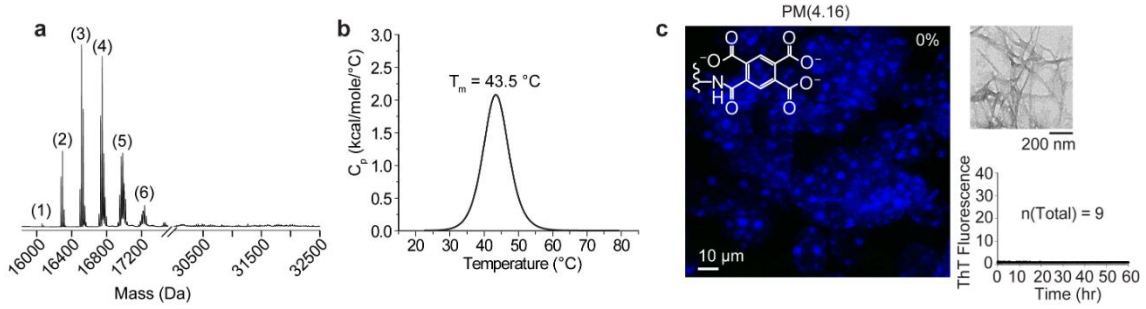

Figure 2.10 Pyromellitylation of 4.16 lysine residues (37 % of all lysines in SOD1) abolishes the ability of SOD1 to form ThT-positive fibrils in microplate assays and inhibits seeding in organotypic spinal cord cultures. (a) Electrospray ionization mass spectrum and **(b)** DSC thermogram of pyromellitylated WT apo-SOD1 (4.16 acylated lysine per monomer). **(c)** Representative confocal micrograph of spinal cord slices from transgenic G85R-SOD1:YFP mice that were exposed with apo-SOD1-PM(4.16) fibril homogenates. The value on the top right of the confocal image represents the percentage of discrete spinal cord slices that showed SOD1 inclusions (n = 5). Plots next to the confocal image show TEM micrograph (upper panel) and ThT fluorescence traces (lower panel) corresponding to the microplate well/fibril solution that was added to spinal cord.

Because pyromellitylation had the greatest inhibitory effect on SOD1 fibrillization, I became interested in determining whether the pyromellitylation of a larger fraction of lysine residues in WT apo-SOD1 protein would completely abolish its ability to form ThT-positive fibrils. To this end, I acylated an average of 4.16 lysines in apo-SOD1 (per monomeric protein) with pyromellitic dianhydride (Figure 2.10a). This higher degree of lysine pyromellitylation did not abolish the tertiary structure of native apo-SOD1, but did destabilize it by ΔT_m = -8.9 °C (Figure 2.10b). After performing 9 replicate ThT fluorescence aggregation assays, I observed that none of the iterate wells containing apo-SOD1-PM (4.16) fibrillized into ThT-positive species (Figure 2.10c). The addition of these ThT-negative fibrils to spinal cord cultures did not seed aggregation (Figure 2.10c), in accordance with our results from singly pyromellitylated SOD1 fibrils that were ThT-

negative. Thus, the pyromellitylation of ~ 4 stoichiometric equivalents of lysine in SOD1 abolishes its ability to seed ALS-variant SOD1 aggregation in organotypic spinal cord cultures of transgenic mice.

I also compared the *in vitro* seeding activity of singly pyromellitylated SOD1 fibrils that were ThT-negative and ThT-positive. These experiments were performed on soluble, unacylated "native" apo-SOD1, by addition of 5 μL of acylated fibril seeds (formed from *in vitro* microplate assays) (Figure 4.13a). The rate of unseeded nucleation of SOD1 fibrils were statistically similar to rate of nucleation of SOD1 fibrils that were seeded with ThT-negative, acylated fibrils ($p = 0.5$; Figure 4.13b). In contrast, SOD1 fibrils nucleated faster (by ~ 5 hr) when seeded with ThT-positive, acylated fibrils compared to unseeded controls ($p = 0.005$; Figure 4.13b). The rate of fibril propagation was faster in the presence of ThT-negative and ThT-positive seeds than in the absence of seeds, however, the increase in propagation rate was more significant for SOD1 oligomers seeded with ThT-positive fibrils ($p = 0.02$ for ThT-negative vs. $p = 0.007$ for ThT-positive; Figure 4.13c). ThT-positive seeds also increased the probability of SOD1 fibrillization according to Kaplan-Meier analysis ($p = 0.04$; Figure 4.13d), whereas no significant changes in probability of fibrillization were observed in the presence of ThT-negative seeds ($p = 0.21$; Figure 4.13d).

In conclusion, the results from our *in vitro* seeding assays support our seeding assays in organotypic spinal cord: ThT-negative SOD1 fibrils lack the ability to seed the fibrillization of soluble apo-SOD1.

Conclusion

This chapter demonstrates that attachment of negatively charged acyl groups to a fraction of lysine residues in SOD1 can inhibit its aggregation into ThT-positive fibrils that lack seeding activity in organotypic spinal cord, while promoting the formation of ThT-negative fibrils and amorphous complexes that lack seeding activity in organotypic spinal cord. These protective effects appear to be electrostatic in nature, that is, they are not caused by increases in native state thermostability and are not caused by steric disruptions to polypeptide packing in fibrils and amorphous complexes. I am hesitant to refer to the seeding activity of ThT-positive SOD1 fibrils, as "prion-like activity". For example, I do not know whether ThT-positive aggregates crossed cell membranes in cultured spinal cord and directly catalyzed the aggregation of intracellular SOD1 proteins, or whether the ThT-positive aggregates merely lurked in extracellular space and aggregated with soluble SOD1 that existed in extracellular space (SOD1 exists in cerebrospinal fluid at nM concentrations).[104]

One limitation of this study is that it did not test the toxicity of acylated SOD1 fibrils, as it is difficult to comprehensively assay the cytotoxicity of SOD1 aggregates among the entire population of motor neurons in organotypic spinal cord slabs. Recently, Eisenberg and coworkers have cultured primary motor neurons (2D cultures derived from embryonic stem cells) to assay the toxicity of ThT-positive SOD1 fibrils and oligomers (ThT-negative aggregates were not reported or studied).[105] The primary motor neurons in this study were assayed 12 hr after incubation with aggregates, which is shorter than the lag phase of the seeded fibrillization processes I measure *in vitro*. These cultured cells and others (e.g., neuroblastoma cells) are viable for only a few days to a maximum of 2 weeks.

Our organotypic spinal cord—a 3D culture, *per se*—is incubated with fibrils for four weeks and the only conventional assay that might be appropriate is the ethidium homodimer-1 assay. This assay requires manual counting of cells on the surface of the tissue slab,[106] i.e., spinal cord cross sections used in our current study are ~ 300 μm thick and the bulk of cells are not observed with microscopy. I do note that in our experience with organotypic spinal cord slabs, substantial toxicity would be directly observed by a change in the spinal cord morphology and a shrinking of the sections over time. None of the fibril preparations, even those that induced SOD1 inclusions, were observed to result in shrinking, suggesting either a low level and/or a slow rate of toxicity. Future studies will be needed to address the issue of fibril toxicity.

Another caveat—perhaps a perceived weakness—of this study is that it generated and analyzed mixtures of acylated and unacylated apo-SOD1 proteins. For example, 10.7 % to 40.9 % of apo-SOD1 remained unacylated in samples used in this study (Table 2.1), and the fraction that was acylated included multiple regioisomers (Tables 4.1-4.2). Thus, this study analyzed the aggregation of mixtures of unmodified and quasi-randomly modified SOD1 proteins. This statistical feature is, however, an asset not a liability. Our results suggest that subpopulations of SOD1 bearing randomly acylated lysine residues can be potent inhibitors of SOD1 self-assembly into ThT-positive fibrils, that is, the acylation of almost any lysine residue in SOD1 can impede its fibrillization into ThT-positive fibrils. Our explanation for this non-specific effect is that acylation increases long-range Coulombic repulsions between SOD1 polypeptides, that is, it does not matter which lysine is acylated because acylation of any of the 11 lysine in SOD1 will increase its net negative charge by ~ 0.9 units and increase electrostatic repulsion of subunits. An interesting finding

of this study deals with the polydispersity of SOD1 and with how polydispersity affects its rate and probability of fibrillization. When a single lysine is randomly acylated in SOD1, a theoretical maximum of 11 regioisomers are generated; when two lysines are acylated, a maximum of 55 regioisomers can be generated (i.e., r = 11!/[N!(11-N)!], where N is the number of acylated lysines for a particular CE rung).[107] Acylation of lysines is of course not entirely random, but is at least partially random according to tandem mass spectrometry (Tables 4.1-4.2). Thus, the sequence homology (monodispersity) of SOD1 chains is diminished to less than 100 % by fractional acylation. How might a decrease in monodispersity affect the rate of formation or free energy of fibrillar SOD1? The threshold level of polydispersity/sequence homology required for two chains to self-assemble into amyloid has not been quantified. I presume that an SOD1 protein with an acetylated K91 (for example) will pack better with another SOD1 protein that possesses an acetylated K91, compared to an SOD1 chain with unacetylated K91. This study suggests that the increase in polydispersity associated with fractional lysine acylation is not a major factor in disfavoring SOD1 fibrillization. For example, pyromellitylated SOD1 proteins have the same approximate polydispersity as tricarboxycyclobutylated SOD1 proteins (according to MS/MS; Table 4.1), yet have divergent effects on fibrillization.

This chapter represents the first systematic determination of how acylation of a protein affects its net surface charge and rate of fibril nucleation and propagation.[108, 109] These data will assist us (and others) in the design of small molecules that electrostatically control the self-assembly of amyloid-like oligomers via acylation.[54, 110] For example, recent studies have shown that the simplest aryl ester, aspirin, can impede the aggregation of multiple proteins linked to neurodegeneration, presumably via acetylation of proteins

(other than aspirin's primary target, cyclooxygenase).[62] Can more complex pharmacons be designed to transfer more electrostatically potent groups than the acetyl group of aspirin ($\Delta Z = -1$)? Our results suggest that single acyl groups can electrostatically disrupt the formation of classical prion-like amyloid assemblies if the acyl group is sufficiently charged. Towards this goal of "drugging Z", we have recently imagined, and are now synthesizing, "ball and chain flail" compounds that contain amyloid binding motifs (the "handle") attached to flexible linkers (the "chain") that are capped with an acylating head group (the "ball"). We hypothesize that these small molecules will selectively acylate amyloid-like oligomers or fibrils and electrostatically disrupt their propagation.

CHAPTER THREE

Glycerolipid Headgroups Control Rate and Mechanism of Superoxide Dismutase-1 Aggregation and Accelerate Fibrillization of Slowly Aggregating Amyotrophic Lateral Sclerosis Mutants

This chapter is published as:
Rasouli S, Abdolvahabi A, Croom CM, Plewman DL, Shi Y, Shaw BF.
Glycerolipid headgroups control rate and mechanism of superoxide dismutase-1 aggregation and accelerate fibrillization of slowly aggregating amyotrophic lateral sclerosis mutants (2018) *ACS Chem Neurosci* .[111]

Abstract

Interactions between superoxide dismutase-1 (SOD1) and lipid membranes might be directly involved in the toxicity and intercellular propagation of aggregated SOD1 in amyotrophic lateral sclerosis (ALS), but the chemical details of lipid-SOD1 interactions and their effects on SOD1 aggregation remain unclear. This chapter determined the rate and mechanism of nucleation of fibrillar apo-SOD1 catalyzed by liposomal surfaces with identical hydrophobic chains ($RCH_2(O_2C_{18}H_{33})_2$), but headgroups of different net charge and hydrophobicity (i.e., $R(CH_2)N^+(CH_3)_3$, $RPO_4^-(CH_2)_2N^+(CH_3)_3$, and RPO_4^-). Under semi-quiescent conditions (within a 96 well microplate, without a gyrating bead), the aggregation of apo-SOD1 into thioflavin-T-positive (ThT(+)) amyloid fibrils did not occur over 120 h in the absence of liposomal surfaces. Anionic liposomes triggered aggregation of apo-SOD1 into ThT(+) amyloid fibrils; cationic liposomes catalyzed fibrillization but at slower rates and across a narrower lipid concentration; zwitterionic liposomes produced non-fibrillar (amorphous) aggregates. The inability of zwitterionic liposomes to catalyze fibrillization and dependence of fibrillization rate on anionic lipid concentration

suggests that membranes catalyze SOD1 fibrillization by a primary nucleation mechanism. Membrane-catalyzed fibrillization was also examined for eight ALS variants of apo-SOD1, including G37R, G93R, D90A, and E100G apo-SOD1 that nucleate slower than or equal to WT SOD1 in lipid-free, non-quiescent amyloid assays. All ALS variants (with one exception) nucleated faster than WT SOD1 in presence of anionic liposomes, wherein the greatest acceleratory effects were observed among variants with lower net negative surface charge (G37R, G93R, D90A, E100G). The exception was H46R apo-SOD1, which did not form ThT(+) fibrils.

Introduction

The aggregation of superoxide dismutase-1 (SOD1) into prion-like oligomers is causally linked to amyotrophic lateral sclerosis (ALS).[112] Some type of interaction—transient or stable—between monomeric or oligomeric SOD1 and cellular or vesicular membranes[42, 47] might occur during the intercellular, prion-like transmission of its oligomers.[113] As with other proteins, membrane surfaces might also be as critical in catalyzing the oligomerization of SOD1 as in mediating the intercellular transmission or toxicity of oligomers.[48, 49] The probability of protein-membrane interactions is presumably higher for proteins such as SOD1 that are localized to mitochondria.[114] Interactions between SOD1 and inner- and outer-mitochondrial membrane surfaces are reported to be involved in SOD1 aggregation[115, 116] *in vivo* and misfolded SOD1 binds mitochondrial membranes.[51]

In general, interactions between cytosolic proteins and surfactants remain the least understood interactions between biological macromolecules.[117-119] For example, do ion-specific processes[120] that might be solvent-mediated dominate interactions,[121] or do long-

range electrostatic interactions that scale with the net charge of protein and lipid surfaces control rates? Is the lipid headgroup—its net charge, hydrophobicity, H-bond donor/acceptor ability, solvation—more crucial than the alkyl chain in catalyzing the formation of amyloid-like oligomers or in facilitating their intercellular transmission?

In this chapter, I determine the rate, mechanism of formation, and morphology of aggregated forms of metal-free (apo) wild-type (WT) human SOD1 in the presence of small unilamellar vesicles (SUVs) composed of identical hydrophobic chains, but headgroups of variable charge i.e., anionic, zwitterionic, and cationic (Scheme 1). The aggregation of eight different ALS variants of apo-SOD1 in the presence of anionic SUVs was also examined.

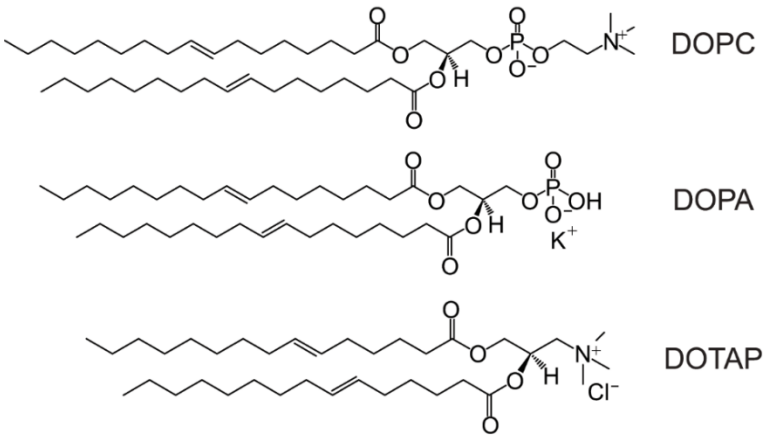

Scheme 3.1 Lipids used to prepare SUVs. DOPC = 1,2-di-(9Z-octadecenoyl)-*sn*-glycero-3-phosphocholine. DOPA = 1,2-di-(9Z-octadecenoyl)-*sn*-glycero-3-phosphate. DOTAP = 1,2-di-(9Z-octadecenoyl)-3-trimethylammonium-propane. Anionic and cationic SUVs were prepared by combining a 1:1 molar ratio of zwitterionic DOPC with anionic DOPA or cationic DOTAP lipids, and are denoted "DOPCA" and "DOTAPC", respectively. Zwitterionic (neutral) SUVs are comprised entirely of DOPC lipids (denoted DOPC).

Because unseeded SOD1 fibrillization is a stochastic process,[55, 122-126] I used high-throughput microplate-based aggregation assays to properly characterize (with statistical significance) the distribution of rates of nucleation and elongation, and used Kaplan-Meier estimators to approximate the probability of fibrillization.[123]

The microplate-based amyloid assays used in this study involve semi-quiescent conditions, that is, minimal agitation without a Teflon bead. I am specifically interested in membranes composed entirely of zwitterionic lipids, and mixed membranes composed of anionic and zwitterionic lipids, or mixtures of cationic and zwitterionic lipids. Motor neuron membranes are primarily composed of zwitterionic lipids (including phosphoethanolamine and phosphatidylcholine); less than 30 % of neuronal membrane lipids have anionic headgroups.[127] Cationic lipids exist at even lower concentrations than anionic lipids (in neuronal membranes), but play a critical role in membrane integrity and permeability.[128] The lipid composition of mitochondrial membranes is somewhat similar to that of the neuronal plasma membrane: zwitterionic phosphoethanolamine and phosphatidylcholine comprise ~ 70 % of total lipids in inner- and outer-mitochondrial membranes.[129] The anionic phospholipid cardiolipin constitutes 16 % of lipids in the inner mitochondrial membrane, and 6 % of lipids in the outer mitochondrial membrane.[20]

This paper also examines how different ALS-SOD1 missense mutations affect the aggregation of SOD1 in the presence of lipid surfaces. The self-assembly of SOD1 into amyloid-like fibrils is sigmoidal (*in vitro*) and involves an initial nucleation step followed by an elongation or propagation step that might involve secondary nucleation (fibril breaking, followed by re-elongation of daughter fibrils).[21] Several ALS-linked SOD1 missense mutations do not increase the rate of amyloid nucleation of apo-SOD1 in non-

quiescent, non-liposomal *in vitro* assays (e.g., G37R, D90A, G93R, E100G).[22] This surprising result is in conflict with prevailing "protein only" amyloid hypotheses, and is also consistent with the need of additional physiological components, membrane surfaces in particular, for promoting aggregation. One ALS variant, H46R apo-SOD1, does not form ThT(+) fibrils during *in vitro* or *ex vivo* assays,[123, 130] but does produce inclusions in mice/rat spinal cord.[131, 132] I wished to determine whether these ALS mutations uniformly accelerate fibrillization, relative to WT SOD1 in the presence of anionic membrane surfaces that are more biologically relevant than the previous standard assays I performed.[123]

The results of this study demonstrate that the surface headgroups of membranes can switch the mechanism of SOD1 aggregation from amorphous to fibrillar pathways. Lipid vesicles that possess a net electrostatic charge (in particular anionic SUVs) trigger the amyloidogenesis of apo-SOD1, whereas zwitterionic vesicles favor the formation of amorphous aggregates. This study also found that anionic lipid membranes promote SOD1 fibrillization through primary nucleation events,[133] i.e., lipid surfaces promote the formation of new nuclei from SOD1 monomers. This study also shows that ALS mutations (almost) uniformly accelerate the nucleation of amyloid-like fibrils of SOD1 in the presence of anionic vesicles. Mutations that lower net charge (eliminate anionic groups and/or introduce cationic groups; G37R, D90A, E100G, G93R) underwent the greatest acceleration of fibril nucleation among anionic vesicles, relative to non-liposomal, non-quiescent assays that employ a Teflon bead.[28] These results suggest that some ALS mutations might promote aggregation by lowering electrostatic repulsion between SOD1 and anionic membrane surfaces. The H46R SOD1 protein did not, however, fibrillize *in*

vitro into ThT(+) or ThT(-) species, which suggests that liposomal assays lack some critical component—perhaps time (months)—required to form the type of H46R SOD1 complexes observed *in vivo*.

Results and Discussion

Characterization of Anionic, Cationic, and Zwitterionic SUVs:

Small unilamellar vesicles were synthesized by combining anionic or cationic lipids with zwitterionic lipids (Scheme 3.1) in a 1:1 molar ratio. Vesicles were characterized with dynamic light scattering (DLS) and transmission electron microscopy (TEM).

According to DLS, the average diameter of synthesized SUVs ranged from 67 ± 1 nm to 87 ± 1 nm (Figure 4.14a-c). Visual analysis of TEM micrographs for each type of SUV (Figure 4.14 a-c) enabled us to estimate the size and lamellarity of synthesized SUVs. Each type of SUV contained ~ 85-90 % unilamellar and ~ 10-15 % multilamellar structures (Figure 4.14d). The average polydispersity was < 10 %. Polydispersity was defined as the ratio of peak width and peak median (i.e., size distributions in Figure 4.14a-c), where polydispersity values between 1-10 % suggest sample homogeneity. Together, these data suggest that the majority of SUVs were unilamellar and fairly monodisperse (Figure 4.14). Aggregation assays in the presence of SUVs were performed at 37 °C, that is, at a temperature which is > 40 °C above the gel-to-fluid transition temperature for each liposome type (T_m(DOPC) = -16.5 °C,[134] T_m(DOPA) = -4 °C,[135] and T_m(DOTAP) = -11.9 °C [136]).

Fibrillization of WT apo-SOD1 Requires Anionic and Cationic SUVs under Semi-quiescent Conditions:

Unless otherwise noted, all proteins examined in this study are demetallated to yield a metal:protein stoichiometry of ≤ 0.04 Cu^{2+} and ≤ 0.08 Zn^{2+} per SOD1 dimer, according to ICP-MS (Table 4.3). The types of microtiter plate-based amyloid assays used in this study were similar to our previous studies,[122] but differed in two key aspects. In this study, I did not use a stirring bead in the microplate well, as in all previous studies. Stirring beads are typically used in SOD1 assays of fibrillization because the fibrillization of apo-SOD1 *in vitro* is a slow process (in the absence of stirring beads and mechanical agitation[124]) and can take days-to-weeks to initiate.[124, 137] I avoided using a bead in the presence of SUVs because I found that gyrating beads disrupted SUVs. The microplate was also agitated at a 6-fold lower rate in this study (60 rpm) compared to our previous study (360 rpm)[122] in order to preserve the integrity of SUVs.

In the absence of SUVs (i.e., [Lipid]:[SOD1] = 0:1) WT apo-SOD1 proteins did not self-assemble into fibrillar structures that are detectable by ThT fluorescence, even after 120 h (Figure 3.1). Instead, TEM analysis showed that SOD1 formed amorphous aggregates in the absence of SUVs (Figure 3.1).

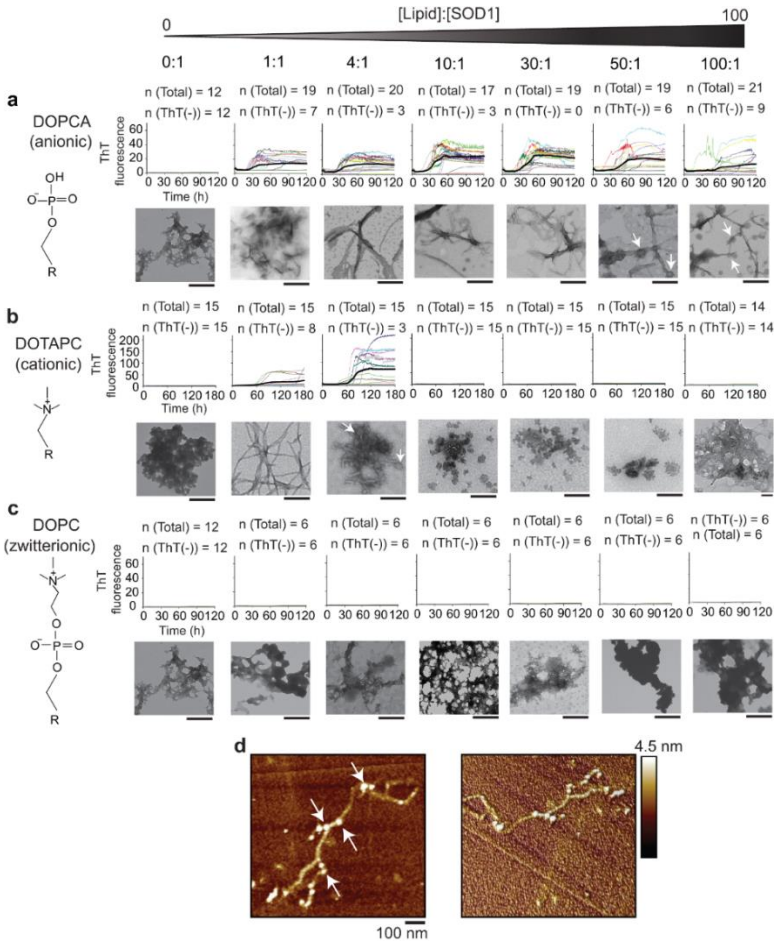

Figure 3.1 Iterate thioflavin-T fluorescence assays of WT apo-SOD1 fibrillization in the presence of anionic, cationic, and zwitterionic liposomes. Replicates of ThT fluorescence from semi-quiescent microplate assays of WT apo-SOD1 fibrillization. Panels represent different ratios of [Lipid]:[SOD1] for **(a)** anionic (DOPCA), **(b)** cationic (DOTAPC), and **(c)** zwitterionic (DOPC) liposomes. The thick black trace in each panel illustrates the average of all replicate data points. Scale bars = 200 nm (except at [Lipid]:[SOD1] = 4:1 and at highest DOTAPC concentration where scale bars = 100 nm and 400 nm, respectively). **(d)** Two-dimensional (left panel) and 3D (right panel) atomic force micrographs of mature WT SOD1 amyloid fibrils interacting with anionic DOPCA SUVs ([Lipid]:[SOD1] = 30:1). White arrows in both TEM and AFM images point to DOPCA SUVs. TEM and AFM were performed on aggregation solutions after the termination of assays. Note: the number of iterate measurements was at least 19 for cationic and anionic liposomes, where higher numbers of iterate measurements were made per availability of protein. Zwitterionic liposomes were repeated at fewer iterations because increases in ThT fluorescence were never observed and statistically significant lag times or elongation rates were therefore not obtainable. Some traces are characterized by a decrease in ThT fluorescence after reaching a maximum intensity. This phenomenon has been observed in several previous reports and is caused by adhesion of macroscopic precipitates of protein to sides of the well (as inferred from manual inspection of wells exhibiting diminished intensity).

I also imaged the binding of fibrillar SOD1 to lipid vesicles. TEM analysis showed that fibrillar SOD1 species interact with anionic liposomes (Figure 3.1a). To image the interactions between SOD1 oligomers and SUVs at higher resolution, I performed atomic force microscopy on mature SOD1 fibrils formed in the presence of DOPCA vesicles. Results obtained from AFM analysis suggest that: (i) liposomes decorate the surface of mature SOD1 fibrils at linear and branched regions, and (ii) SOD1 fibrils interact with small liposomes ($R_H \approx 30$ nm), and not large liposomes (Figure 3.1d). These interactions might represent points of nucleation of protein aggregates upon biological membranes. In so much as the liposomes studied in this paper are structurally similar to vesicles and exosomes formed *in vivo*, the lipid portion of liposome-bound fibrils also represent potential points of fusion with cellular and organellar membranes, which could facilitate the cellular entry or exiting of misfolded SOD1.

AFM imaging showed that small liposomes (~ 30 nm) interact with fibrillar SOD1 (in addition to the 100 nm liposomes observed with TEM). Previous studies have shown that small liposomes ($\leq$ 50 nm) trigger the amyloid nucleation of α-synuclein and $A\beta_{1\text{-}40}$ more significantly than large liposomes (> 50 nm).[36, 37] This effect was explained by the higher water penetration and solvent exposure of hydrophobic regions in small vesicles.[38, 39]

Anionic and cationic SUVs promoted the fibrillization of WT apo-SOD1, however, the range of concentration that triggered fibrillization—and the upper concentration of lipid where fibrillization was inhibited—was higher for anionic than cationic liposomes (Figure 3.1a-b and Figure 3.2a-b). Fibrillization occurred across a wider range of [Lipid]:[SOD1] for anionic (DOPCA) lipids—from 1:1 to 100:1—compared to cationic (DOTAPC) lipids,

wherein fibrillization only occurred from 1:1 to 4:1 (Figure 3.1a-b and Figure 3.2b). Fibrillization was not observed for purely zwitterionic lipids (Figure 3.1c and Figure 3.2c). Increasing [DOPCA]:[SOD1] ratios up to 50:1 increased the maximal ThT fluorescence (Figure 3.2d), increased the lag time, and decreased the propagation rate of SOD1 aggregation (Figure 3.2e-f). A similar trend was observed in the case of cationic SUVs. For example, increasing [Lipid]:[SOD1] up to 4:1 led to faster fibrillization and higher maximal fluorescence (Figure 3.2a). Higher concentrations of cationic SUVs (e.g., [Lipid]:[SOD1] = 10:1) did not promote SOD1 aggregation (Figure 3.2b) and produced predominantly amorphous species (Figure 3.1b).

Zwitterionic Vesicles Promote Non-fibrillar SOD1 Aggregation:

The inability of zwitterionic DOPC liposomes to trigger the fibrillization of SOD1 (Figure 3.1c and Figure 3.2c) has been observed for other toxic amyloidogenic proteins (e.g., human islet amyloid polypeptide, hIAPP).[138] The morphology of SOD1/DOPC solutions was observed with TEM in order to verify that the absence of ThT fluorescence was caused by the absence of fibrillar species (and not a false negative result, for example, caused by ThT-lipid interactions that quench ThT fluorescence[139]). TEM micrographs of SOD1/DOPC solutions showed amorphous species across all DOPC concentrations (Figure 3.1c). These results demonstrate that the ability of vesicles to accelerate fibrillization is highly sensitive to the functional groups present on the lipid headgroups of the vesicle. For example, zwitterionic and cationic lipids that I used contain the same terminal, cationic amine group, and the only difference between the zwitterionic and cationic lipids is the presence of a phosphate ester in the zwitterionic lipid (Scheme 3.1).

Higher Lipid Concentrations Decrease the Probability of SOD1 Fibrillization:

Although data presented in Figure 3.2 suggest that increasing ratios of DOPCA:SOD1 resulted in increased lag time and decreased propagation rates, the statistical significance of some these correlations is low (see p-values in Figure 3.2). This low significance persists in part because many wells (10-20 %) failed to aggregate (i.e., flat lines or ThT-negative wells) and were therefore excluded from analysis. To account for these ThT-negative wells and to express SOD1 fibrillization into ThT-positive species with greater statistical significance—that takes into account stochastic nucleation processes that sometimes do not result in amyloid fibrils[122]—I also expressed the effect of lipid concentration on SOD1 fibrillization in probabilistic terms using Kaplan-Meier estimators (Figure 3.2a-b).[55, 123]

We recently demonstrated that Kaplan-Meier estimators can be useful in quantifying the probability of stochastic aggregation in the form of a Hazard ratio of aggregation. We hypothesize that the probability of SOD1 aggregation might be a more physiologically relevant expression of rates of aggregation *in vivo*—where aggregation only needs to occur in an isolated population of cells and propagate to neighboring cells—compared to classical kinetic metrics such as mean lag time or propagation rate.[123] For some ALS variants of SOD1, Hazard ratios of fibrillization in a microplate equal Hazard ratios of patient survival.[123]

To construct the Kaplan-Meier plots (Figure 3.2g) an "event" was defined as the point in time when an individual microplate well containing SOD1 solution had reached 50 % of its maximum ThT fluorescence (t_0 in Equation 3.1). Control wells (i.e., [Lipid] = 0 mM) did not show ThT fluorescence throughout the entire time course of the experiment,

and therefore no aggregation "event" occurred (gray horizontal line in Figure 3.2g). The probability of SOD1 aggregation at each concentration of DOPCA was expressed as a Hazard ratio, relative to that of the wells with [Lipid]:[SOD1] = 1:1 (Figure 3.2h). In other words, the computed Hazard ratios in Figure 3.2h reflect the probability that SOD1/SUV mixtures will aggregate relative to the probability of aggregation at [Lipid]:[SOD1] = 1:1. Hazard ratios > 1 demonstrate a greater probability of fibrillization at that ratio, relative to [Lipid]:[SOD1] = 1:1; Hazard ratios < 1 demonstrate a lower probability. The Hazard ratios of SOD1 fibrillization at different DOPCA concentrations suggest that maximal SOD1 aggregation occurs at [Lipid]:[SOD1] = 30:1, and that higher DOPCA concentrations (e.g., [Lipid]:[SOD1] = 100:1) diminish the probability of SOD1 aggregation (Figure 3.2h). In our opinion, Kaplan-Meier estimators provide a more statistically reliable (and simpler) expression of the effect of lipid concentration on the nucleation and elongation of apo-SOD1 fibrils than classical metrics such as mean lag time.

Mechanisms of Lipid-catalyzed Fibrillization of Apo-SOD1:

There are two general mechanisms by which cationic and anionic liposomes might accelerate WT apo-SOD1 fibrillization. One is primary nucleation, wherein liposomes are somehow accelerating the formation of an oligomer nucleus from monomeric SOD1. The second mechanism is secondary nucleation, wherein SUVs directly cause the fragmentation of an oligomer or fibril, at which point two or more nuclei are produced from oligomers or fibrils. For example, fragmentation of fibrils would produce 2-fold more propagating ends per break. This type of fragmentation might be caused by shear forces between liposomes, similar to how the shear forces of gyrating beads of increasing mass produce shorter fibrils at faster elongation rates.[124]

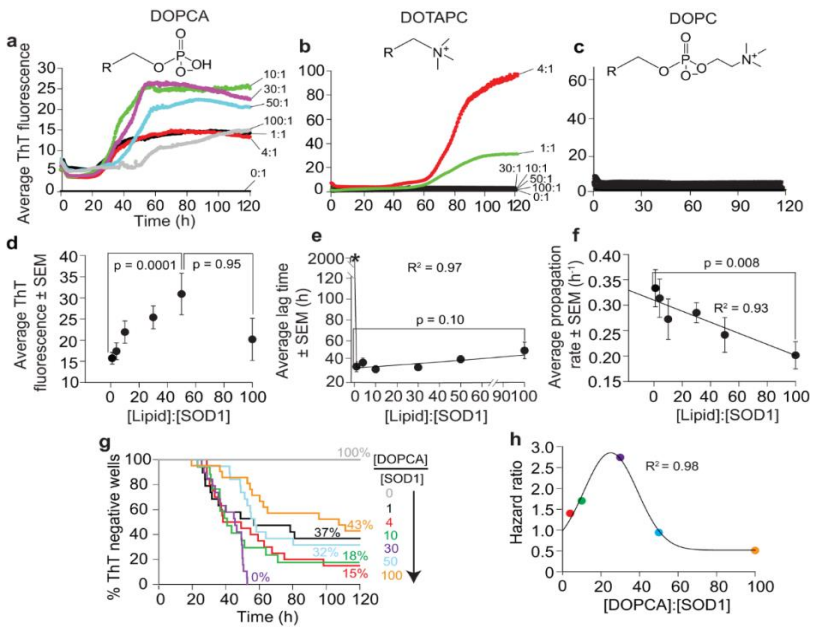

Figure 3.2 Average ThT fluorescence of WT apo-SOD1 as a function of [Lipid]:[SOD1] for **(a)** anionic, **(b)** cationic, and **(c)** zwitterionic liposomes. Each plot is an average of data points from plots in Figure 3.1 Plots of **(d)** average ThT fluorescence intensity, **(e)** average lag time, and **(f)** average propagation rate versus increasing [Lipid]:[SOD1] ratios for the aggregation of WT apo-SOD1 in the presence of anionic DOPCA liposomes. Error bars appear smaller than expected from stochastic aggregation (as inferred from ThT traces in Figure 3.1a), because they represent standard error of the mean (SEM), not standard deviation. The first data point in each plot is not [Lipid]:[SOD1] = 0:1, but rather [Lipid]:[SOD1] = 1:1. ThT(+) fibrils do not form at [Lipid]:[SOD1] = 0:1. Asterisk in the middle panel denotes artificial data point added for purpose of fitting, as no aggregation/lag time could be observed for SOD1 in absence of lipid, but will presumably occur at some time point outside experimental time scale. **(g)** Kaplan-Meier plots of WT apo-SOD1 aggregation into ThT(+) species in the presence of increasing concentrations of DOPCA liposomes. . Values next to each plot indicate the percentage of wells that showed no increase in ThT fluorescence over experimental time course (i.e., ThT(-) wells). **(h)** Plot of Hazard ratio at each lipid concentration (calculated with respect to data from [Lipid]:[SOD1] = 1:1) versus increasing concentrations of lipids in DOPCA liposomes.

The strongest support for a primary nucleation mechanism for lipid-catalyzed SOD1 fibrillization is the inability of zwitterionic SUVs to promote SOD1 fibrillization. This result suggests that shear forces (generated by liposomes) are not dominant in triggering fibrillization, as shear forces would be generated by zwitterionic liposomes, as well as anionic and cationic liposomes.

The dependence of Hazard ratio (and fibril lag time and propagation rate, albeit with moderate statistical significant) on anionic lipid concentration that we observed—the increase in aggregation probability with increasing lipid concentration, followed by a decrease in aggregation at higher concentrations (Figure 3.2)—provides additional support for a primary nucleation mechanism.[49] In this mechanism, SOD1 binds to the liposome and this interaction alters the structure of apo-SOD1 in a way that accelerates amyloid nucleation. Higher liposome concentrations lead to higher lag times and lower elongation rates because of a decrease in the concentration of free monomeric SOD1, per its binding to liposomes and sequestering of bound SOD1 to myriad liposomes (this mechanism is illustrated at the end of this chapter, Fig 3.7).

Primary nucleation mechanisms have been observed for the liposome-induced fibrillization of α-synuclein.[49] If liposomes were accelerating amyloid formation by a secondary nucleation pathway, then higher liposome concentrations would not necessarily affect nucleation rates and would result in faster elongation/propagation.

Structural Integrity of Lipid Vesicles During Assay:

I suspected that lipid vesicles in the aggregation solution might disassemble or partially monomerize due to (i) local shear forces generated upon agitating the plate at 60 rpm; and (ii) the presence of large SOD1 aggregates. To test this possibility, I centrifuged solutions at the end of the aggregation assays at high speed (13,000 × g) for both DOPCA and DOPC samples. Supernatants were collected and UV-vis spectroscopy was performed to measure the total concentration of lipids in the supernatant. As shown in Figure 4.15, no statistical difference was observed between lipid concentrations for control solutions (i.e.,

[SOD1] = 0) and aggregated soluions ([SOD1] = 30 μM). These data demonstrate that disintegration of vesicles was minimal during the course of assay.

Strong Binding of Native and Fibrillar WT apo-SOD1 to Anionic DOPCA SUVs:

The effect of headgroup charge on the pathway of SOD1 aggregation raises a few immediate questions. Does apo-SOD1 need to bind tightly to a liposome in order to fibrillize? Is SOD1 *not* fibrillizing in the presence of zwitterionic liposomes because it is not binding zwitterionic liposomes or because it binds in a particular way that does not promote fibrillization? To begin to answer these questions, we used a filter-trap assay to investigate the binding of native SOD1 to SUVs prior to fibrillization (Figure 3.3). In filter-trap assays, the pores of the filter (10 nm in diameter, i.e., 100-kDa molecular weight cut-off) are smaller than the size of liposomes, but larger than the size of monomeric or dimeric SOD1 (hydrodynamic radius, $R_H \approx 2$ nm for dimeric SOD1, according to DLS). SOD1 proteins were incubated with all three types of liposomes at two different ratios: [Lipid]:[SOD1] = 100:1 and 4:1. Incubation time varied between 0.25 to 2.0 h (i.e., before stochastic nucleation and elongation, which occurs across a range of 10-100 h, Figure 3.1a). SDS-PAGE was performed on the effluent of each centrifugal washing cycle, which will contain unbound SOD1, and on the solution retained by the filter after the last of seven washing cycles (i.e., liposome-bound and/or aggregated SOD1). The concentration of SOD1 decreased in effluents after each washing cycle (Figure 3.3).

At [Lipid]:[SOD1] = 4:1, ~ 20 % of SOD1 bound to both anionic DOPCA and cationic DOTAPC liposomes with a slightly greater affinity for DOTAPC liposomes (~ 16 % binding for DOPCA and ~ 22 % binding for DOTAPC; Figure 3.3a-b). There was no detectable amount of SOD1 bound to zwitterionic DOPC liposomes (Figure 3.3a-b).

At [Lipid]:[SOD1] = 100:1, SOD1 was retained to a greater degree by the anionic DOPCA vesicles (~ 76 % binding, compared to ~ 14 % binding to cationic liposomes, and ~ 0 % binding to zwitterionic liposomes) after seven cycles of washing, demonstrating that SOD1 binds strongly to anionic liposomes (Figure 3.3c-d). A lower amount of SOD1 is retained in cationic DOTAPC samples, however, this amount is similar in quantity to the retained samples at [Lipid]:[SOD1] = 4:1 (Figure 3.3d). Thus, increasing the [DOPCA]:[SOD1] from 4:1 to 100:1 increases binding, whereas increasing [DOTAPC]:[SOD1] from 4:1 to 100:1 does not result in greater binding.

To investigate the kinetics of SOD1 binding to SUVs, I performed filter-trap binding assays with DOPCA/SOD1 at different incubation times (i.e., 0.25 h, 0.5 h, and 1.0 h; [Lipid]:[SOD1] = 100:1). As shown in Figure 3.3e-f, SOD1 binding to DOPCA SUVs reaches apparent equilibrium by 0.25 h, as inferred from almost identical SDS-PAGE band intensities for DOPCA/SOD1 samples at different incubation times.

Why does the anionic WT apo-SOD1 protein ($Z_{apo\text{-}SOD1}$ = -12.13 ± 0.08 units at pH 7.4, per dimer[64]) bind more strongly to anionic liposome surfaces than cationic surfaces at [Lipid]:[SOD1] = 100:1? Why does SOD1 not bind to zwitterionic surfaces? The results in Figure 3.3 suggest that long-range electrostatic (Coulombic) interactions between net negatively charged SOD1 and net positively charged (or neutral or negative) surfaces cannot entirely account for binding affinities. The observed effects are the reverse of what I would expect. Moreover, hydrophobic interactions between SOD1 and methyl groups of choline are not apparently strong enough to facilitate binding to zwitterionic lipids. One explanation for this electrostatically non-intuitive effect is that local patterns of cationic charge on the surface of SOD1 interact with anionic phosphate headgroups more favorably

than local anionic surfaces of SOD1 interact with cationic and hydrophobic choline headgroups (or zwitterionic and hydrophobic choline headgroups). Thus, the most reasonable set of explanations that I can find for these effects are: (i) the first residues on proteins to interact with lipid surfaces are cationic (Arg and Lys), due to the greater length of these residues (compared to Asp and Glu[140]); and (ii) ion-specific solvation effects at liposomal surfaces.[141]

Regarding solvation and ion-specific effects, phosphate residues on the surface of DOPCA vesicles have been observed by Song et al. to be more strongly hydrated than choline surfaces of DOTAPC and DOPC vesicles.[141] The structural rigidity of water and hydration levels at headgroups of DOTAPC, DOPC, and DOPCA vesicles were previously approximated by measuring rates of water diffusion across the membrane[141] (via Overhauser dynamic nuclear polarization on water protons coupled to nitroxide paramagnetic spin labels on the surface of liposomes[141, 142]). If the binding of SOD1 to liposomes is solvent-mediated, then solvent will bridge interactions between SOD1 and lipid surfaces (lowering the transition state energy of binding). I do not know, however, the degree to which these interactions are solvent-mediated. Elucidating mechanisms of solvent-mediated interactions between chemically asymmetric surfaces is an active area of research.[143]

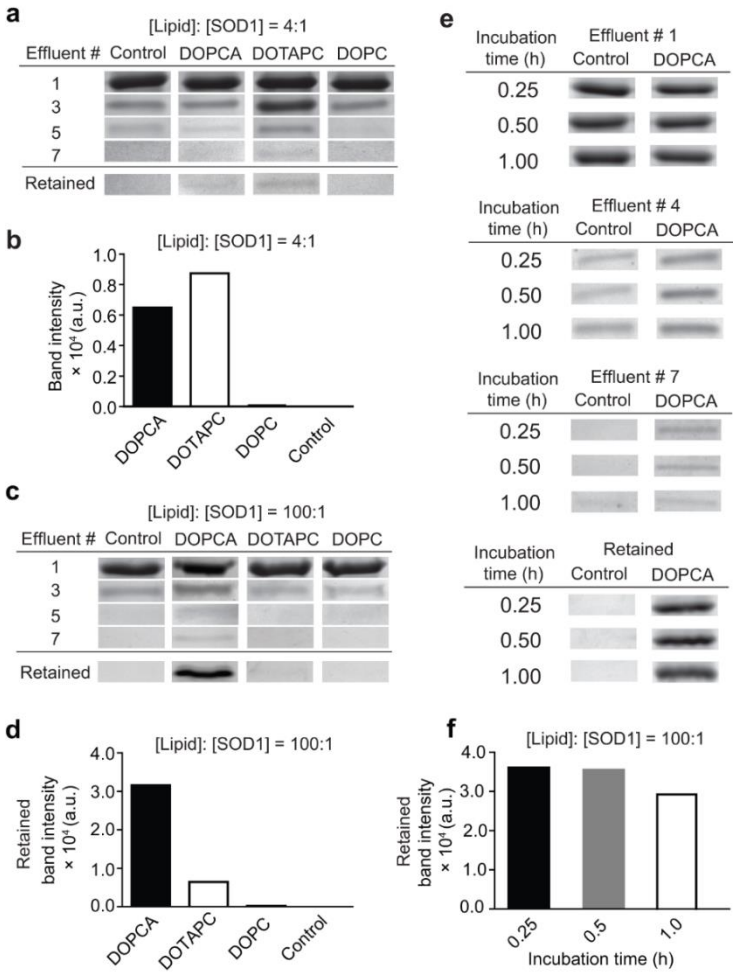

Figure 3.3 Filter-trap assays of binding of soluble WT apo-SOD1 to liposomes before fibrillization. SDS-PAGE analysis of effluent (soluble SOD1 unbound to liposome) and retained (liposome-bound or oligomeric apo-SOD1) samples, and densitometry analysis for **(a-b)** [Lipid]:[SOD1] = 4:1, and **(c-d)** [Lipid]:[SOD1] = 100:1. Assays were performed after 2 h incubation of SOD1 with liposomes. **(e-f)** Kinetics of SOD1 binding to anionic DOPCA SUVs using filter-trap assay at 0.25 h, 0.5 h, and 1 h incubation times. SDS-PAGE was used to analyze the amount of SOD1 protein in effluent (unbound SOD1) and retained (liposome-bound SOD1) samples from binding assays. Bar graphs show the comparison of band intensities for SOD1 bound to DOPCA SUVs (taken from retained samples) as a function of incubation time (the time that native SOD1 was incubated with liposomes). Densitometry analyses were performed using ImageJ® software.

Effect of Anionic Liposomes on Aggregation of Holo-SOD1:

In order to determine if liposomes could catalyze the fibrillization of fully metallated SOD1—which does not fibrillize in non-quiescent unseeded *in vitro* assays[72]—I incubated anionic liposomes with WT Cu_2, Zn_2 SOD1. The fully metallated SOD1 that I used was isolated from human erythrocytes and was purchased from Sigma Aldrich. Liposomes failed to catalyze the fibrillization of metallated SOD1, under a variety of conditions that involved the presence and absence of EDTA and reducing agents (Figure 3.4). A fraction of wells did undergo small sigmoidal and exponential increases in ThT fluorescence, but the intensity was so low, relative to samples of fibrillized WT apo-SOD1, that I consider the well to not have undergone aggregation (see insets in Figure 3.4).

Moreover, TEM analysis showed that holo-SOD1 did not form fibrillar species in the presence (or absence) of anionic DOPCA liposomes, even in wells that showed small increases in ThT fluorescence (Figure 3.4, insets). SDS-PAGE analysis of the supernatant of wells containing holo-SOD1 proteins also showed that these proteins remained soluble and did not aggregate (Figure 3.4).

It is generally accepted that the highly thermostable holo-SOD1 protein will not readily nucleate into amyloid or form aggregates when Cu^{2+} and Zn^{2+} are properly coordinated at the active site and the disulfide bond of each subunit is intact.[53-55] Our results suggest that this rule holds true in the presence of lipid surfaces. We do not know, however, whether the metals prevent aggregation by the presence of coordinate covalent bonds *per se*, that is, by increasing the structural rigidity of the protein, or rather by inhibiting the

reduction of the disulfide bond.[54] The presence of the disulfide bond has been reported to be more critical in preventing fibrillization into amyloid, than the coordination of Zn^{2+} (but not necessarily Cu^{2+}).[56, 57]

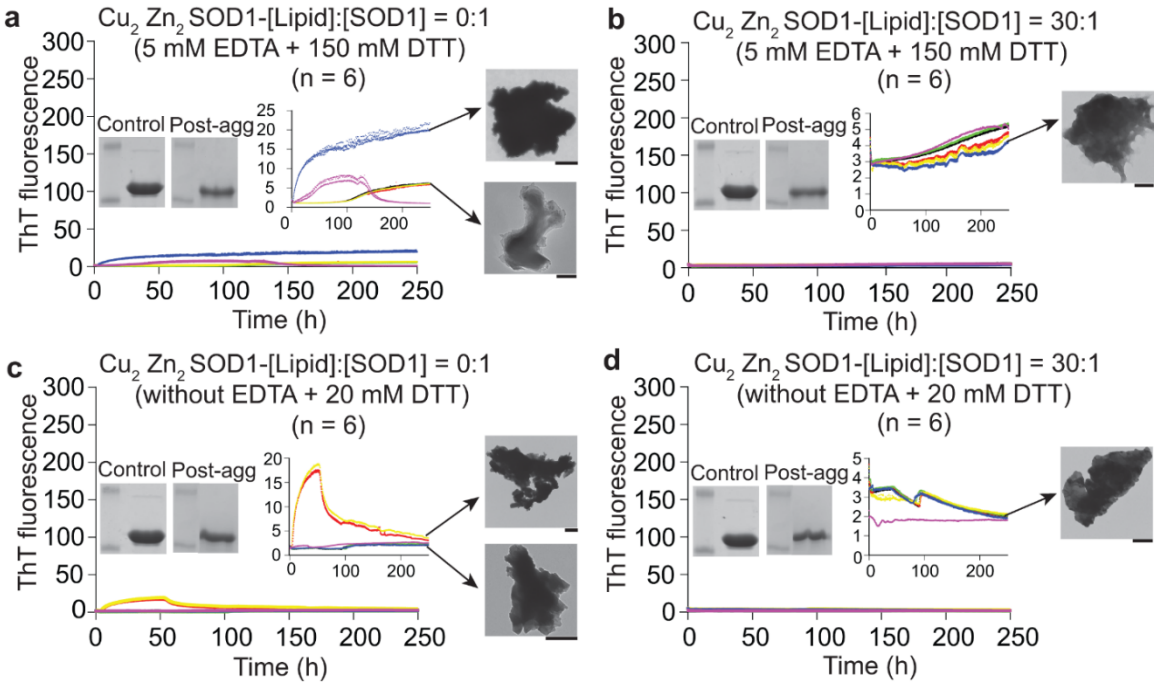

Figure 3.4 Fully metallated SOD1 does not fibrillize into ThT(+) species in the absence or presence of DOPCA liposomes. Replicate plots of ThT fluorescence for the aggregation of holo-SOD1 in the absence (left) and presence (right) of DOPCA liposomes in **(a-b)** 5 mM EDTA/150 mM DTT, and **(c-d)** 0 mM EDTA/20 mM DTT. Holo-SOD1 remained soluble during the course of aggregation assay, but a fraction aggregated into amorphous species under all conditions, according to TEM. Scale bar = 200 nm in all micrographs. Inset SDS-PAGE gels show the presence of soluble protein after the termination of aggregation assays (i.e., post-agg). SDS-PAGE gel of soluble WT apo-SOD1 from a 30 µM stock solution is shown as a control in each panel.

Effect of ALS-linked Mutations on Lipid-catalyzed SOD1 Fibrillization:

The effect of ALS mutations on the nucleation and elongation of fibrillar apo-SOD1 was studied in the presence of anionic liposomes at a molar ratio of [Lipid]:[SOD1] = 30:1 (i.e., under conditions that resulted in the most rapid nucleation of WT apo-SOD1 fibrils). I chose eight ALS variants of SOD1 (A4V, G37R, L38V, D90A, G93R, E100G, I113T, and H46R) that together represent the known biophysical diversity of ALS-linked mutations. I chose G37R, D90A, G93R, and E100G because these proteins have been reported to have lag times of fibrillization higher than or equal to WT apo-SOD1 (in non-quiescent microplate assays that lack liposomes but employ a gyrating Teflon bead). The H46R variant does not coordinate copper and zinc properly and has been reported by our group and others to not fibrillize in microplate-based amyloid assays.[123, 130] The remaining variants (which are isoelectric with WT SOD1) were chosen because they are commonly studied variants that fibrillize faster than WT apo-SOD1 in non-quiescent microplate assays.

ALS variants exhibited a broad range of maximum ThT intensity, fibril lag time, and elongation rate (Figure 3.5; Table 3.1). The A4V, G37R, E100G, and I113T variants exhibited lower fluorescence intensity than WT, D90A, and G93R SOD1 (Figure 3.5). All ALS-variant apo-SOD1 proteins (except for H46R) formed fibrillar species, even among wells that showed no ThT fluorescence (denoted ThT(-) wells;[55] Figure 4.16a-b), however, ThT(-) wells exhibited a higher concentration of soluble protein at the end of aggregation assay than ThT(+) wells according to SDS-PAGE (Figure 4.16c-d). The H46R apo-SOD1 protein did not fibrillize and aggregated exclusively into amorphous species in some wells and remained soluble in others (according to SDS-PAGE, Figure 4.16).

In the presence of anionic liposomes, all mutant proteins that fibrillized underwent nucleation faster than WT apo-SOD1 (Figure 3.6a-b; Table 3.1). I point out that these acceleratory effects are all statistically significant ($p < 0.0007$; Table 3.1), with the exception of G37R ($p = 0.82$). In contrast to this uniform acceleration in fibril nucleation, ALS mutations did not uniformly accelerate fibril elongation/propagation in the presence of anionic liposomes, relative to WT apo-SOD1 (Figure 3.6c-d). The variants A4V, G37R, D90A, and E100G exhibited slower rates of elongation in liposomal assays; all other variants (besides H46R SOD1) underwent fibril elongation at faster rates than WT apo-SOD1 (Figure 3.6c-d; Table 3.1).

I also expressed rates of apo-SOD1 fibrillization as Kaplan Meier estimators (Hazard ratios (Table 3.1, Figure 3.6e-f). Our previous analyses have shown that Kaplan-Meier estimators of ALS-variant SOD1 fibrillization correlate weakly with Hazard ratios of survival for patients expressing that mutation.[123]

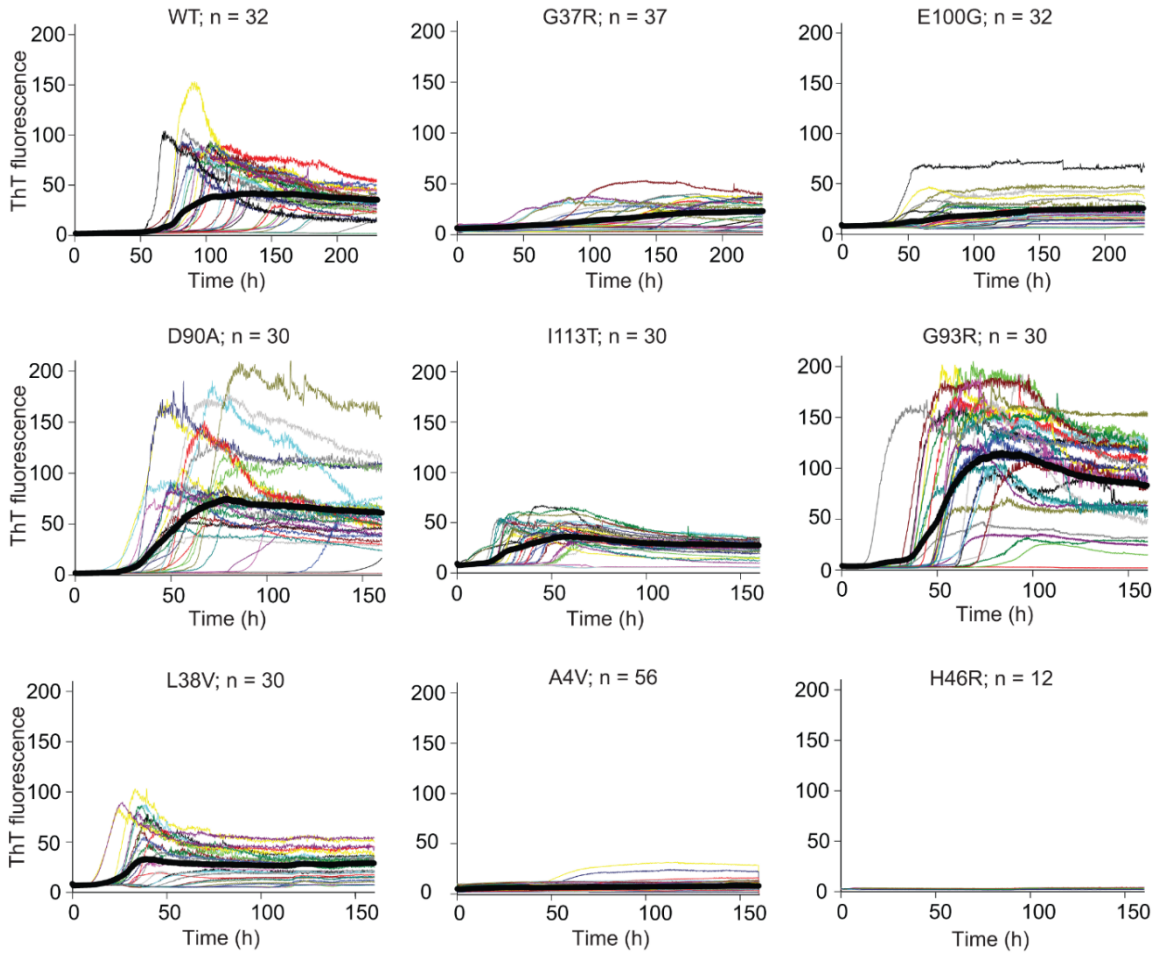

Figure 3.5 Iterate thioflavin-T fluorescence assays of fibrillization of WT and ALS-variant apo-SOD1 in the presence of anionic DOPCA liposomes ([Lipid]:[SOD1] = 30:1) (pH 7.4, 37ºC). The thick black trace in each panel represents the average of all replicate data points for WT and each mutant. Note: some traces are characterized by a decrease in ThT fluorescence after reaching a maximum intensity. This phenomenon has been observed in several previous reports,[122, 125, 144] and is caused by adhesion of macroscopic precipitates of protein to sides of the well (as inferred from manual inspection of wells exhibiting diminished intensity).

Table 3.1 Kinetic parameters of non-liposomal (T) and liposomal (L) assays of apo-SOD1 fibrillization (10 mM TCEP, 37 °C, pH 7.4).

SOD1 Variant[a]	τ_L (h)[b]	τ_T (h)[c]	k_L (h^{-1})[b]	k_T (h^{-1})[c]	HR_L[b,d]	HR_T[c,d]
WT (n = 32)	109.8 ± 6.6	13.4 ± 0.5	0.29 ± 0.01	0.20 ± 0.01	1.00	1.00
A4V (n = 60)[e]	47.90 ± 11.6 (p = 0.0007)	11.5 ± 0.5 (p = 0.013)	0.17 ± 0.07 (p = 0.018)	0.50 ± 0.02 (p < 0.0001)	0.56 (p = 0.37)	2.50 (p < 0.0001)
G37R (n = 37)	107.1 ± 10.9 (p = 0.82)	23.0 ± 0.8 (p < 0.0001)	0.10 ± 0.01 (p < 0.0001)	0.35 ± 0.01 (p < 0.0001)	0.28 (p < 0.0001)	0.40 (p < 0.0001)
L38V (n = 30)	28.3 ± 1.7 (p < 0.0001)	12.8 ± 0.5 (p = 0.44)	0.48 ± 0.02 (p < 0.0001)	0.46 ± 0.02 (p < 0.0001)	14.49 (p < 0.0001)	1.60 (p = 0.03)
H46R[f] (n = 12)	N/A	N/A	N/A	N/A	~ 0.00	~ 0.00
D90A (n = 30)	48.2 ± 4.3 (p < 0.0001)	14.5 ± 0.7 (p = 0.22)	0.27 ± 0.02 (p = 0.53)	0.41 ± 0.02 (p < 0.0001)	5.26 (p = 0.49)	0.95 (p = 0.76)
G93R (n = 30)	49.8 ± 2.7 (p < 0.0001)	13.6 ± 0.3 (p = 0.80)	0.35 ± 0.02 (p = 0.017)	0.57 ± 0.03 (p < 0.0001)	15.10 (p = 0.46)	2.58 (p < 0.0001)
E100G (n = 32)	62.3 ± 4.2 (p < 0.0001)	20.7 ± 0.8 (p < 0.0001)	0.14 ± 0.02 (p < 0.0001)	0.46 ± 0.02 (p < 0.0001)	0.95 (p = 0.74)	0.69 (p = 0.05)
I113T (n = 30)	29.9 ± 2.4 (p < 0.0001)	12.0 ± 0.5 (p = 0.089)	0.58 ± 0.06 (p < 0.0001)	0.39 ± 0.03 (p < 0.0001)	25 (p < 0.0001)	1.65 (p = 0.02)

Table 3.1 Caption:
[a]Data are from previous studies that agitated SOD1 at 360 rpm with a Teflon bead (T), which are compared with data from this study using agitation at 60 rpm with liposomes (L). Data are shown as mean ± standard error of the mean (SEM). N= number of iterate measurements for each variant, which varied per availability of each protein. HR: Hazard ratio. Average R^2 of sigmoidal fits for all replicate assays was 0.98. [b]The reducing conditions of these assays were adjusted to be identical with conditions of our previously published assays that involved gyrating Teflon beads,[123] i.e., 30 min incubation in 10 mM TCEP prior to plate gyration instead of 6 h in 100 mM TCEP, resulting in longer lag times than experiments shown in Figure 3.1. [c]Data obtained from our previous study.[123] [d]P values are calculated from the statistical comparison between Kaplan-Meier plots of each mutant SOD1 and that of WT SOD1, using Log-Rank (Mantel-Cox) algorithm at 95 % confidence interval ($p < 0.05$). [e]Only 3 out of 60 replicate aggregation assays of A4V apo-SOD1 (in the presence of DOPCA liposomes) resulted in a sigmoidal increase in ThT fluorescence. [f]H46R apo-SOD1 did not fibrillize in the presence of either Teflon beads or DOPCA liposomes.

The ranking of Hazard ratios was as follows: I113T > G93R > L38V > D90A > E100G > A4V > G37R > H46R (Figure 3.6f). These Hazard ratios do not correlate at all with Hazard ratios from patients with these same mutations ($R^2 = 0.070$). Thus, Hazard ratios of fibrillization that were obtained from our previous study, using non-quiescent microplate assays and a gyrating Teflon bead, produced kinetic data that correlated better with patient Hazard ratios than the liposomal assays in this study. A large factor in this lack of correlation was the A4V variant, which exhibited one of the highest Hazard ratios in non-quiescent amyloid assays but exhibited one of the lowest Hazard ratios in semi-quiescent liposomal assays (Table 3.1, Figure 3.6f).

Another feature of the Kaplan Meier Hazard ratio is that it expresses the proportion of iterate wells that did not form ThT(+) amyloid fibrils. Previous studies have shown that SOD1 can form ThT(-) fibrils that do not register in fluorescence assays (and have weaker seeding activity for SOD1 aggregation in organotypic spinal cord, compared to ThT(+)

amyloid fibrils[55]). Qualitatively, the most striking acceleratory effects on fibrillization into ThT(+) species were observed for G37R, D90A, G93R, and E100G mutations.

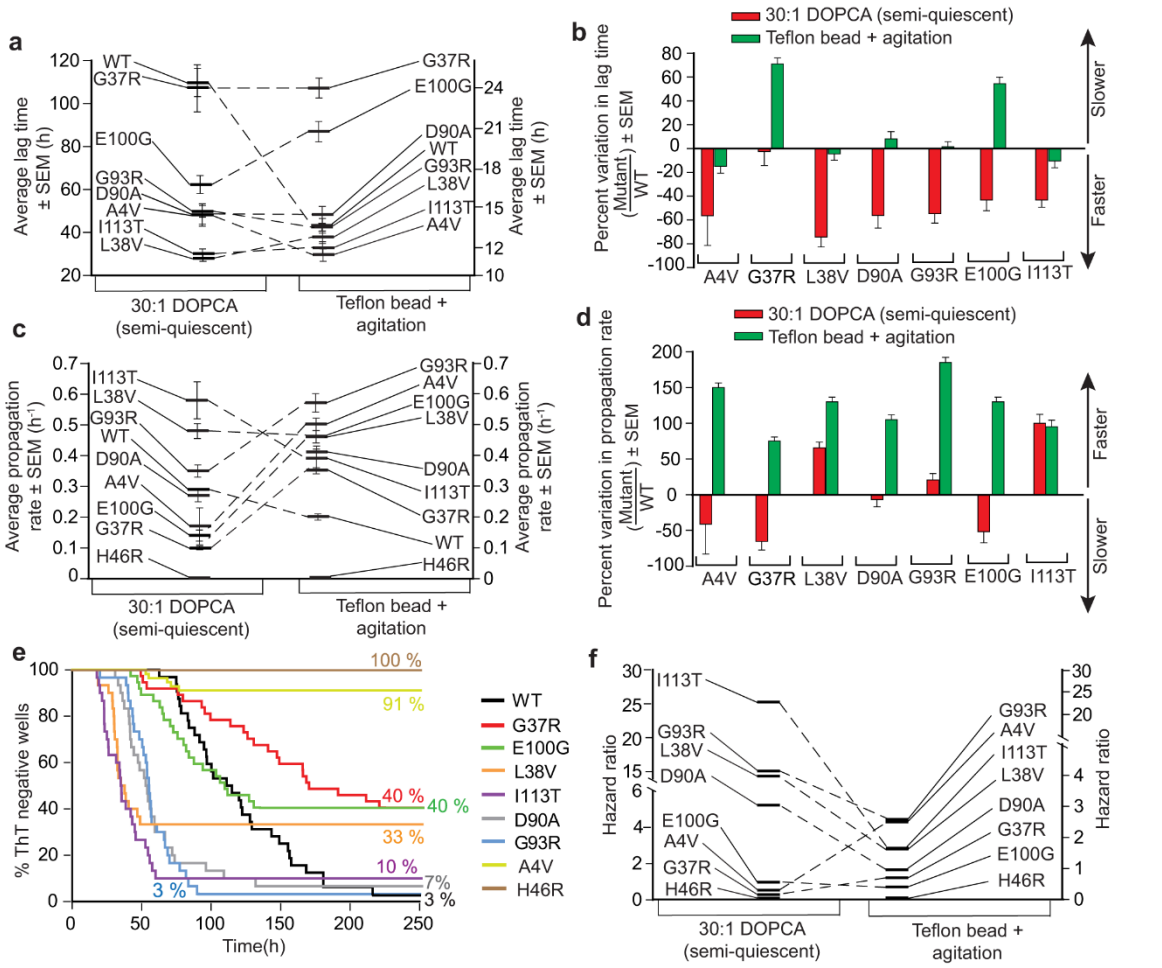

Figure 3.6 Comparison of rank order of **(a-b)** fibril nucleation, and **(c-d)** fibril elongation rate of ALS variant apo-SOD1 proteins when assays are carried out semi-quiescently in the presence of anionic DOPCA liposomes (without a Teflon bead) versus agitation with a Teflon bead (without liposomes). Reducing conditions were modified in these liposomal experiments to match reducing conditions of previous membrane-free ThT assays that utilized gyrating beads,[123] and thus differ from experiments described in Figure 3.1. **(e)** Kaplan-Meier analysis of aggregation of WT and 8 ALS-variant apo-SOD1 proteins in the presence of anionic DOPCA liposomes ([Lipid]:[SOD1] = 30:1). Values next to each plot indicate the percent of wells that did not exhibit an increase in ThT fluorescence during the course of assay. **(f)** Comparison of Hazard ratio of ALS-variant apo-SOD1 fibrillization when assays are carried out semi-quiescently in the presence of anionic DOPCA liposomes (without a Teflon bead) versus agitation with a Teflon bead (without liposomes).

For example, these variants have been previously shown[123] to diminish (or not affect) the rate of fibril nucleation in non-liposomal assays, compared to WT apo-SOD1, however, these variants do accelerate nucleation in liposomal assays. These four mutations are the only mutants in this study—with the exception of H46R SOD1—that decrease the magnitude of net negative charge of SOD1. Among this set, the D90A, G93R and E100G mutants aggregated much faster than G37R and exhibited lag times > 40 hours lower than G37R. These effects might be electrostatic nature and reflect how local changes in surface charge affect interactions with SOD1 and anionic surfactants of the liposome. For example, the D90A, G93R and E100G mutations occur in the so-called "gel shifting" domain of SOD1 (residues 80-101).[145]

These substitutions, and others that lower the net negative charge of this ~ 20 residue domain, have been previously shown to increase the binding of anionic surfactants to SOD1 by reducing electrostatic repulsion between surfactant and SOD1 (e.g., D90A results in the additional binding of ~ 3 SDS molecules per SOD1 monomer at equilibrium).[145]

Identical amino acid substitutions outside domain ~ 80-101 (e.g., G37R, E21G) do not result in changes in surfactant binding (and do not cause gel shifting during SDS-PAGE) and neither do isoelectric substitutions that increase hydrophobicity of this domain.[145] Similarly, local electrostatic effects might explain why D90A, G93R, and E100G mutations accelerate SOD1 fibrillization in anionic liposomes more than G37R, and why these four accelerate fibrillization more than the remaining isoelectric mutations that were examined.

Conclusion

This study demonstrates that the surface charge of a membrane can determine whether that surface catalyzes the primary nucleation of SOD1 fibrils or the amorphous aggregation of SOD1. To our knowledge, these data are the first to demonstrate that membrane surfaces catalyze SOD1 fibrillization (previous studies demonstrated amorphous aggregation[47]). The general trend that I observed between rate of fibrillization and charge of the headgroup was anionic > cationic > zwitterionic (Figure 3.2a). Long-range Coulombic interactions between liposomes and SOD1, which would depend upon the net charge of SOD1 and liposomes, cannot uniformly explain these observed trends in binding and fibrillization as SOD1 is a negatively charged protein.[64] Ion-specific effects might adequately explain these trends as headgroups with greater solvation lead to more rapid SOD1 fibrillization.

An important trend that I observed in this study was that increasing the ratio of [Lipid]:[SOD1] generally decreased the rate of SOD1 fibril nucleation and elongation. This trend can be explained in terms of primary nucleation mechanism, as illustrated in Figure 3.7. At low [Lipid]:[SOD1] ratios (e.g., 4:1), a fraction of SOD1 proteins bind to the surface of liposomes, which creates nucleation sites for the recruitment of free SOD1 proteins from solution, thus leading to fibril elongation (Figure 3.7a). At high [Lipid]:[SOD1] ratios (e.g., 100:1), however, SUVs bind a larger fraction of free SOD1 polypeptides, which depletes free SOD1 in solution and sequesters more SOD1 to a now greater number of liposomes. Therefore, although a higher number of potential nucleation sites are formed, there is not enough free SOD1 for elongation (and fibrillization) to occur, and there is a lower number of SOD1 chains bound per liposome (Figure 3.7b).

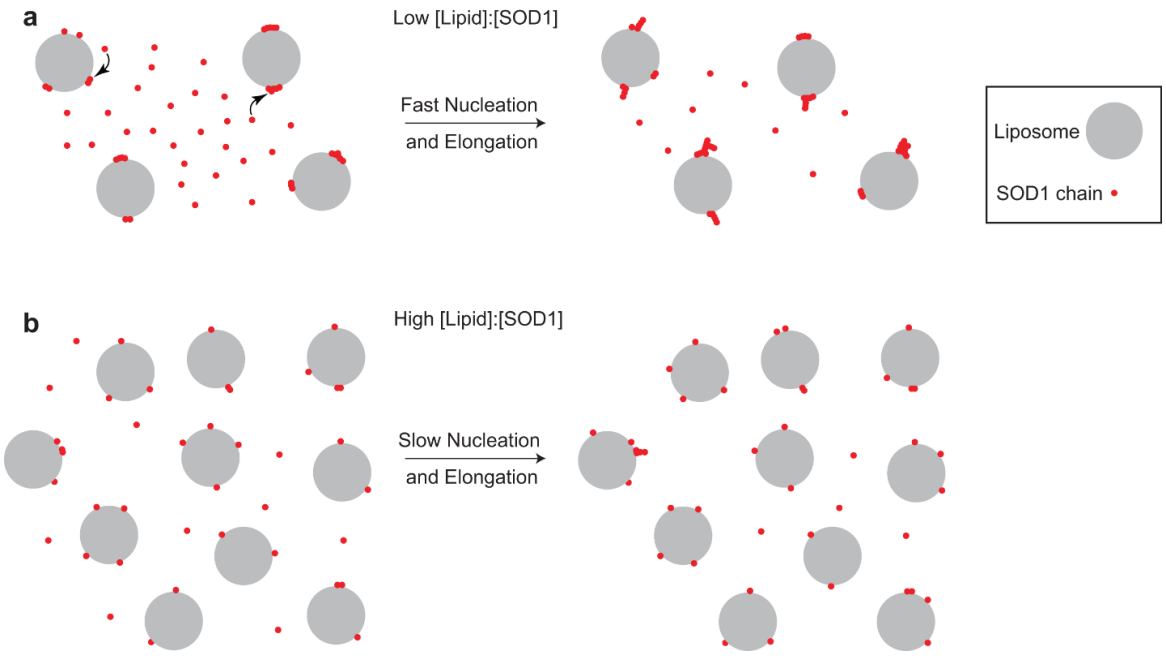

Figure 3.7 Primary nucleation mechanism of lipid-catalyzed SOD1 fibrillization. (a) At low [Lipid]:[SOD1] ratios, a critical amount of free SOD1 attaches to nucleation sites on the surface of SUVs and elongates to from mature fibrils. **(b)** At high [Lipid]:[SOD1] ratios, a greater concentration of SOD1 is bound to the surface of SUVs, which separates SOD1 from free monomers and causes an increase in the number of bound SOD1 per vesicle, leaving fewer SOD1 monomers for nucleation and elongation.

In the context of ALS, these results suggest that changes in the composition of membrane or vesicle surfaces from zwitterionic to anionic or cationic can promote the primary nucleation of amyloid-like SOD1 oligomers *in vivo*.[146, 147] Variations in lipid homeostasis have been reported in patients with ALS, but the link to ALS pathogenesis or progression (i.e., causative, coincidental, or protective) is unclear.[147, 148] Elevated levels of phosphatidylcholine lipids (including DOPC) have been reported in blood of G93A SOD1 mice.[75] Although it might not be prudent to extrapolate our simple *in vitro* results to *in vivo* systems, our results do suggest that the elevation of phosphatidylcholine lipids in membrane surfaces would be protective against the formation of amyloid-like oligomers of SOD1. Mitochondrial membranes might represent the lipid surface that

SOD1 has the highest probability of encountering. A higher abundance of phospholipids has been observed in neuronal mitochondria compared to non-neuronal mitochondria[76] and the content of zwitterionic lipids increases with age.[77]

Characterizing the effects of membrane surfaces on SOD1 aggregation is not only relevant to understanding interactions between SOD1 and intact cellular or organellar membranes,[149] but is also relevant to understanding interactions between SOD1 and small inter- or intracellular vesicles that are 30-50 nm in diameter in neurons.[150] The migration and transmission of neurotoxic SOD1 oligomers between cells has been shown to occur via pinocytosis, a process in which SOD1 proteins are engulfed by the cell membrane in the form of small vesicles—similar in size to the SUVs studied here—and transported into the extracellular matrix.[151] This study suggests that the headgroup composition of such vesicles is directly related to their ability to catalyze the self-assembly of neurotoxic oligomers. Moreover, this study finds that liposomes bind directly to fibrillar SOD1. These liposome-fibril complexes will have, I hypothesize, a greater affinity for cell membranes than fibrils alone. These fibril-bound liposomes might represent points-of-fusion (or attachment) to cell membranes.

Perhaps the most important result in this study is that apo-SOD1 fibrillization is more uniformly accelerated by ALS mutations in the presence of anionic liposomes compared to the absence of liposomes. Considering that the inclusion of liposomes renders the assay more biologically relevant, I suggest that these aggregation metrics are more physiologically relevant than assays that do not involve liposomes but rather utilize rapidly gyrating beads. That being said, there is very little correlation between fibrillization kinetics of each ALS-variant SOD1 protein in the presence of anionic liposomes, and the

clinical phenotype of patients expressing each variant. The mystery that continues to linger is why the H46R apo-protein does not form ThT(+) fibrils in the presence or absence[123, 130] of liposomes. This mutation is associated with a clinically mild form of ALS with a mean patient survival time of ~ 15 years.[152]

Materials and Methods

SOD1 Purification, Demetallation, and Characterization:

Recombinant human apo-SOD1 protein was expressed in *Saccharomyces cerevisiae*, purified using ammonium sulfate precipitation and three consecutive chromatographic separations, as previously described.[153]

SOD1 proteins were demetallated using a three-step dialysis procedure, as previously described.[153] Inductively coupled plasma mass spectrometry (ICP-MS) analysis confirmed that all apo-SOD1 proteins contained ≤ 0.08 equivalents of zinc or copper (Table 4.3).

Preparation and Characterization of Lipid Vesicles:

Small unilamellar vesicles (SUVs) were prepared using the thin film hydration method described by Yanasarn et al.[154] Zwitterionic 1,2-di-(9Z-octadecenoyl)-*sn*-glycero-3-phosphocholine (DOPC), anionic 1,2-di-(9Z-octadecenoyl)-*sn*-glycero-3-phosphate (DOPA), and cationic 1,2-di-(9Z-octadecenoyl)-3-trimethylammonium-propane (DOTAP) lipids were purchased from Avanti Polar Lipids (Alabaster, AL, USA), and used without further purification. SUVs were prepared upon mixing anionic DOPA or cationic DOTAP with zwitterionic DOPC lipids (1:1 molar ratio). Briefly, lipid solutions (in chloroform) were dried through rotary evaporation, leaving behind a "lipid cake" along the

walls of the round bottom flask. Upon hydration of the lipid cake with 10 mM KPO_4 buffer (containing 5 mM EDTA, pH 7.4), amphiphilic lipids within the lipid cake self-assembled into double-membrane, circular vesicles with a heterogeneous size distribution. High-energy sonication followed by mechanical extrusion through polycarbonate membranes (pore size = 100 nm) led to the formation of homogeneous, unilamellar liposome solutions with an accurate size distribution. The size, polydispersity, and lamellarity of SUVs were assessed with dynamic light scattering and transmission electron microscopy.

Dynamic Light Scattering (DLS):

The size distribution and homogeneity of SUV solutions were measured with a DynaPro NanoStar DLS instrument (Wyatt Technology, Goleta, CA, USA). The DLS operated with a 100 mW laser at 663 nm. The acquisition time was 5 seconds (n = 10), and data were collected at 25 °C, with the detector placed perpendicular to the light path. A sample volume of 10 µL was analyzed in a Cyclic Olefin Copolymer (COC) cuvette. Size distribution of SUVs was obtained via fitting the corresponding autocorrelation functions, using DYNAMICS software, version 7.1.

Thioflavin-T (ThT) Fluorescence Aggregation Assays:

The effect of zwitterionic, anionic, and cationic SUVs on apo-SOD1 aggregation was studied at varying [Lipid]:[SOD1] molar ratios with high-throughput, microplate-based ThT fluorescence aggregation assays. For experiments with neutral and anionic liposomes, apo-SOD1 proteins (30 µM per dimer) in aggregation buffer (10 mM KPO_4/5 mM EDTA, pH 7.4) were incubated for 6 hours in 100 mM tris-(2-carboxyethyl) phosphine (TCEP) at 22 °C, with agitation (110 rpm). In the case of aggregation assays with cationic

liposomes, 150 mM dithiothreitol (DTT) was used as the reducing agent (under identical conditions used for zwitterionic and anionic liposomes). I used DTT instead of TCEP because cationic liposomes precipitate in the presence of TCEP. In the case of ALS-variant apo-SOD1, protein solutions were incubated in 10 mM TCEP for 30 min. Reduced SOD1 samples were then filtered with a syringe filter (200 nm), in order to remove possible preformed oligomers that might seed SOD1 fibrillization. Liposome solutions (of varying concentrations) were added to each well of the 96-well polystyrene microplate, followed by the addition of reduced protein solutions to each well (total final lipid concentrations ranged from 30 μM to 3 mM). The final concentration of ThT was 50 μM in each well. The plate was completely sealed with a transparent polypropylene cover and was placed in a Thermo Scientific® Fluoroskan Ascent equipped with a temperature controller. Fluorescence was recorded every 15 min, and plate was agitated at minimum speed (60 rpm) every 15 sec.

Fully metallated holo-SOD1 (isolated from human erythrocytes) was purchased from Sigma Aldrich. The aggregation assays of holo-SOD1 were performed identically to those of apo-SOD1 (i.e., using microplate assays, pH 7.4, 30 μM dimer). However, I varied the reducing conditions by performing assays in 20 mM or 150 mM DTT, and I also performed assays with and without 5 mM EDTA.

Longitudinal plots of ThT fluorescence followed a sigmoidal trace and were fit with a 4-parameter sigmoidal function (Equation 1) using SigmaPlot® software, version 11.0:

$$I = I_0 + \frac{I_{\max}}{1 + e^{k(t - t_0)}} \qquad \text{(Equation 3.1)}$$

Where I is the ThT fluorescence intensity at each time point t; I_0 and I_{max} are the minimum and maximum ThT fluorescence, respectively; t_0 is the time at which the sigmoid reaches half of its maximum, and k is the rate of fibril propagation. The lag time of SOD1 fibrillization was calculated as $\tau = t_0 - 2k^{-1}$. For iterate longitudinal plots of ThT fluorescence that were characterized by a decrease in ThT fluorescence after reaching a maximum intensity (see Figures 3.1 and 3.5), I only included the sigmoidal increase to maximum I in the curve fitting. I note that this phenomenon has been observed repeatedly and is likely caused by adhesion of macroscopic precipitates of protein to sides of the well (as inferred from manual inspection of wells exhibiting diminished intensity[55, 125, 144]). Kaplan-Meier analyses on individual aggregating wells were performed using Graphpad Prism® 5, as previously described.[123]

Transmission Electron Microscopy (TEM):

To determine the lamellarity of SUVs as well as the morphology of SOD1 aggregates, I performed TEM microscopy using a JEOL JEM-1010 transmission electron microscope (JEOL Ltd., MA, USA). Sample preparation for both SUVs and SOD1 aggregates were performed as previously described.[55]

Filter-trap Assay to investigate the Binding of SOD1 to SUVs:

In order to determine the extent of SOD1 binding to variably charged liposomes, WT apo-SOD1 proteins were incubated with all three types of liposomes ([Lipid]:[SOD1] = 4:1 and 100:1) for 2.0 h (and for 0.25 h, 0.5 h, and 1.0 h in the case of binding kinetics of SOD1 to DOPCA liposomes). All binding assays were performed in the presence of 150 mM DTT at 37 °C, with minimal orbital gyration (60 rpm). An identical solution of WT

apo-SOD1 (without liposomes) was incubated with 150 mM DTT as control. All solutions were then transferred to centrifugal filtration devices (100-kDa molecular weight cut-off, 10 nm pore size), and washed with 10 mM KPO_4/5 mM EDTA buffer. Each washing cycle consisted of ~ 10-fold concentration and dilution in wash buffer. Solutions of species that were retained by the filter and all other effluents were analyzed with SDS-PAGE.

Atomic Force Microscopy (AFM):

To study the interaction of fibrillar SOD1 and SUVs, I centrifuged the post-aggregation homogenates of SOD1 fibrils/DOPCA SUVs ([Lipid]:[SOD1] = 30:1), and imaged the pellets using a Dimension Icon AFM, equipped with NanoScope V software (Bruker, Santa Barbara, CA).

Topography images were obtained with tapping mode probes (NSC35/ALBS, 5.4 N/m). The cantilever oscillated at a frequency of 150 kHz and micrographs were analyzed using NanoScope Analysis software.

CHAPTER FOUR

Supporting Information

Lysine Acylation in Superoxide Dismutase-1 Electrostatically Inhibits Formation of Fibrils with Prion-like Seeding.

Supporting Figures and Tables

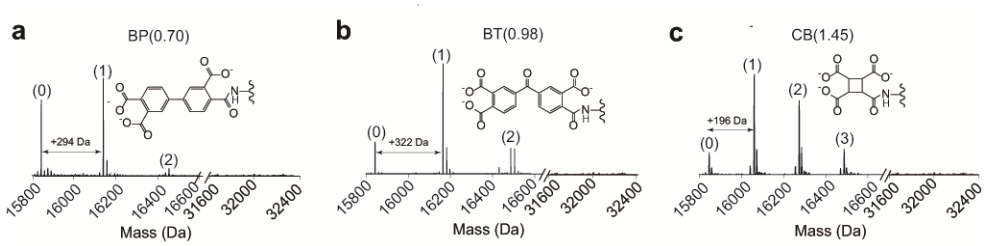

Figure 4.1 Mass spectra of WT apo-SOD1 proteins modified with **(a)** BP (0.70), **(b)** BT (0.98), and **(c)** CB (1.45).

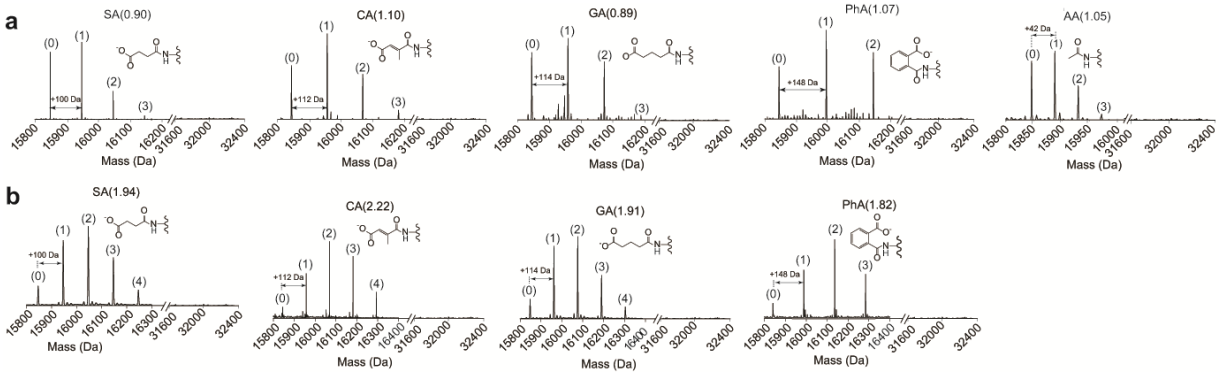

Figure 4.2 Mass spectra of WT apo-SOD1 proteins modified with **(a)** SA(0.90), CA(1.10), GA(0.89), PhA(1.07), AA(1.05), and **(b)** SA(1.94), CA(2.22), GA(1.91), and PhA(1.82). Modified proteins in panel **(b)** were only used in protein charge ladder experiments to determine the charge regulation associated with each modification.

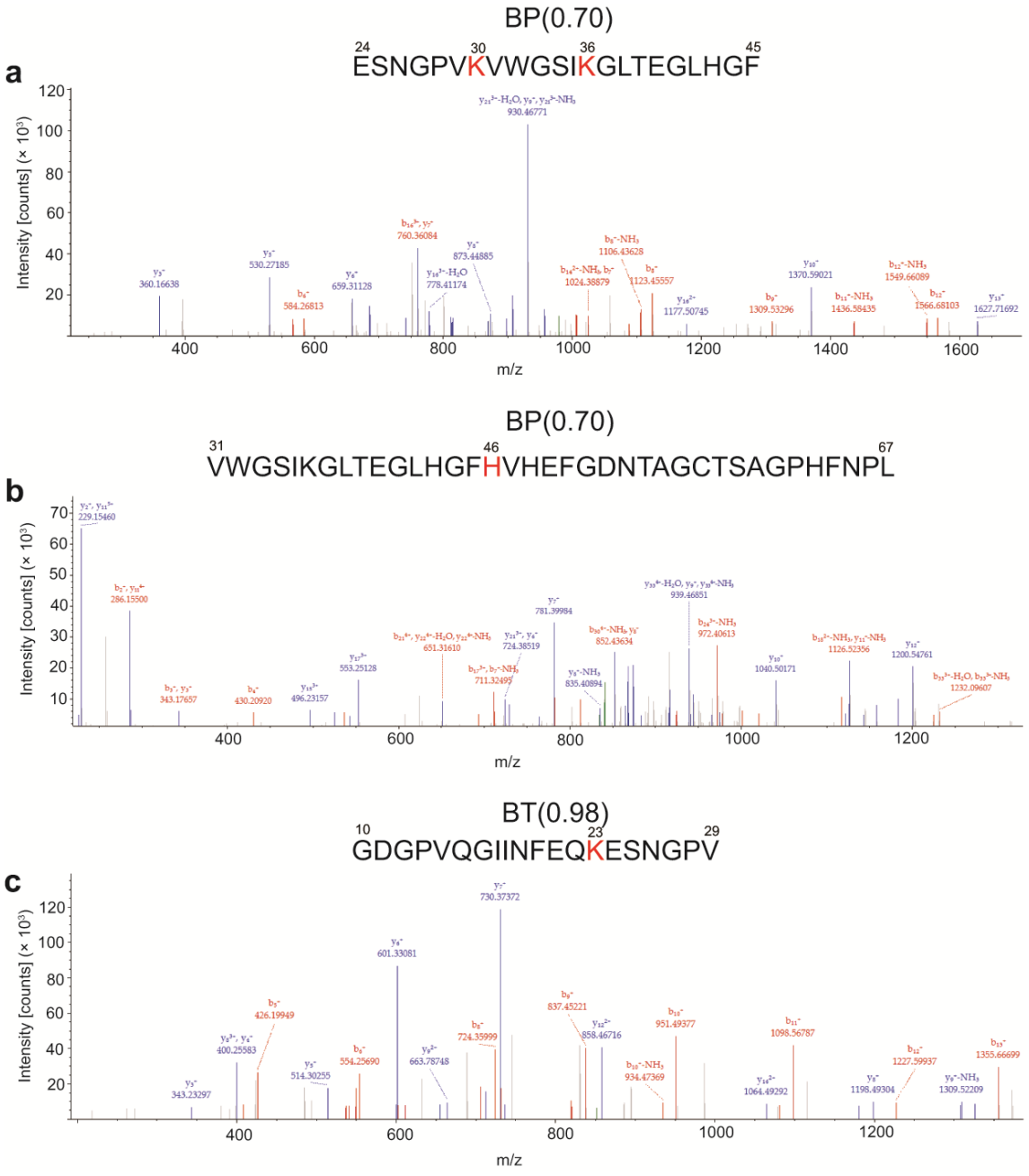

Figure 4.3 Acylation of WT apo-SOD1 with BP and BT modifications. Tandem mass spectra for acylated WT apo-SOD1 **(a-b)** BP(0.70), and **(c)** BT(0.98).

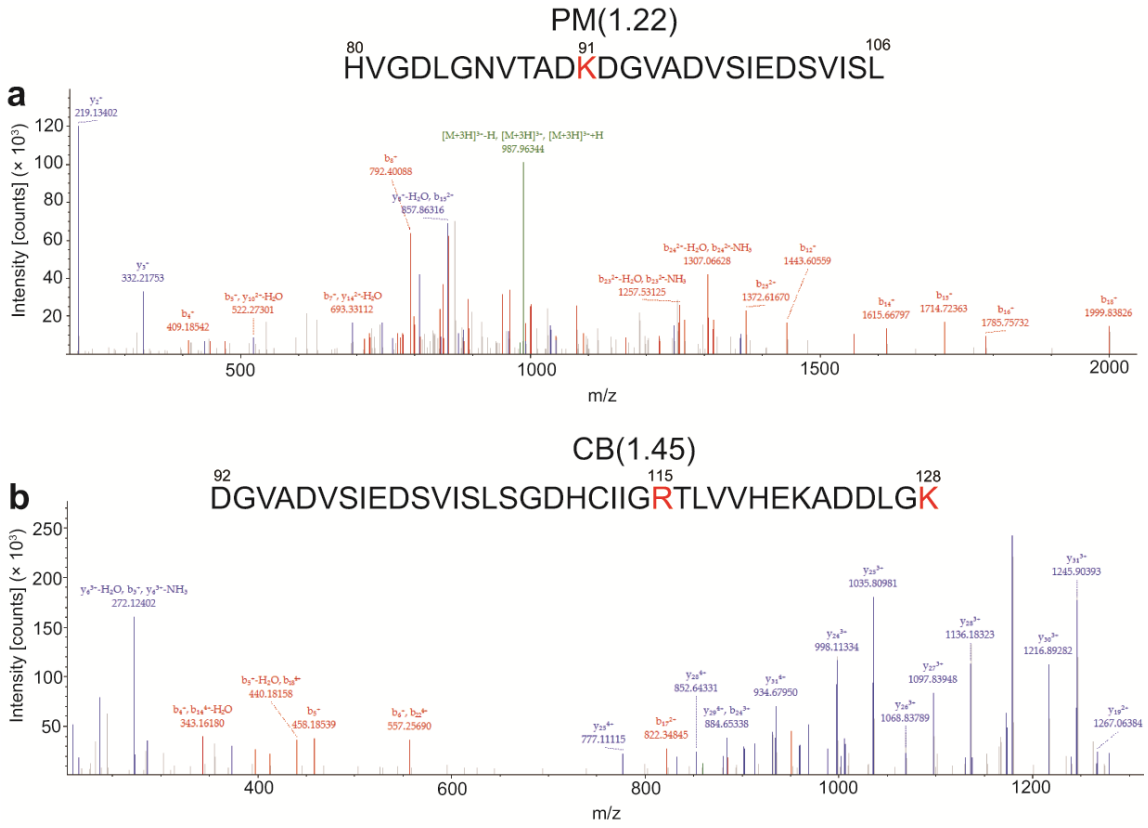

Figure 4.4 Acylation of WT apo-SOD1 with PM and CB modifications. Tandem mass spectra for acylated WT apo-SOD1 **(a)** PM(1.22), and **(b)** CB(1.45).

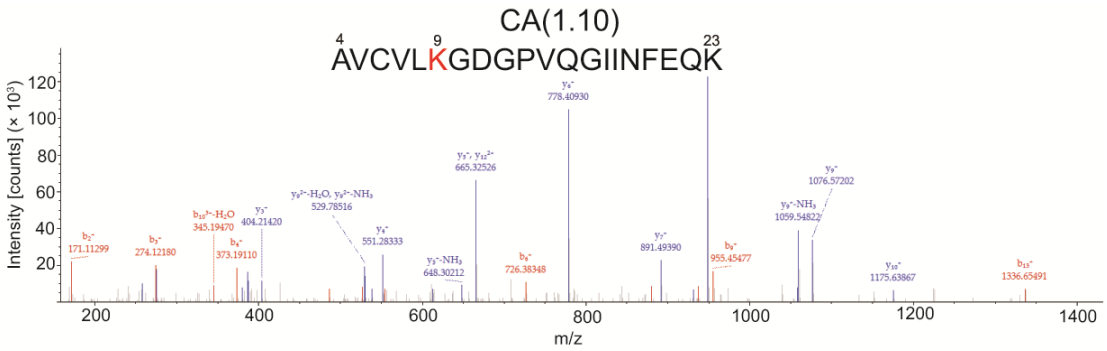

Figure 4.5 Acylation of WT apo-SOD1 with CA modification. Tandem mass spectrum of acylated WT apo-SOD1 (CA(1.10)).

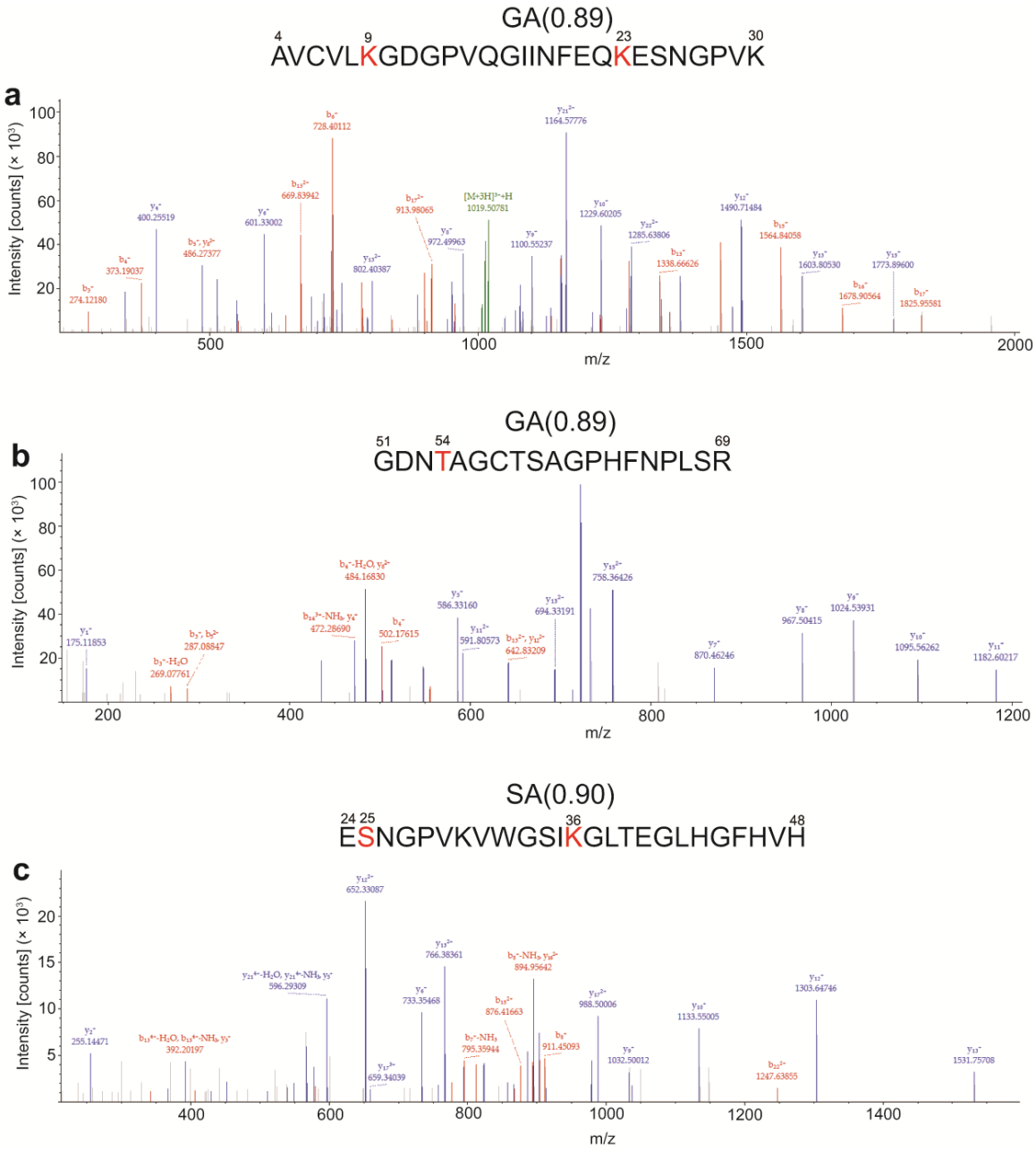

Figure 4.6 Acylation of WT apo-SOD1 with GA and SA modifications. Tandem mass spectra for acylated WT apo-SOD1 **(a-b)** GA(0.89), and **(c)** SA(0.90).

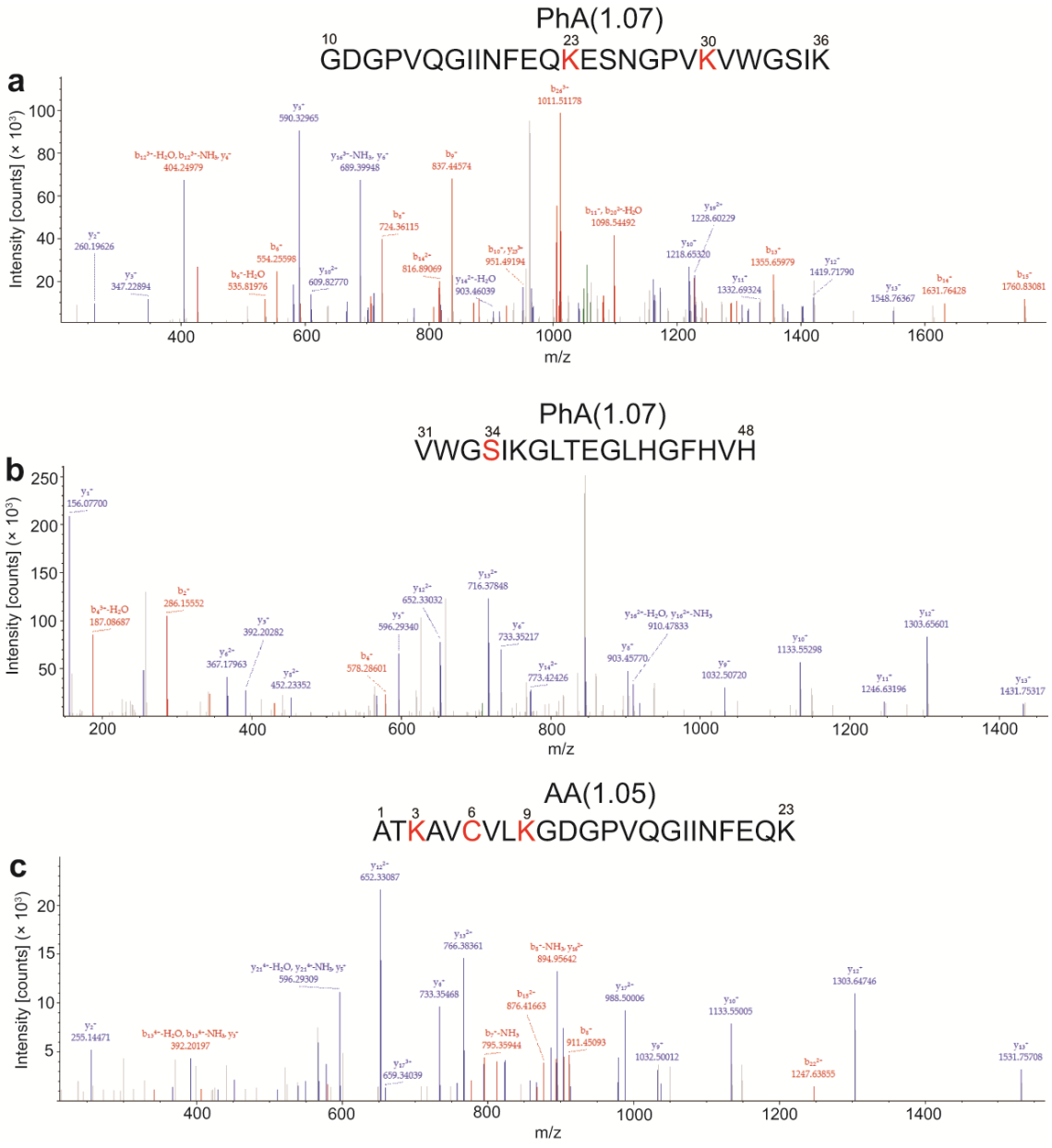

Figure 4.7 Acylation of WT apo-SOD1 with PhA and AA modifications. Tandem mass spectra for acylated WT apo-SOD1 **(a-b)** PhA(1.07), and **(c)** AA(1.05).

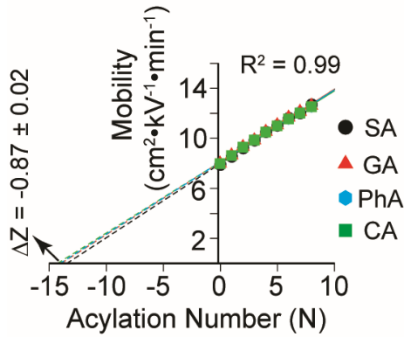

Figure 4.8 Charge calculation for the minor charge ladder observed in the electropherograms of SOD1 proteins modified with acyl groups with ΔZ_{formal} = -2 (see asterisks in Figure 2.3d of the main text).

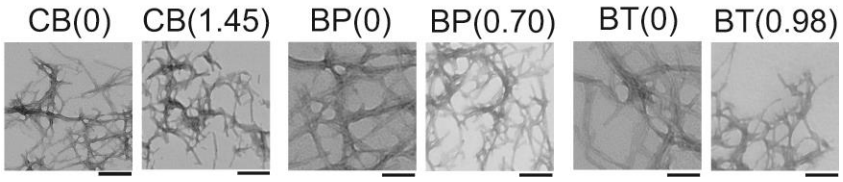

Figure 4.9 TEM micrographs of acylated and unacylated apo-SOD1 proteins collected after the termination of ThT assay (ΔZ_{formal} = -4). TEM images of pyromellitylated SOD1 and its corresponding unmodified protein are shown in Figure 2.5 in chapter 2. Scale bar = 200 nm in all micrographs.

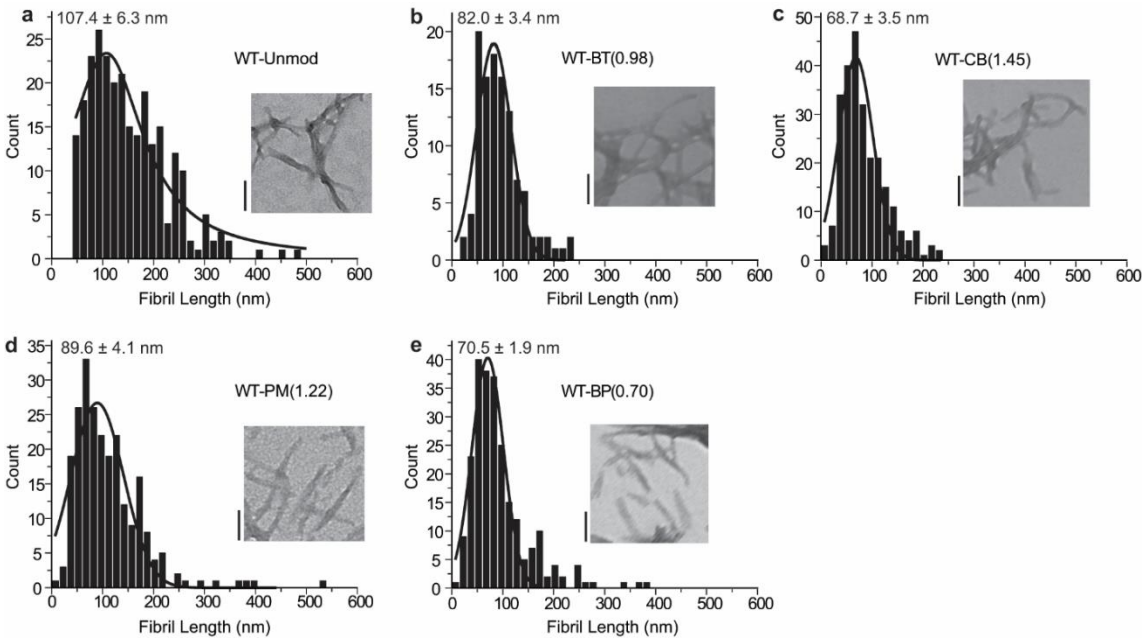

Figure 4.10 (a-e) Histograms of fibril length (average ± SD) for variably acylated and unmodified apo-SOD1 proteins ($\Delta Z_{formal} = -4$), measured from TEM micrographs ($n_{unmod} = 265$; $n_{PM} = 234$; $n_{BT} = 112$; $n_{BP} = 239$; $n_{CB} = 214$). Scale bar = 200 nm in all micrographs.

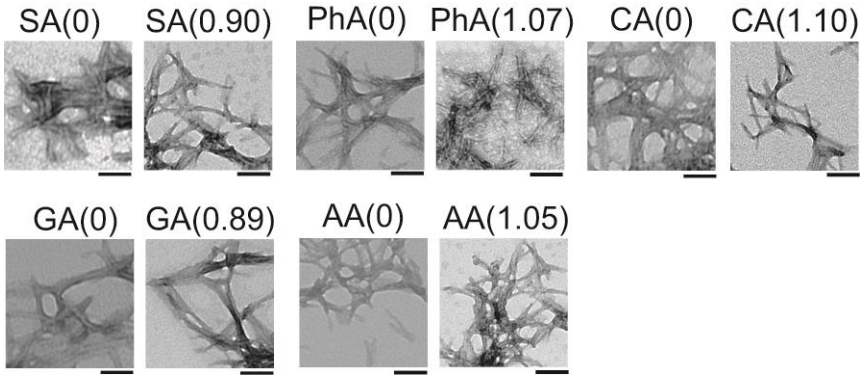

Figure 4.11 TEM micrographs of acylated and unacylated apo-SOD1 proteins collected after the termination of ThT assay ($\Delta Z_{formal} \leq -2$). Scale bar = 200 nm in all micrographs.

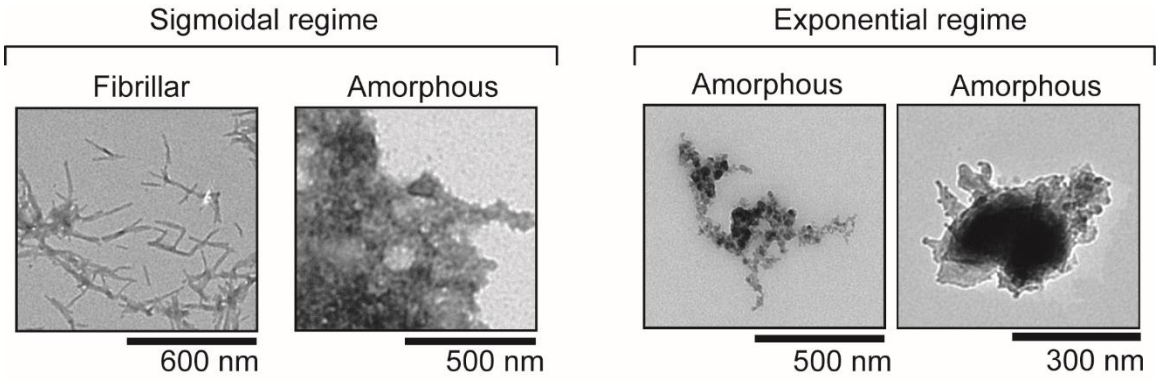

Figure 4.12 Representative TEM micrographs taken from wells that show sigmoidal (left) and exponential (right) kinetics, during ANS fluorescence aggregation assays of acylated and unmodified apo-SOD1 proteins.

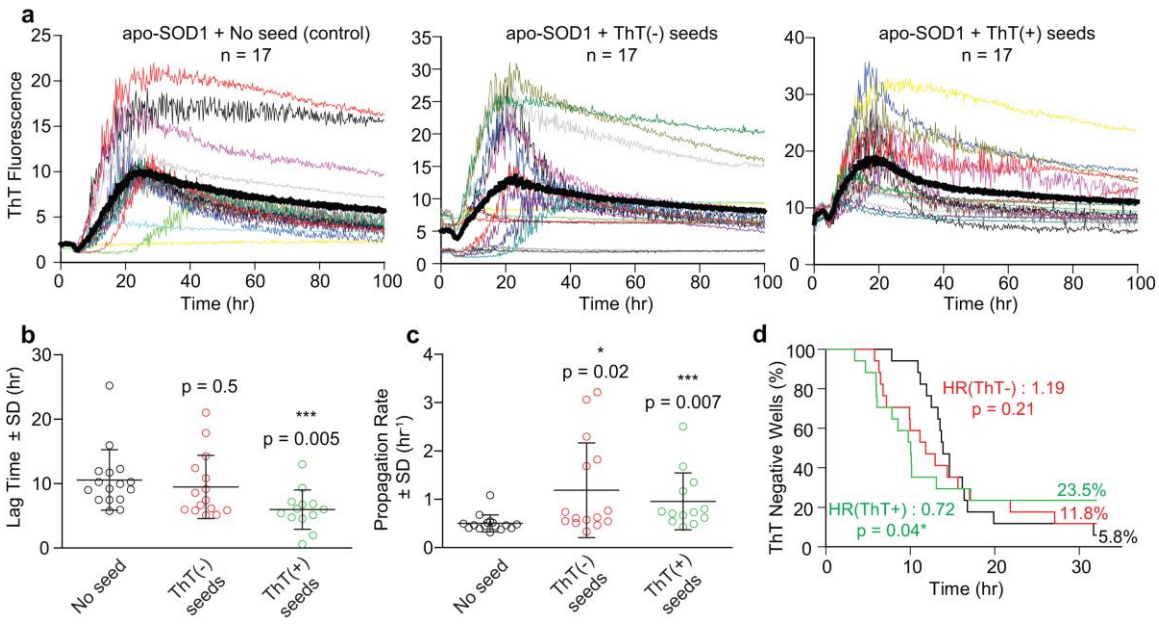

Figure 4.13 (a) Replicate ThT fluorescence assays of aggregation of WT apo-SOD1 seeded with acylated SOD1 fibrils that were ThT-negative and ThT-positive. The fibrils that were used to seed SOD1 are composed of preformed, singly pyromellitylated SOD1. The black trace in each panel shows the average of all replicate traces for each condition. Plots of **(b)** average lag time, and **(c)** average propagation rate for SOD1 aggregation in the absence and presence of different seeds (SD: standard deviation). P-values for ThT-negative and ThT-positive conditions are calculated with respect to control (unseeded) data, using an Unpaired Student's t-test. **(d)** Kaplan-Meier analysis of aggregation of WT apo-SOD1 seeded with ThT-negative and ThT-positive SOD1 fibrils. Hazard ratios (HR) and p-values are calculated with respect to control (unseeded) data, using Mantel-Cox algorithm.

Table 4.1 MS/MS analysis of WT apo-SOD1 tryptic digests modified with different acylating groups (Ac(~1)). The peptide sequence coverage varied from 98 % to 100 % in all proteomics analyses. Listing of Xcorr value for each residue in the grid denotes detection of acylation of that residue by each modification. Only peptides with Xcorr ≥ 4.0 and ppm ≤ 0.05 were considered as positive hits.

Modified residues	Ac(~1)									
		BP(0.70)	BT(0.98)	PM(1.22)	CB(1.45)	PhA(1.07)	SA(0.90)	GA(0.89)	CA(1.10)	AA(1.05)
	K3									4.9
	K9					6.6		10.0	4.9	7.0
	K23	5.6		5.7	5.9	6.6	5.9	9.9		7.0
	K30	4.0		4.0	7.0	6.5	6.6	7.3		5.0
	K36	4.0	4.0	5.8	6.9	5.4	6.6	4.0		4.0
	K70									
	K75									
	K91	8.8		6.7	8.2	8.4		7.7		9.3
	K122	5.1		4.5	4.0		5.2	5.2		4.8
	K128	5.1	4.9	4.7	5.8		5.2			4.8
	K136	4.8		4.0	5.7		4.3	4.0		4.6

Modified residues	Ac(~1)									
		BP(0.70)	BT(0.98)	PM(1.22)	CB(1.45)	PhA(1.07)	SA(0.90)	GA(0.89)	CA(1.10)	AA(1.05)
	H46	4.0								
	T54							4.5		
	S34					4.6				
	S25			5.8			4.4			
	C6									4.9
	S68							4.9		
	R115				5.3					

Table 4.2 MS/MS analysis of WT apo-SOD1 tryptic digests modified with different acylating groups with ΔZ_{formal} = -2 for the purpose of measuring ΔZ of acylation (Ac(~2)). The peptide sequence coverage was varied from 98 % to 100 % in all proteomics analyses. Listing of Xcorr value for each residue in the grid denotes detection of acylation of that residue by each modification. Only peptides with Xcorr ≥ 4.0 and ppm ≤ 0.05 were considered as positive hits.

Modified residues	Ac(~2)		
	PhA(1.82)	SA(1.94)	GA(1.91)
K3			
K9	4.6	8.6	5.8
K23	6.0	8.6	
K30	6.0	6.6	
K36	5.6	6.5	
K70			
K75			
K91		4.8	
K122	4.2	7.6	
K128	4.2	7.6	
K136	4.3	6.2	4.4

Modified residues	Ac(~2)		
	PhA(1.82)	SA(1.94)	GA(1.91)
S34	4.9		
S25	4.2		
S98			5.2

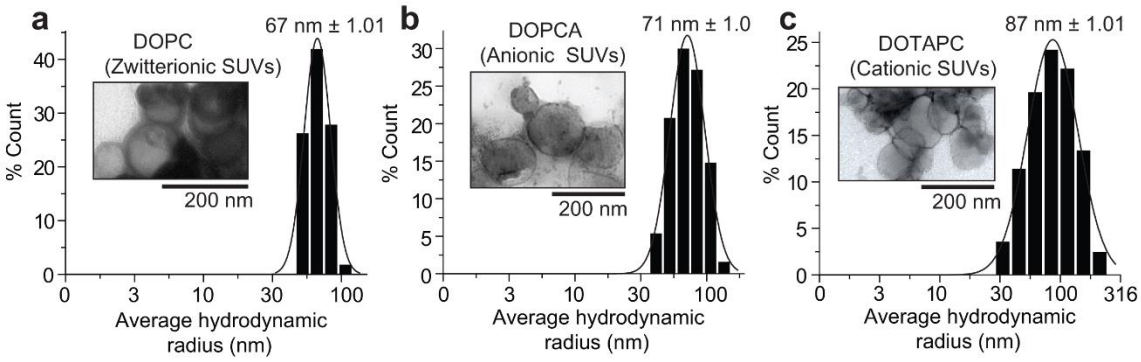

d

Lipid	SUV count	MLV count	Total count	SUV (%)
DOPC	79	14	93	84.9 ± 3.5
DOPCA	142	15	157	90.4 ± 0.05
DOTAPC	131	18	149	87.9 ± 0.06

Figure 4.14 Characterization of zwitterionic, anionic, and cationic SUVs. Dynamic light scattering and transmission electron microscopy of **(a)** DOPC (zwitterionic), **(b)** DOPCA (anionic), and **(c)** DOTAPC (cationic) SUVs prepared from lipids shown in Scheme 3.1. Average hydrodynamic radius above each histogram represents the average of three separate measurements (± standard deviation). **(d)** Lamellarity values were determined via visual inspection of TEM micrographs for each vesicle type. SUV: small unilamellar vesicle; MLV: multilamellar vesicle.

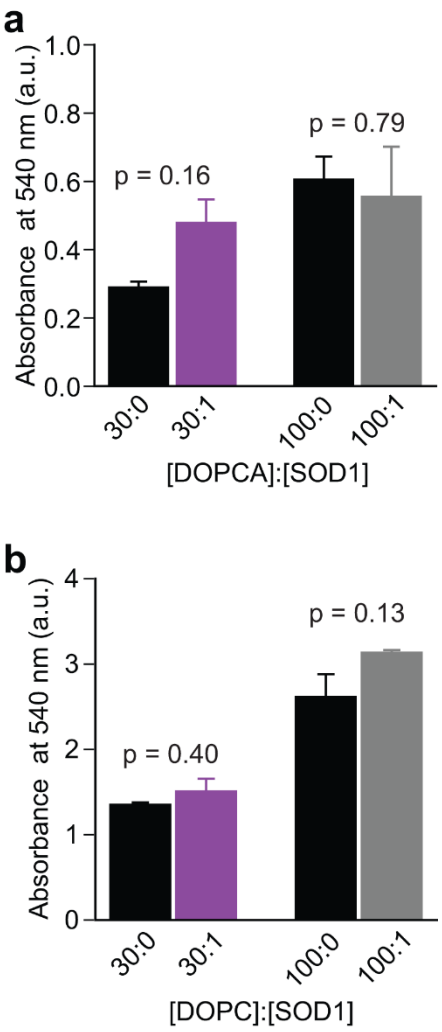

Figure 4.15 Small lipid vesicles do not disassemble during the course of aggregation assays. Comparison of UV-vis absorption performed on the supernatant of control solutions ([Lipid]:[SOD1] = 30:0 and 100:0) prior to and after SOD1 aggregation assays in the presence of **(a)** DOPCA ([Lipid]:[SOD1] = 30:1 and 100:1) SUVs, and **(b)** DOPC ([Lipid]:[SOD1] = 30:1 and 100:1) SUVs.

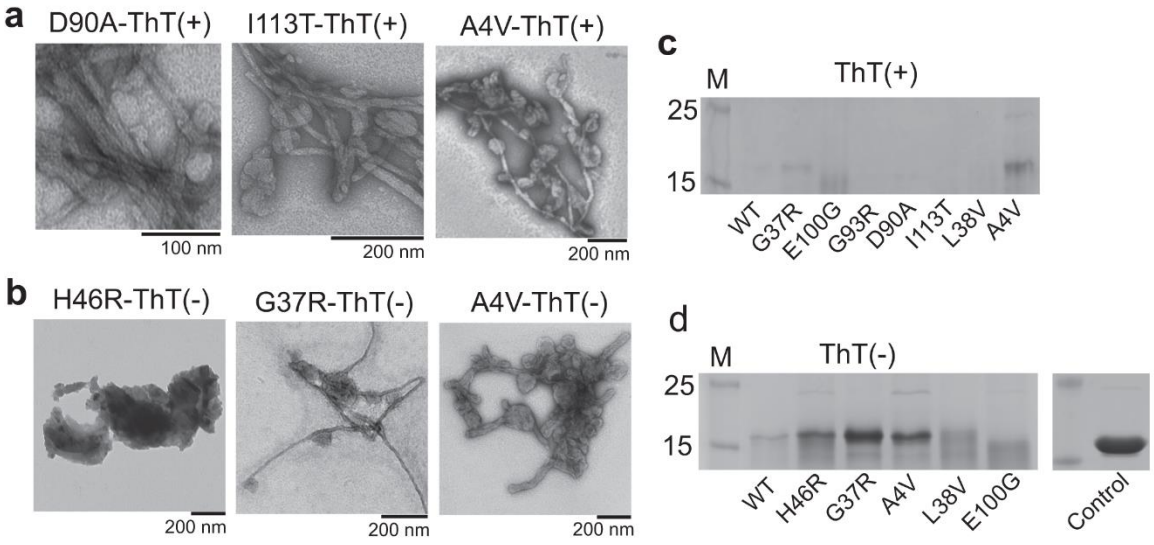

Figure 4.16 TEM micrographs of **(A)** ThT(+), and **(B)** ThT(-) wells after completion of aggregation assays of ALS-variant apo-SOD1 proteins in the presence of anionic DOPCA liposomes, [Lipid]:[SOD1] = 30:1. SDS-PAGE gels of the supernatants from **(C)** ThT(+), and **(D)** ThT(-) wells containing ALS-variant apo-SOD1 proteins in the presence of anionic DOPCA liposomes ([Lipid]:[SOD1] = 30:1) after the termination of aggregation assay. SDS-PAGE gel of soluble control WT apo-SOD1 from a 30 μM stock solution is shown in panel D as control (right gel).

Table 4.3 Metal content of WT and ALS-variant apo-SOD1 proteins measured with ICP-MS.

SOD1 variant	Zn^{2+} (per dimer)	Cu^{2+} (per dimer)
WT	0.08	0.04
A4V	0.03	0.01
G37R	0.04	0.04
L38V	0.02	0.02
H46R	0.01	0.01
D90A	0.07	0.03
G93R	0.05	0.02
E100G	0.02	0.04
I113T	0.02	0.01

REFERENCES

1. Ross, C. A.; Poirier, M. A., Protein aggregation and neurodegenerative disease. *Nat Med* **2004,** *10 Suppl*, S10-7.

2. Combs, B. L.; Cox, A. G., Update on the treatment of Parkinson's disease psychosis: role of pimavanserin. *Neuropsychiatr Dis Treat* **2017,** *13*, 737-744.

3. Skovronsky, D. M.; Lee, V. M.; Trojanowski, J. Q., Neurodegenerative diseases: new concepts of pathogenesis and their therapeutic implications. *Annu Rev Pathol* **2006,** *1*, 151-70.

4. Selkoe, D. J.; Hardy, J., The amyloid hypothesis of Alzheimer's disease at 25 years. *EMBO Mol Med* **2016,** *8* (6), 595-608.

5. Roychaudhuri, R.; Yang, M.; Hoshi, M. M.; Teplow, D. B., Amyloid beta-protein assembly and Alzheimer disease. *J Biol Chem* **2009,** *284* (8), 4749-53.

6. Brown, R. H., Jr., SOD1 aggregates in ALS: cause, correlate or consequence? *Nat Med* **1998,** *4* (12), 1362-4.

7. Desplats, P.; Lee, H. J.; Bae, E. J.; Patrick, C.; Rockenstein, E.; Crews, L.; Spencer, B.; Masliah, E.; Lee, S. J., Inclusion formation and neuronal cell death through neuron-to-neuron transmission of alpha-synuclein. *Proc Natl Acad Sci U S A* **2009,** *106* (31), 13010-5.

8. Knowles, T. P.; Waudby, C. A.; Devlin, G. L.; Cohen, S. I.; Aguzzi, A.; Vendruscolo, M.; Terentjev, E. M.; Welland, M. E.; Dobson, C. M., An analytical solution to the kinetics of breakable filament assembly. *Science* **2009,** *326* (5959), 1533-7.

9. Knowles, T. P.; Vendruscolo, M.; Dobson, C. M., The amyloid state and its association with protein misfolding diseases. *Nat Rev Mol Cell Biol* **2014,** *15* (6), 384-96.

10. Eisenberg, D.; Jucker, M., The amyloid state of proteins in human diseases. *Cell* **2012,** *148* (6), 1188-203.

11. Sawaya, M. R.; Sambashivan, S.; Nelson, R.; Ivanova, M. I.; Sievers, S. A.; Apostol, M. I.; Thompson, M. J.; Balbirnie, M.; Wiltzius, J. J.; McFarlane, H. T.; Madsen, A. O.; Riekel, C.; Eisenberg, D., Atomic structures of amyloid cross-beta spines reveal varied steric zippers. *Nature* **2007,** *447* (7143), 453-7.

12. Rowland, L. P.; Shneider, N. A., Amyotrophic lateral sclerosis. *N Engl J Med* **2001,** *344* (22), 1688-700.

13. Silverman, J. M.; Fernando, S. M.; Grad, L. I.; Hill, A. F.; Turner, B. J.; Yerbury, J. J.; Cashman, N. R., Disease Mechanisms in ALS: Misfolded SOD1 Transferred Through Exosome-Dependent and Exosome-Independent Pathways. *Cell Mol Neurobiol* **2016,** *36* (3), 377-81.

14. Hartl, F. U., Protein Misfolding Diseases. *Annu Rev Biochem* **2017,** *86*, 21-26.

15. Gruzman, A.; Wood, W. L.; Alpert, E.; Prasad, M. D.; Miller, R. G.; Rothstein, J. D.; Bowser, R.; Hamilton, R.; Wood, T. D.; Cleveland, D. W.; Lingappa, V. R.; Liu, J., Common molecular signature in SOD1 for both sporadic and familial amyotrophic lateral sclerosis. *Proc Natl Acad Sci U S A* **2007,** *104* (30), 12524-9.

16. Fernandez-Trapero, M.; Espejo-Porras, F.; Rodriguez-Cueto, C.; Coates, J. R.; Perez-Diaz, C.; de Lago, E.; Fernandez-Ruiz, J., Upregulation of CB2 receptors in reactive astrocytes in canine degenerative myelopathy, a disease model of amyotrophic lateral sclerosis. *Dis Model Mech* **2017,** *10* (5), 551-558.

17. Field, L. S.; Furukawa, Y.; O'Halloran, T. V.; Culotta, V. C., Factors controlling the uptake of yeast copper/zinc superoxide dismutase into mitochondria. *J Biol Chem* **2003,** *278* (30), 28052-9.

18. Lamb, A. L.; Torres, A. S.; O'Halloran, T. V.; Rosenzweig, A. C., Heterodimeric structure of superoxide dismutase in complex with its metallochaperone. *Nat Struct Biol* **2001,** *8* (9), 751-5.

19. Furukawa, Y.; Torres, A. S.; O'Halloran, T. V., Oxygen-induced maturation of SOD1: a key role for disulfide formation by the copper chaperone CCS. *EMBO J* **2004,** *23* (14), 2872-81.

20. Sturtz, L. A.; Diekert, K.; Jensen, L. T.; Lill, R.; Culotta, V. C., A fraction of yeast Cu,Zn-superoxide dismutase and its metallochaperone, CCS, localize to the intermembrane space of mitochondria. A physiological role for SOD1 in guarding against mitochondrial oxidative damage. *J Biol Chem* **2001,** *276* (41), 38084-9.

21. Sheng, Y.; Abreu, I. A.; Cabelli, D. E.; Maroney, M. J.; Miller, A. F.; Teixeira, M.; Valentine, J. S., Superoxide dismutases and superoxide reductases. *Chem Rev* **2014,** *114* (7), 3854-918.

22. Corson, L. B.; Strain, J. J.; Culotta, V. C.; Cleveland, D. W., Chaperone-facilitated copper binding is a property common to several classes of familial amyotrophic lateral sclerosis-linked superoxide dismutase mutants. Proc Natl Acad Sci U S A 1998, 95 (11), 6361-6.

23. Carroll, M. C.; Girouard, J. B.; Ulloa, J. L.; Subramaniam, J. R.; Wong, P. C.; Valentine, J. S.; Culotta, V. C., Mechanisms for activating Cu- and Zn-containing. superoxide dismutase in the absence of the CCS Cu chaperone. *Proc Natl Acad Sci U S A* **2004,** *101* (16), 5964-9.

24. McCord, J. M.; Fridovich, I., Superoxide dismutase. An enzymic function for erythrocuprein (hemocuprein). *J Biol Chem* **1969,** *244* (22), 6049-55.

25. Ogihara, N. L.; Parge, H. E.; Hart, P. J.; Weiss, M. S.; Goto, J. J.; Crane, B. R.; Tsang, J.; Slater, K.; Roe, J. A.; Valentine, J. S.; Eisenberg, D.; Tainer, J. A., Unusual trigonal-planar copper configuration revealed in the atomic structure of yeast copper-zinc superoxide dismutase. *Biochemistry* **1996,** *35* (7), 2316-21.

26. Forman, H. J.; Fridovich, I., On the stability of bovine superoxide dismutase. The effects of metals. *J Biol Chem* **1973,** *248* (8), 2645-9.

27. Parge, H. E.; Hallewell, R. A.; Tainer, J. A., Atomic structures of wild-type and thermostable mutant recombinant human Cu,Zn superoxide dismutase. *Proc Natl Acad Sci U S A* **1992,** *89* (13), 6109-13.

28. Furukawa, Y.; Kaneko, K.; Yamanaka, K.; O'Halloran, T. V.; Nukina, N., Complete loss of post-translational modifications triggers fibrillar aggregation of SOD1 in the familial form of amyotrophic lateral sclerosis. *J Biol Chem* **2008,** *283* (35), 24167-76.

29. Cleveland, D. W.; Rothstein, J. D., From Charcot to Lou Gehrig: deciphering selective motor neuron death in ALS. *Nat Rev Neurosci* **2001,** *2* (11), 806-19.

30. Rosen, D. R.; Siddique, T.; Patterson, D.; Figlewicz, D. A.; Sapp, P.; Hentati, A.; Donaldson, D.; Goto, J.; O'Regan, J. P.; Deng, H. X.; et al., Mutations in Cu/Zn superoxide dismutase gene are associated with familial amyotrophic lateral sclerosis. *Nature* **1993,** *362* (6415), 59-62.

31. Abel, O.; Shatunov, A.; Jones, A. R.; Andersen, P. M.; Powell, J. F.; Al-Chalabi, A., Development of a Smartphone App for a Genetics Website: The Amyotrophic Lateral Sclerosis Online Genetics Database (ALSoD). *JMIR Mhealth Uhealth* **2013,** *1* (2), e18.

32. Saccon, R. A.; Bunton-Stasyshyn, R. K.; Fisher, E. M.; Fratta, P., Is SOD1 loss of function involved in amyotrophic lateral sclerosis? *Brain* **2013,** *136* (Pt 8), 2342-58.

33. Rodriguez, J. A.; Shaw, B. F.; Durazo, A.; Sohn, S. H.; Doucette, P. A.; Nersissian, A. M.; Faull, K. F.; Eggers, D. K.; Tiwari, A.; Hayward, L. J.; Valentine, J. S., Destabilization of apoprotein is insufficient to explain Cu,Zn-superoxide dismutase-linked ALS pathogenesis. *Proc Natl Acad Sci U S A* **2005,** *102* (30), 10516-21.

34. Marklund, S. L.; Andersen, P. M.; Forsgren, L.; Nilsson, P.; Ohlsson, P. I.; Wikander, G.; Oberg, A., Normal binding and reactivity of copper in mutant superoxide dismutase isolated from amyotrophic lateral sclerosis patients. *J Neurochem* **1997,** *69* (2), 675-81.

35. Broom, W. J.; Johnson, D. V.; Auwarter, K. E.; Iafrate, A. J.; Russ, C.; Al-Chalabi, A.; Sapp, P. C.; McKenna-Yasek, D.; Andersen, P. M.; Brown, R. H., Jr., SOD1A4V-mediated ALS: absence of a closely linked modifier gene and origination in Asia. *Neurosci Lett* **2008,** *430* (3), 241-5.

36. Shaw, B. F.; Moustakas, D. T.; Whitelegge, J. P.; Faull, K. F., Taking charge of proteins from neurodegeneration to industrial biotechnology. *Adv Protein Chem Struct Biol* **2010,** *79*, 127-64.

37. Shi, Y.; Abdolvahabi, A.; Shaw, B. F., Protein charge ladders reveal that the net charge of ALS-linked superoxide dismutase can be different in sign and magnitude from predicted values. *Protein Sci* **2014,** *23* (10), 1417-33.

38. Deng, H. X.; Hentati, A.; Tainer, J. A.; Iqbal, Z.; Cayabyab, A.; Hung, W. Y.; Getzoff, E. D.; Hu, P.; Herzfeldt, B.; Roos, R. P.; et al., Amyotrophic lateral sclerosis and structural defects in Cu,Zn superoxide dismutase. *Science* **1993,** *261* (5124), 1047-51.

39. Ratovitski, T.; Corson, L. B.; Strain, J.; Wong, P.; Cleveland, D. W.; Culotta, V. C.; Borchelt, D. R., Variation in the biochemical/biophysical properties of mutant superoxide dismutase 1 enzymes and the rate of disease progression in familial amyotrophic lateral sclerosis kindreds. *Hum Mol Genet* **1999,** *8* (8), 1451-60.

40. Polymenidou, M.; Cleveland, D. W., The seeds of neurodegeneration: prion-like spreading in ALS. *Cell* **2011,** *147* (3), 498-508.

41. Brettschneider, J.; Del Tredici, K.; Lee, V. M.; Trojanowski, J. Q., Spreading of pathology in neurodegenerative diseases: a focus on human studies. *Nat Rev Neurosci* **2015,** *16* (2), 109-20.

42. Grad, L. I.; Yerbury, J. J.; Turner, B. J.; Guest, W. C.; Pokrishevsky, E.; O'Neill, M. A.; Yanai, A.; Silverman, J. M.; Zeineddine, R.; Corcoran, L.; Kumita, J. R.; Luheshi, L. M.; Yousefi, M.; Coleman, B. M.; Hill, A. F.; Plotkin, S. S.; Mackenzie, I. R.; Cashman, N. R., Intercellular propagated misfolding of wild-type Cu/Zn superoxide dismutase occurs via exosome-dependent and -independent mechanisms. *Proc Natl Acad Sci U S A* **2014,** *111* (9), 3620-5.

43. Lee, S.; Kim, H. J., Prion-like Mechanism in Amyotrophic Lateral Sclerosis: are Protein Aggregates the Key? *Exp Neurobiol* **2015,** *24* (1), 1-7.

44. Munch, C.; O'Brien, J.; Bertolotti, A., Prion-like propagation of mutant superoxide dismutase-1 misfolding in neuronal cells. *Proc Natl Acad Sci U S A* **2011,** *108* (9), 3548-53.

45. Furukawa, Y.; Kaneko, K.; Watanabe, S.; Yamanaka, K.; Nukina, N., Intracellular seeded aggregation of mutant Cu,Zn-superoxide dismutase associated with amyotrophic lateral sclerosis. *FEBS Lett* **2013,** *587* (16), 2500-5.

46. Chia, R.; Tattum, M. H.; Jones, S.; Collinge, J.; Fisher, E. M.; Jackson, G. S., Superoxide dismutase 1 and tgSOD1 mouse spinal cord seed fibrils, suggesting a propagative cell death mechanism in amyotrophic lateral sclerosis. *PLoS One* **2010,** *5* (5), e10627.

47. Choi, I.; Yang, Y. I.; Song, H. D.; Lee, J. S.; Kang, T.; Sung, J. J.; Yi, J., Lipid molecules induce the cytotoxic aggregation of Cu/Zn superoxide dismutase with structurally disordered regions. *Biochim Biophys Acta* **2011,** *1812* (1), 41-8.

48. Terakawa, M. S.; Yagi, H.; Adachi, M.; Lee, Y. H.; Goto, Y., Small liposomes accelerate the fibrillation of amyloid beta (1-40). *J Biol Chem* **2015,** *290* (2), 815-26.

49. Galvagnion, C.; Buell, A. K.; Meisl, G.; Michaels, T. C.; Vendruscolo, M.; Knowles, T. P.; Dobson, C. M., Lipid vesicles trigger alpha-synuclein aggregation by stimulating primary nucleation. *Nat Chem Biol* **2015,** *11* (3), 229-34.

50. Abu-Hamad, S.; Kahn, J.; Leyton-Jaimes, M. F.; Rosenblatt, J.; Israelson, A., Misfolded SOD1 Accumulation and Mitochondrial Association Contribute to the Selective Vulnerability of Motor Neurons in Familial ALS: Correlation to Human Disease. *ACS Chem Neurosci* **2017,** *8* (10), 2225-2234.

51. Vande Velde, C.; Miller, T. M.; Cashman, N. R.; Cleveland, D. W., Selective association of misfolded ALS-linked mutant SOD1 with the cytoplasmic face of mitochondria. *Proc Natl Acad Sci U S A* **2008,** *105* (10), 4022-7.

52. Sandelin, E.; Nordlund, A.; Andersen, P. M.; Marklund, S. S.; Oliveberg, M., Amyotrophic lateral sclerosis-associated copper/zinc superoxide dismutase mutations preferentially reduce the repulsive charge of the proteins. *J Biol Chem* **2007,** *282* (29), 21230-6.

53. Chiti, F.; Taddei, N.; Baroni, F.; Capanni, C.; Stefani, M.; Ramponi, G.; Dobson, C. M., Kinetic partitioning of protein folding and aggregation. *Nat Struct Biol* **2002,** *9* (2), 137-43.

54. Abdolvahabi, A.; Shi, Y.; Rhodes, N. R.; Cook, N. P.; Marti, A. A.; Shaw, B. F., Arresting amyloid with coulomb's law: acetylation of ALS-linked SOD1 by aspirin impedes aggregation. *Biophys J* **2015,** *108* (5), 1199-212.

55. Rasouli, S.; Abdolvahabi, A.; Croom, C. M.; Plewman, D. L.; Shi, Y.; Ayers, J. I.; Shaw, B. F., Lysine acylation in superoxide dismutase-1 electrostatically inhibits formation of fibrils with prion-like seeding. *J Biol Chem* **2017,** *292* (47), 19366-19380.

56. Mompean, M.; Chakrabartty, A.; Buratti, E.; Laurents, D. V., Electrostatic Repulsion Governs TDP-43 C-terminal Domain Aggregation. *PLoS Biol* **2016,** *14* (4), e1002447.

57. Taylor, J. D.; Hawthorne, W. J.; Lo, J.; Dear, A.; Jain, N.; Meisl, G.; Andreasen, M.; Fletcher, C.; Koch, M.; Darvill, N.; Scull, N.; Escalera-Maurer, A.; Sefer, L.; Wenman, R.; Lambert, S.; Jean, J.; Xu, Y.; Turner, B.; Kazarian, S. G.; Chapman, M. R.; Bubeck, D.; de Simone, A.; Knowles, T. P.; Matthews, S. J., Electrostatically-guided inhibition of Curli amyloid nucleation by the CsgC-like family of chaperones. *Sci Rep* **2016,** *6*, 24656.

58. Chiti, F.; Stefani, M.; Taddei, N.; Ramponi, G.; Dobson, C. M., Rationalization of the effects of mutations on peptide and protein aggregation rates. *Nature* **2003,** *424* (6950), 805-8.

59. Lawrence, M. S.; Phillips, K. J.; Liu, D. R., Supercharging proteins can impart unusual resilience. *J Am Chem Soc* **2007,** *129* (33), 10110-10112.

60. Gitlin, I.; Carbeck, J. D.; Whitesides, G. M., Why are proteins charged? Networks of charge-charge interactions in proteins measured by charge ladders and capillary electrophoresis. *Angew Chem Int Edit* **2006,** *45* (19), 3022-3060.

61. Shi, Y.; Acerson, M. J.; Shuford, K. L.; Shaw, B. F., Voltage-Induced Misfolding of Zinc-Replete ALS Mutant Superoxide Dismutase-1. *ACS Chem Neurosci* **2015,** *6* (10), 1696-707.

62. Ayyadevara, S.; Balasubramaniam, M.; Alla, R.; Mehta, J. L.; Shmookler Reis, R. J., Aspirin-mediated acetylation protects against multiple neurodegenerative pathologies by impeding protein aggregation. *Antioxid Redox Signal* **2017**.

63. Profit, A. A.; Vedad, J.; Desamero, R. Z. B., Peptide Conjugates of Benzene Carboxylic Acids as Agonists and Antagonists of Amylin Aggregation. *Bioconjugate Chem* **2017,** *28* (2), 666-677.

64. Shi, Y. H.; Mowery, R. A.; Shaw, B. F., Effect of Metal Loading and Subcellular pH on Net Charge of Superoxide Dismutase-1. *J Mol Biol* **2013,** *425* (22), 4388-4404..

65. Shi, Y.; Abdolvahabi, A.; Shaw, B. F., Protein charge ladders reveal that the net charge of ALS-linked superoxide dismutase can be different in sign and magnitude from predicted values. *Protein Sci* **2014,** *23* (10), 1417-1433.

66. Alfonso, L. F.; Srivenugopal, K. S.; Bhat, G. J., Does aspirin acetylate multiple cellular proteins? (Review). *Mol Med Rep* **2009,** *2* (4), 533-7.

67. Tatham, M. H.; Cole, C.; Scullion, P.; Wilkie, R.; Westwood, N. J.; Stark, L. A.; Hay, R. T., A Proteomic Approach to Analyze the Aspirin-mediated Lysine Acetylome. *Mol Cell Proteomics* **2017,** *16* (2), 310-326.

68. Bateman, L. A.; Zaro, B. W.; Miller, S. M.; Pratt, M. R., An alkyne-aspirin chemical reporter for the detection of aspirin-dependent protein modification in living cells. *J Am Chem Soc* **2013,** *135* (39), 14568-73.

69. Schmitt, N. D.; Agar, J. N., Parsing Disease-relevant Protein Modifications from Epiphenomena: Perspective on the Structural Basis of SOD1-Mediated ALS. *J Mass Spectrom* **2017**.

70. Felder, C. E.; Prilusky, J.; Silman, I.; Sussman, J. L., A server and database for dipole moments of proteins. *Nucleic Acids Res* **2007,** *35*, W512-W521.

71. Chattopadhyay, M.; Durazo, A.; Sohn, S. H.; Strong, C. D.; Gralla, E. B.; Whitelegge, J. P.; Valentine, J. S., Initiation and elongation in fibrillation of ALS-linked superoxide dismutase. *Proc Natl Acad Sci U S A* **2008,** *105* (4 8), 18663-8.

72. Oztug Durer, Z. A.; Cohlberg, J. A.; Dinh, P.; Padua, S.; Ehrenclou, K.; Downes, S.; Tan, J. K.; Nakano, Y.; Bowman, C. J.; Hoskins, J. L.; Kwon, C.; Mason, A. Z.; Rodriguez, J. A.; Doucette, P. A.; Shaw, B. F.; Valentine, J. S., Loss of metal ions, disulfide reduction and mutations related to familial ALS promote formation of amyloid-like aggregates from superoxide dismutase. *PLoS One* **2009,** *4* (3), e5004.

73. Renton, A. E.; Chio, A.; Traynor, B. J., State of play in amyotrophic lateral sclerosis genetics. *Nat Neurosci* **2014,** *17* (1), 17-23.

74. Rotunno, M. S.; Bosco, D. A., An emerging role for misfolded wild-type SOD1 in sporadic ALS pathogenesis. *Front Cell Neurosci* **2013,** *7*, 253.

75. Furukawa, Y.; Anzai, I.; Akiyama, S.; Imai, M.; Cruz, F. J.; Saio, T.; Nagasawa, K.; Nomura, T.; Ishimori, K., Conformational Disorder of the Most Immature Cu, Zn-Superoxide Dismutase Leading to Amyotrophic Lateral Sclerosis. *J Biol Chem* **2016,** *291* (8), 4144-55.

76. Choudhary, C.; Weinert, B. T.; Nishida, Y.; Verdin, E.; Mann, M., The growing landscape of lysine acetylation links metabolism and cell signalling. *Nat Rev Mol Cell Biol* **2014,** *15* (8), 536-50.

77. Oueslati, A.; Fournier, M.; Lashuel, H. A., Role of post-translational modifications in modulating the structure, function and toxicity of alpha-synuclein: implications for Parkinson's disease pathogenesis and therapies. *Prog Brain Res* **2010,** *183*, 115-45.

78. Cohen, T. J.; Hwang, A. W.; Restrepo, C. R.; Yuan, C. X.; Trojanowski, J. Q.; Lee, V. M., An acetylation switch controls TDP-43 function and aggregation propensity. *Nat Commun* **2015,** *6*, 5845.

79. Cook, C.; Stankowski, J. N.; Carlomagno, Y.; Stetler, C.; Petrucelli, L., Acetylation: a new key to unlock tau's role in neurodegeneration. *Alzheimers Res Ther* **2014,** *6* (3), 29.

80. Banks, C. J.; Rodriguez, N. W.; Gashler, K. R.; Pandya, R.; Mortenson, J. B.; Whited, M. D.; Soderblom, E. J.; Thompson, J. W.; Moseley, M. A.; Reddi, A. R.; Tessem, J. S.; Torres, M. P.; Bikman, B. T.; Andersen, J. L., Acylation of Superoxide Dismutase 1 (SOD1) at K122 Governs SOD1-mediated Inhibition of Mitochondrial Respiration. *Mol Cell Biol* **2017**.

81. Antinone, S. E.; Ghadge, G. D.; Lam, T. T.; Wang, L. J.; Roos, R. P.; Green, W. N., Palmitoylation of Superoxide Dismutase 1 (SOD1) Is Increased for Familial Amyotrophic Lateral Sclerosis-linked SOD1 Mutants. *Journal of Biological Chemistry* **2013,** *288* (30), 21606-21617.

82. Abdolvahabi, A.; Shi, Y.; Chuprin, A.; Rasouli, S.; Shaw, B. F., Stochastic Formation of Fibrillar and Amorphous Superoxide Dismutase Oligomers Linked to Amyotrophic Lateral Sclerosis. *ACS Chem Neurosci* **2016**.

83. Gitlin, I.; Mayer, M.; Whitesides, G. M., Significance of charge regulation in the analysis of protein charge ladders. *J Phys Chem B* **2003,** *107* (6), 1466-1472.

84. Menon, M. K.; Zydney, A. L., Determination of effective protein charge by capillary electrophoresis: effects of charge regulation in the analysis of charge ladders. *Anal Chem* **2000,** *72* (22), 5714-7.

85. Walker, J. M., The Bicinchoninic Acid (BCA) Assay for Protein Quantitation. *Springer Protoc Hand* **2009**, 11-15.

86. Kruger, N. J., The Bradford Method For Protein Quantitation. *Springer Protoc Hand* **2009**, 17-24.

87. Abdolvahabi, A.; Shi, Y.; Rasouli, S.; Croom, C. M.; Aliyan, A.; Marti, A. A.; Shaw, B. F., Kaplan-Meier meets chemical kinetics: intrinsic rate of SOD1 amyloidogenesis decreased by subset of ALS mutations and cannot fully explain age of disease onset. *ACS Chem Neurosci* **2017**.

88. Wang, J.; Farr, G. W.; Zeiss, C. J.; Rodriguez-Gil, D. J.; Wilson, J. H.; Furtak, K.; Rutkowski, D. T.; Kaufman, R. J.; Ruse, C. I.; Yates, J. R.; Perrin, S.; Feany, M. B.; Horwich, A. L., Progressive aggregation despite chaperone associations of a mutant SOD1-YFP in transgenic mice that develop ALS. *P Natl Acad Sci USA* **2009,** *106* (5), 1392-1397.

89. Ayers, J. I.; Diamond, J.; Sari, A.; Fromholt, S.; Galaleldeen, A.; Ostrow, L. W.; Glass, J. D.; Hart, P. J.; Borchelt, D. R., Distinct conformers of transmissible misfolded SOD1 distinguish human SOD1-FALS from other forms of familial and sporadic ALS. *Acta Neuropathol* **2016,** *132* (6), 827-840.

90. Shi, Y. H.; Rhodes, N. R.; Abdolvahabi, A.; Kohn, T.; Cook, N. P.; Marti, A. A.; Shaw, B. F., Deamidation of Asparagine to Aspartate Destabilizes Cu, Zn Superoxide Dismutase, Accelerates Fibrillization, and Mirrors ALS-Linked Mutations. *J Am Chem Soc* **2013,** *135* (42), 15897-15908.

91. Shaw, B. F.; Arthanari, H.; Narovlyansky, M.; Durazo, A.; Frueh, D. P.; Pollastri, M. P.; Lee, A.; Bilgicer, B.; Gygi, S. P.; Wagner, G.; Whitesides, G. M.,Neutralizing positive charges at the surface of a protein lowers its rate of amide hydrogen exchange without altering its structure or increasing its thermostability. *J.Am Chem Soc* **2010,** *132* (49), 17411-25.

92. Shaw, B. F.; Schneider, G. F.; Bilgicer, B.; Kaufman, G. K.; Neveu, J. M.; Lane, W. S.; Whitelegge, J. P.; Whitesides, G. M., Lysine acetylation can generate highly charged enzymes with increased resistance toward irreversible inactivation. *Protein Science* **2008,** *17* (8), 1446-1455.

93. Rich, J. T.; Neely, J. G.; Paniello, R. C.; Voelker, C. C. J.; Nussenbaum, B.; Wang, E. W., A practical guide to understanding Kaplan-Meier curves. *Otolaryng Head Neck* **2010,** *143* (3), 331-336.

94. Ferrone, F., Analysis of protein aggregation kinetics. *Methods Enzymol* **1999,** *309*, 256-74.

95. Yoshimura, Y.; Lin, Y.; Yagi, H.; Lee, Y. H.; Kitayama, H.; Sakurai, K.; So, M.; Ogi, H.; Naiki, H.; Goto, Y., Distinguishing crystal-like amyloid fibrils and glass-like amorphous aggregates from their kinetics of formation. *Proc Natl Acad Sci U S A* **2012,** *109* (36), 14446-51.

96. Younan, N. D.; Viles, J. H., A Comparison of Three Fluorophores for the Detection of Amyloid Fibers and Prefibrillar Oligomeric Assemblies. ThT (Thioflavin T); ANS (1-Anilinonaphthalene-8-sulfonic Acid); and bisANS (4,4'-Dianilino-1,1'-binaphthyl-5,5'-disulfonic Acid). *Biochemistry* **2015,** *54* (28), 4297-306.

97. Kundu, B.; Guptasarma, P., Hydrophobic dye inhibits aggregation of molten carbonic anhydrase during thermal unfolding and refolding. *Proteins* **1999,** *37* (3), 321-4.

98. Deng, H. X.; Shi, Y.; Furukawa, Y.; Zhai, H.; Fu, R. G.; Liu, E. D.; Gorrie, G. H.; Khan, M. S.; Hung, W. Y.; Bigio, E. H.; Lukas, T.; Dal Canto, M. C.; O'Halloran, T. V.; Siddique, T., Conversion to the amyotrophic lateral sclerosis phenotype is associated with intermolecular linked insoluble aggregates of SOD1 in mitochondria. *P Natl Acad Sci USA* **2006,** *103* (18), 7142-7147.

99. Fukada, K.; Nagano, S.; Satoh, M.; Tohyama, C.; Nakanishi, T.; Shimizu, A.; Yanagihara, T.; Sakoda, S., Stabilization of mutant Cu/Zn superoxide dismutase (SOD1) protein by coexpressed wild SOD1 protein accelerates the disease progression in familial amyotrophic lateral sclerosis mice. *Eur J Neurosci* **2001,** *14* (12), 2032-2036.

100. Wang, L. J.; Deng, H. X.; Grisotti, G.; Zhai, H.; Siddique, T.; Roos, R. P., Wild-type SOD1 overexpression accelerates disease onset of a G85R SOD1 mouse. *Human Molecular Genetics* **2009,** *18* (9), 1642-1651.

101. Xu, G. L.; Ayers, J. I.; Roberts, B. L.; Brown, H.; Fromholt, S.; Green, C.; Borchelt, D. R., Direct and indirect mechanisms for wild-type SOD1 to enhance the toxicity of mutant SOD1 in bigenic transgenic mice. *Human Molecular Genetics* **2015,** *24* (4), 1019-1035.

102. Rothstein, J. D.; Jin, L.; Dykes-Hoberg, M.; Kuncl, R. W., Chronic inhibition of glutamate uptake produces a model of slow neurotoxicity. *Proc Natl Acad Sci U S A* **1993,** *90* (14), 6591-5.

103. Nagy, M.; Fenton, W. A.; Li, D.; Furtak, K.; Horwich, A. L., Extended survival of misfolded G85R SOD1-linked ALS mice by transgenic expression of chaperone Hsp110. *P Natl Acad Sci USA* **2016,** *113* (19), 5424-5428.

104. Frutiger, K.; Lukas, T. J.; Gorrie, G.; Ajroud-Driss, S.; Siddique, T., Gender difference in levels of Cu/Zn superoxide dismutase (SOD1) in cerebrospinal fluid of patients with amyotrophic lateral sclerosis. *Amyotroph Lateral Scler* **2008,** *9* (3), 184-7.

105. Sangwan, S.; Zhao, A.; Adams, K. L.; Jayson, C. K.; Sawaya, M. R.; Guenther, E. L.; Pan, A. C.; Ngo, J.; Moore, D. M.; Soriaga, A. B.; Do, T. D.; Goldschmidt, L.; Nelson, R.; Bowers, M. T.; Koehler, C. M.; Shaw, D. E.; Novitch, B. G.; Eisenberg, D. S., Atomic structure of a toxic, oligomeric segment of SOD1 linked to amyotrophic lateral sclerosis (ALS). *Proc Natl Acad Sci U S A* **2017,** *114* (33), 8770-8775.

106. De Lavor, M. S. L.; Binda, N. S.; Fukushima, F. B.; Caldeira, F. M. C.; da Silva, J. F.; Silva, C. M. O.; de Oliveira, K. M.; Martins, B. D.; Torres, B. B. J.; Rosado, I. R.; Gomez, R. S.; Gomez, M. V.; de Melo, E. G., Ischemia-reperfusion model in rat spinal cord: cell viability and apoptosis signaling study. *Int J Clin Exp Patho* **2015,** *8* (9), 9941-9949.

107. Carbeck, J. D.; Colton, I. J.; Gao, J. M.; Whitesides, G. M., Protein charge ladders, capillary electrophoresis, and the role of electrostatics in biomolecular recognition. *Accounts Chem Res* **1998,** *31* (6), 343-350.

108. Tanaka, M.; Komi, Y., Layers of structure and function in protein aggregation. *Nat Chem Biol* **2015,** *11* (6), 373-7.

109. Iyer, A.; Roeters, S. J.; Schilderink, N.; Hommersom, B.; Heeren, R. M.; Woutersen, S.; Claessens, M. M.; Subramaniam, V., The Impact of N-terminal Acetylation of Alpha Synuclein on Phospholipid Membrane Binding and Fibril Structure. *J Biol Chem* **2016**.

110. Eisele, Y. S.; Monteiro, C.; Fearns, C.; Encalada, S. E.; Wiseman, R. L.; Powers, E. T.; Kelly, J. W., Targeting protein aggregation for the treatment of degenerative diseases. *Nat Rev Drug Discov* **2015,** *14* (11), 759-80.

111. Rasouli, S.; Abdolvahabi, A.; Croom, C. M.; Plewman, D. L.; Shi, Y.; Shaw, B. F., Glycerolipid Headgroups Control Rate and Mechanism of Superoxide Dismutase-1 Aggregation and Accelerate Fibrillization of Slowly Aggregating Amyotrophic Lateral Sclerosis Mutants. *ACS Chem Neurosci* **2018**.

112. Sangwan, S.; Eisenberg, D. S., Perspective on SOD1 mediated toxicity in Amyotrophic Lateral Sclerosis. *Postepy Biochem* **2016,** *62* (3), 362-369.

113. Sibilla, C.; Bertolotti, A., Prion Properties of SOD1 in Amyotrophic Lateral Sclerosis and Potential Therapy. *Cold Spring Harb Perspect Biol* **2017,** *9* (10).

114. Pickles, S.; Semmler, S.; Broom, H. R.; Destroismaisons, L.; Legroux, L.; Arbour, N.; Meiering, E.; Cashman, N. R.; Vande Velde, C., ALS-linked misfolded SOD1 species have divergent impacts on mitochondria. *Acta Neuropathol Commun* **2016,** *4* (1), 43.

115. Abu-Hamad, S.; Kahn, J.; Leyton-Jaimes, M. F.; Rosenblatt, J.; Israelson, A., Misfolded SOD1 Accumulation and Mitochondrial Association Contribute to the Selective Vulnerability of Motor Neurons in Familial ALS: Correlation to Human Disease. *ACS Chem Neurosci* **2017**.

116. Palomo, G. M.; Manfredi, G., Exploring new pathways of neurodegeneration in ALS: the role of mitochondria quality control. *Brain Res* **2015,** *1607*, 36-46.

117. Shaw, B. F.; Schneider, G. F.; Arthanari, H.; Narovlyansky, M.; Moustakas, D.; Durazo, A.; Wagner, G.; Whitesides, G. M., Complexes of native ubiquitin and dodecyl sulfate illustrate the nature of hydrophobic and electrostatic interactions in the binding of proteins and surfactants. *J Am Chem Soc* **2011,** *133* (44), 17681-95.

118. Shaw, B. F.; Schneider, G. F.; Whitesides, G. M., Effect of surfactant hydrophobicity on the pathway for unfolding of ubiquitin. *J Am Chem Soc* **2012,** *134* (45), 18739-45.

119. Otzen, D. E., Proteins in a brave new surfactant world. *Current Opinion in Colloid & Interface Science* **2015,** *20* (3), 161-169.

120. Okur, H. I.; Hladilkova, J.; Rembert, K. B.; Cho, Y.; Heyda, J.; Dzubiella, J.; Cremer, P. S.; Jungwirth, P., Beyond the Hofmeister Series: Ion-Specific Effects on Proteins and Their Biological Functions. *J Phys Chem B* **2017,** *121* (9), 1997-2014.

121. Chong, S. H.; Ham, S., Distinct Role of Hydration Water in Protein Misfolding and Aggregation Revealed by Fluctuating Thermodynamics Analysis. *Accounts Chem Res* **2015,** *48* (4), 956-965.

122. Abdolvahabi, A.; Shi, Y.; Chuprin, A.; Rasouli, S.; Shaw, B. F., Stochastic Formation of Fibrillar and Amorphous Superoxide Dismutase Oligomers Linked to Amyotrophic Lateral Sclerosis. *ACS Chem Neurosci* **2016,** *7* (6), 799-810.

123. Abdolvahabi, A.; Shi, Y.; Rasouli, S.; Croom, C. M.; Aliyan, A.; Marti, A. A.; Shaw, B. F., Kaplan-Meier Meets Chemical Kinetics: Intrinsic Rate of SOD1 Amyloidogenesis Decreased by Subset of ALS Mutations and Cannot Fully Explain Age of Disease Onset. *ACS Chem Neurosci* **2017,** *8* (6), 1378-1389.

124. Abdolvahabi, A.; Shi, Y.; Rasouli, S.; Croom, C. M.; Chuprin, A.; Shaw, B. F., How Do Gyrating Beads Accelerate Amyloid Fibrillization? *Biophys J* **2017,** *112* (2), 250-264.

125. Abdolvahabi, A.; Shi, Y. H.; Rhodes, N. R.; Cook, N. P.; Marti, A. A.; Shaw, B. F., Arresting Amyloid with Coulomb's Law: Acetylation of ALS-Linked SOD1 by Aspirin Impedes Aggregation. *Biophysical Journal* **2015,** *108* (5), 1199-1212.

126. Lang, L.; Zetterstrom, P.; Brannstrom, T.; Marklund, S. L.; Danielsson, J.; Oliveberg, M., SOD1 aggregation in ALS mice shows simplistic test tube behavior. *Proc Natl Acad Sci U S A* **2015,** *112* (32), 9878-83.

127. Takamori, S.; Holt, M.; Stenius, K.; Lemke, E. A.; Gronborg, M.; Riedel, D.; Urlaub, H.; Schenck, S.; Brugger, B.; Ringler, P.; Muller, S. A.; Rammner, B.; Grater, F.; Hub, J. S.; De Groot, B. L.; Mieskes, G.; Moriyama, Y.; Klingauf, J.; Grubmuller, H.; Heuser, J.; Wieland, F.; Jahn, R., Molecular anatomy of a trafficking organelle. *Cell* **2006,** *127* (4), 831-46.

128. Contreras, F. X.; Sot, J.; Alonso, A.; Goni, F. M., Sphingosine increases the permeability of model and cell membranes. *Biophys J* **2006,** *90* (11), 4085-92.

129. Tatsuta, T.; Scharwey, M.; Langer, T., Mitochondrial lipid trafficking. *Trends Cell Biol* **2014,** *24* (1), 44-52.

130. McAlary, L.; Aquilina, J. A.; Yerbury, J. J., Susceptibility of Mutant SOD1 to Form a Destabilized Monomer Predicts Cellular Aggregation and Toxicity but Not In vitro Aggregation Propensity. *Front Neurosci* **2016,** *10*, 499.

131. Sasaki, S.; Nagai, M.; Aoki, M.; Komori, T.; Itoyama, Y.; Iwata, M., Motor neuron disease in transgenic mice with an H46R mutant SOD1 gene. *J Neuropathol Exp Neurol* **2007,** *66* (6), 517-24.

132. Nagai, M.; Aoki, M.; Miyoshi, I.; Kato, M.; Pasinelli, P.; Kasai, N.; Brown, R. H., Jr.; Itoyama, Y., Rats expressing human cytosolic copper-zinc superoxide dismutase transgenes with amyotrophic lateral sclerosis: associated mutations develop motor neuron disease. *J Neurosci* **2001,** *21* (23), 9246-54.

133. Eden, K.; Morris, R.; Gillam, J.; MacPhee, C. E.; Allen, R. J., Competition between primary nucleation and autocatalysis in amyloid fibril self-assembly. *Biophys J* **2015,** *108* (3), 632-43.

134. Ulrich, A. S.; Sami, M.; Watts, A., Hydration of Dopc Bilayers by Differential Scanning Calorimetry. *Bba-Biomembranes* **1994,** *1191* (1), 225-230.

135. Wu, F. G.; Sun, H. Y.; Zhou, Y.; Deng, G.; Yu, Z. W., Molecular-level pictures of the phase transitions of saturated and unsaturated phospholipid binary mixtures. *Rsc Adv* **2015,** *5* (1), 726-733.

136. Hirsch-Lemer, D.; Barenholz, Y., Probing DNA-cationic lipid interactions with the fluorophore trimethylammonium diphenyl-hexatriene (TMADPH). *Bba-Biomembranes* **1998,** *1370* (1), 17-30.

137. Vassall, K. A.; Stubbs, H. R.; Primmer, H. A.; Tong, M. S.; Sullivan, S. M.; Sobering, R.; Srinivasan, S.; Briere, L. A.; Dunn, S. D.; Colon, W.; Meiering, E. M., Decreased stability and increased formation of soluble aggregates by immature superoxide dismutase do not account for disease severity in ALS. *Proc Natl Acad Sci U S A* **2011,** *108* (6), 2210-5.

138. Gao, M.; Winter, R., The Effects of Lipid Membranes, Crowding and Osmolytes on the Aggregation, and Fibrillation Propensity of Human IAPP. *J Diabetes Res* **2015,** *2015*, 849017.

139. Hudson, S. A.; Ecroyd, H.; Kee, T. W.; Carver, J. A., The thioflavin T fluorescence assay for amyloid fibril detection can be biased by the presence of exogenous compounds. *FEBS J* **2009,** *276* (20), 5960-72.

140. Liu, A. P.; Wenzel, N.; Qi, X. Y., Role of lysine residues in membrane anchoring of saposin C. *Arch Biochem Biophys* **2005,** *443* (1-2), 101-112.

141. Song, J.; Kang, T. H.; Kim, M. W.; Han, S., Ion specific effects: decoupling ion-ion and ion-water interactions. *Phys Chem Chem Phys* **2015,** *17* (13), 8306-8322.

142. Armstrong, B. D.; Han, S. G., Overhauser Dynamic Nuclear Polarization To Study Local Water Dynamics. *J Am Chem Soc* **2009,** *131* (13), 4641-4647.

143. Kanduc, M.; Schlaich, A.; Schneck, E.; Netz, R. R., Water-Mediated Interactions between Hydrophilic and Hydrophobic Surfaces. *Langmuir* **2016,** *32* (35), 8767-8782.

144. Shi, Y.; Rhodes, N. R.; Abdolvahabi, A.; Kohn, T.; Cook, N. P.; Marti, A. A.; Shaw, B. F., Deamidation of asparagine to aspartate destabilizes Cu, Zn superoxide dismutase, accelerates fibrillization, and mirrors ALS-linked mutations. *J Am Chem Soc* **2013,** *135* (42), 15897-908.

145. Shi, Y.; Mowery, R. A.; Ashley, J.; Hentz, M.; Ramirez, A. J.; Bilgicer, B.; Slunt-Brown, H.; Borchelt, D. R.; Shaw, B. F., Abnormal SDS-PAGE migration of cytosolic proteins can identify domains and mechanisms that control surfactant binding. *Protein Sci* **2012,** *21* (8), 1197-209.

146. De Groot, N. S.; Burgas, M. T., Is membrane homeostasis the missing link between inflammation and neurodegenerative diseases? *Cell Mol Life Sci* **2015,** *72* (24), 4795-805.

147. Schmitt, F.; Hussain, G.; Dupuis, L.; Loeffler, J. P.; Henriques, A., A plural role for lipids in motor neuron diseases: energy, signaling and structure. *Front Cell Neurosci* **2014,** *8*, 25.

148. Dupuis, L.; Oudart, H.; Rene, F.; Gonzalez de Aguilar, J. L.; Loeffler, J. P., Evidence for defective energy homeostasis in amyotrophic lateral sclerosis: benefit of a high-energy diet in a transgenic mouse model. *Proc Natl Acad Sci U S A* **2004,** *101* (30), 11159-64.

149. Tsang, C. K.; Liu, Y.; Thomas, J.; Zhang, Y.; Zheng, X. F., Superoxide dismutase 1 acts as a nuclear transcription factor to regulate oxidative stress resistance. *Nat Commun* **2014,** *5*, 3446.

150. Jena, B. P., Intracellular Organelle Dynamics at nm Resolution. *Method Cell Biol* **2008,** *90*, 19-37.

151. Zeineddine, R.; Pundavela, J. F.; Corcoran, L.; Stewart, E. M.; Do-Ha, D.; Bax, M.; Guillemin, G.; Vine, K. L.; Hatters, D. M.; Ecroyd, H.; Dobson, C. M.; Turner, B. J.; Ooi, L.; Wilson, M. R.; Cashman, N. R.; Yerbury, J. J., SOD1 protein aggregates stimulate macropinocytosis in neurons to facilitate their propagation. *Mol Neurodegener* **2015,** *10* (1), 57.

152. Wang, Q.; Johnson, J. L.; Agar, N. Y.; Agar, J. N., Protein aggregation and protein instability govern familial amyotrophic lateral sclerosis patient survival. *PLoS Biol* **2008,** *6* (7), e170.

153. Shi, Y.; Acerson, M. J.; Abdolvahabi, A.; Mowery, R. A.; Shaw, B. F., Gibbs Energy of Superoxide Dismutase Heterodimerization Accounts for Variable Survival in Amyotrophic Lateral Sclerosis. *J Am Chem Soc* **2016,** *138* (16), 5351-62.

154. Yanasarn, N.; Sloat, B. R.; Cui, Z., Negatively Charged Liposomes Show Potent Adjuvant Activity When Simply Admixed with Protein Antigens. *Mol Pharmaceut* **2011,** *8* (4), 1174-1185.